



**NTNU – Trondheim**  
Norwegian University of  
Science and Technology

# Coupled Analysis of a Moored Sevan Hull by the use of OrcaFlex

**Erik Byholt Hanssen**

Subsea Technology

Submission date: June 2013

Supervisor: Bernt Johan Leira, IMT

Norwegian University of Science and Technology  
Department of Marine Technology





Master Thesis, Spring 2013

for

Stud. Techn. Erik Byholt Hanssen

## Coupled analysis of a moored Sevan hull by the use of OrcaFlex

*Koblet responsanalyse av en forankret Sevan flyter ved bruk av OrcaFlex*

A coupled analysis is recognized by the dynamics of the floater, mooring lines and risers being solved simultaneously. The aim of a coupled analysis is to determine the floater's mean position and dynamic response due to the mooring and riser system's restoring, damping and inertia forces. Offshore activity is taking place at increasing water depths, and in order to predict the system motion of response these loads must be adequately modeled. The existing laboratories used for design verification of moored vessels are challenged by the water depth increase due to scaling laws. In this context, a coupled analysis can be utilized in collaboration with a truncated model test. Coupled analyses are also the recommended numerical approach in order to predict the low frequency motion of moored structures (Veritas).

The topic of this thesis was initially proposed by 4Subsea, whose main interest was related to OrcaFlex and low frequency motion of moored floaters. A report containing information from a model test conducted on a moored Sevan Floating Storage Unit has been made available for the present master thesis work. The results presented in that report are the basis for comparison with the OrcaFlex numerical analyses to be performed as part of the present work.

The following subjects are to be addressed as part of this work:



1. Give a brief description of the model test for which results were used for comparison with the numerical analyses to be performed as part of the present thesis.
2. Give an overview of the theoretical background for the dynamic response of a moored floater to the combined loading due to wind, waves and current.
3. Run coupled time domain analyses of the moored Sevan FSU subjected to several environmental conditions using OrcaFlex. For the hull this includes the determination of: (i) Frequency and direction dependent first and second order wave excitation coefficients (ii) Frequency dependent added mass and potential damping (iii) Viscous and eddy-making damping. The mooring lines can be modeled as Morison elements.
4. Compare results obtained from the OrcaFlex analyses to model test results and preferably also other software tools.

The work scope may prove to be larger than initially anticipated. Subject to approval from the supervisor, topics may be deleted from the list above or reduced in extent.

In the thesis the candidate shall present his personal contribution to the resolution of problems within the scope of the thesis work.

Theories and conclusions should be based on mathematical derivations and/or logic reasoning identifying the various steps in the deduction.

The candidate should utilise the existing possibilities for obtaining relevant literature.

The thesis should be organised in a rational manner to give a clear exposition of results, assessments, and conclusions. The text should be brief and to the point, with a clear language. Telegraphic language should be avoided.

The thesis shall contain the following elements: A text defining the scope, preface, list of contents, summary, main body of thesis, conclusions with recommendations for further work, list of symbols and acronyms, references and (optional) appendices. All figures, tables and equations shall be numbered.



The supervisor may require that the candidate, in an early stage of the work, presents a written plan for the completion of the work. The plan should include a budget for the use of computer and laboratory resources which will be charged to the department. Overruns shall be reported to the supervisor.

The original contribution of the candidate and material taken from other sources shall be clearly defined. Work from other sources shall be properly referenced using an acknowledged referencing system.

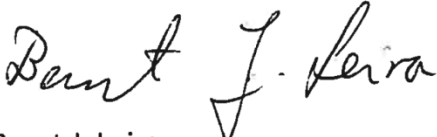
The thesis shall be submitted in 3 copies:

- Signed by the candidate
- The text defining the scope included
- In bound volume(s)
- Drawings and/or computer prints which cannot be bound should be organised in a separate folder.

Supervisor: Professor Bernt J. Leira      Contact person at 4Subsea: Jacob Qvist

Deadline: June 10<sup>th</sup> 2013

Trondheim, January 14<sup>th</sup>, 2013

  
Bernt J. Leira



## Preface

This report is the completion of the Master of Science degree in Marine Technology at the Norwegian University of Science and Technology (NTNU). The paper, written during the last semester of the studies, is weighted with 30 units.

A normal progression at the department of Marine Technology is to perform a literature study during the second last semester, which purpose is to gain knowledge on the topic of the coming master thesis. In my case, this topic was changed, and the work presented in this report was conducted during the last semester.

The topic of this thesis was initially proposed by 4Subsea, whose main interest was related to OrcaFlex and low frequency motion of moored structures.

During the implementation of the analyses several software tools have been utilized. The author was unfamiliar with both GeniE, Wadam (HydroD) and OrcaFlex until this thesis was initiated, and familiarization with these tools consequently took up time. On the other hand, both theoretical and practical knowledge regarding the implementation of coupled analysis was gained.

I would like to thank Professor and supervisor Bernt J. Leira at the Department of Marine Technology for his collaboration during this last semester. Further, both Chittiappa Muthanna and Csaba Pakozdi at Marintek were very helpful to me when I searched for information, and ought to be thanked. Finally, Jacob Qvist from 4Subsea provided good support.

*Erik Byholt Hansen  
Tvedheim 7/6-13*



## **Abstract**

Offshore activity related to the search of energy in terms of hydrocarbons is taking place at increasing water depths. In deeper water, the effects on the floater motion from the mooring and riser systems increase significantly. Viscous damping, inertial mass, current loading and restoring effects from riser and mooring systems need to be adequately modeled in order to predict the system motion of response. Accurate prediction of the system response is vital in the context of design verification of the complete system. The recommended method to analyze the dynamics of a moored structure, especially in deep waters, is by a coupled analysis approach. This is recognized by the dynamics of the floater, mooring lines and risers being solved simultaneously.

This thesis comprises a theoretical part, where key subjects related to the prediction of moored structure motion is addressed. In addition, coupled time domain analyses of a moored Sevan FSU (Floating Storage Unit) were performed. The analyses were initiated by the establishment of a finite element model of the Sevan hull. This was used to conduct a diffraction analysis on FSU. The results obtained from the diffraction analysis were imported to OrcaFlex, where the mooring systems were also modeled. OrcaFlex is a fully 3D non-linear time domain finite element program, which supports Newman's approximation and a method based on Aranha's approximation in order to predict the low frequency motion of moored structures.

Model tests have been previously performed on the moored FSU, and results from these tests were used as the basis for comparison to the OrcaFlex results. In addition, time series of the wave elevation and wind velocities recorded during the FSU model tests were acquired through Sevan and Marintek, enabling these environmental conditions to be integrated in the OrcaFlex analyses. Hence time series results from the OrcaFlex analyses were directly comparable with the FSU model test time series.

The drawback of this approach ultimately proved to be the CPU-cost and the duration of the numerical simulation of relatively short model test time series (scaled to real time). The results obtained from the OrcaFlex analyses show acceptable compliance to the model test results, but the amplitude of the low frequency motion seems to be slightly under predicted.



In order to predict outcomes under specific scenarios e.g. extreme events of the system response, a longer real time simulation is required. This is further discussed at the end of this paper.

## Sammendrag

Søk etter energi i form av hydrokarboner skjer på stadig dypere vann. I dypere vann øker påvirkningen stigerør- og fortøyningsystemer har på flyterens bevegelser. Viskøs demping, tilleggsmasse, strømlaster og stivhetsegenskaper til stigerør- og fortøyningsystemer må da modelleres på en adekvat måte for å kunne forutse systemets bevegelser. Nøyaktig forutsigbarhet av en flyters bevegelse er vitalt i forbindelse med planlegging og verifikasjon av nye flytende offshore systemer. Koblede analyser er den anbefalte metoden, av blant annet DNV, for å analysere forankrede systemer. Koblede analyser kjennetegnes ved at responsen til både flyter, stigerør og forankringssystemer blir beregnet samtidig, og på denne måten blir interaksjonen mellom de ulike systemene også integrert i analysene.

Denne oppgaven inneholder en teoretisk del som beskriver laster og metoder som er viktige for å kunne forutse bevegelser til fortøyde fartøy. Det er også gjennomført koblede responsanalyser av et forankret Sevan skrog. De koblede analysene ble gjennomført i OrcaFlex som er et ikke lineært 3-dimensjonalt tidsdomene dataprogram hvor elementmetoden blir brukt for å modellere systemet. Første og andre ordens eksitasjonslaste, potensial demping og tilleggsmasse for Sevan skroget ble funnet ved hjelp av panelmetodeprogrammet WADAM, og siden importert til OrcaFlex.

Det er tidligere gjennomført modellforsøk av det forankrede Sevan skroget av Marintek. Resultatene fra disse forsøkene ble brukt som sammenlikningsgrunnlag for analysene som er gjort i forbindelse med denne oppgaven. Tidsserier av både vindhastigheter og bølgehevingene som ble målt i forbindelse med disse forsøkene ble i løpet av arbeidet med denne oppgaven også innhentet fra Marintek. Dette muliggjorde at resultatene som ble





funnet gjennom OrcaFlex-analysene kunne sammenliknes direkte med resultatene fra modellforsøket i tidsplanet.

Utfordringen med denne metoden skulle vise seg å være en enorm regnetid for datamaskinen som ble brukt. Dette medførte at lengden på de numeriske simuleringene som er gjort i denne oppgaven er mye kortere enn ønskelig. Resultatene fra de relativt korte tidsseriene gav på en annen side i hovedtrekk akseptabel samsvar med bevegelsen til Sevan skroget i modellforsøket. En svært viktig del av flyter bevegelsen, den lavfrekvente jag bevegelsen, fremstår dog som noe under estimert.



## List of content

Preface.....	iv
Abstract .....	v
List of figures .....	xi
List of tables .....	xiv
Nomenclature.....	xv
1 Introduction .....	- 1 -
2 System description of the moored FSU .....	- 3 -
2.1 Coordinate system and rigid body modes.....	- 4 -
2.2 The FSU.....	- 4 -
2.3 Mooring line systems.....	- 6 -
3 Loads on marine systems.....	- 8 -
3.1 Linear wave theory .....	- 9 -
3.2 Wave excitation loads .....	- 10 -
3.3 Added mass, damping and restoring loads .....	- 11 -
3.4 Panel method for large volume structures .....	- 14 -
3.5 Morison's equation for estimating loads on slender structures.....	- 17 -
3.6 Second order excitation and damping of floaters.....	- 18 -
3.6.1 Newman's approximation for difference frequencies loads .....	- 21 -
3.6.2 Damping of low frequency moored vessel motion .....	- 23 -
3.7 Wind and current loads .....	- 24 -
4 Global analysis of moored floater motion .....	- 26 -
4.1 Coupled analysis of marine systems.....	- 26 -
4.2 Time - and frequency domain representation of response .....	- 28 -



4.3	Implicit time integration: the generalized $\alpha$ -method.....	- 32 -
4.4	Finite element formulation of marine systems.....	- 33 -
5	Implementation of the OrcaFlex coupled analyses .....	- 39 -
5.1	Basis for comparison to the OrcaFlex coupled analyses .....	- 39 -
5.2	Building the model in OrcaFlex.....	- 40 -
5.2.1	Chain-polyester-chain mooring system .....	- 41 -
5.2.2	Chain mooring system.....	- 43 -
5.3	Verification of the mooring stiffness in the numerical model .....	- 44 -
5.4	Diffraction analysis of the FSU by WADAM.....	- 46 -
5.5	Estimating the viscous damping of the FSU .....	- 49 -
5.6	Numerical reconstruction of decay tests .....	- 53 -
5.7	Introducing loads in OrcaFlex.....	- 55 -
5.7.1	Current load in OrcaFlex.....	- 56 -
5.7.2	Wind load in OrcaFlex .....	- 57 -
5.7.3	Import time series of wave elevation to OrcaFlex.....	- 58 -
5.7.4	Second order wave excitation and damping in OraFlex .....	- 59 -
5.8	Irregular wave tests OrcaFlex.....	- 60 -
6	Results from numerical simulations with irregular waves .....	- 64 -
6.1	Test 3021 .....	- 65 -
6.2	Test 3031 .....	- 68 -
6.3	Test 3411 .....	- 69 -
6.4	Test 3710 .....	- 70 -
7	Comparison of power spectra.....	- 72 -
8	Uncertainties related to parameters used in the analyses.....	- 77 -
8.1	Mooring systems .....	- 77 -



8.2	Diffraction analysis .....	- 77 -
8.3	Viscous effects .....	- 78 -
8.4	Second order motion obtained by the OrcaFlex analyses .....	- 79 -
8.5	Power spectra calculation .....	- 80 -
9	Summary and conclusion .....	- 82 -
10	Proposal for further work.....	- 84 -
11	Bibliography.....	- 85 -
Appendices .....		I
Appendix A – Input WADAM analysis.....		I
Appendix B- Estimation of viscous damping coefficients.....		III
Appendix C- Decay tests chain mooring system.....		VII
Appendix D- Orcina support on system stiffness .....		X
Appendix E- Orcina support on dividing period .....		XI
Appendix F- Irregular wave tests chain mooring system .....		XIV
Appendix G - Wave excitation coefficients FSU 1000 .....		XVI
Appendix H– Added mass FSU 1000.....		XVIII
Appendix I - Potential damping FSU 1000 .....		XX
Appendix J- Mean wave drift coefficients FSU 1000 .....		XXII
Appendix K – Converting time series to Gaussian-shaped power spectra .....		XXIII
Appendix L – Smoothing convolution of raw power spectra .....		XXV
Appendix M – Content of attached data folder .....		XXVII



## List of figures

Figure 1: Hybrid verification procedure (Carl Trygve Stansberg, 2002).....	- 1 -
Figure 2: Model test of the FSU at the Marintek basin (Muthanna, 2011) .....	- 3 -
Figure 3: Coordinate system and rigid body modes of the FSU (Greco).....	- 4 -
Figure 4: PDQ relative to the FSU during the model tests (Muthanna, 2011).....	- 5 -
Figure 5: Mooring lines setup (Muthanna, 2011) .....	- 6 -
Figure 6: Wave excitation loads, added mass and damping (Greco).....	- 8 -
Figure 7: Relative importance of mass, viscous drag and diffraction forces on marine structures (Greco) .....	- 8 -
Figure 8: Source and sink illustration (Massie, 2001) .....	- 15 -
Figure 9: Wave drift forces (Massie, 2001) .....	- 19 -
Figure 10: Separated and coupled analysis (Vugts, 1997) .....	- 26 -
Figure 11: Damping normal to the mooring line due to vessel surge.....	- 27 -
Figure 12: Frequency and time domain illustration (Massie, 2001) .....	- 30 -
Figure 13: Simulation of irregular sea (Myrhaug) .....	- 31 -
Figure 14: OrcaFlex discretization of pipe (Orcina).....	- 34 -
Figure 15: Interpolation polynomial 2D-bar (Sigbjörnsson) .....	- 35 -
Figure 16: Newton-Raphson iteration (Moan, 2007).....	- 37 -
Figure 17: Static offset test chain mooring system.....	- 45 -
Figure 18: Static offset test chain-polyester-chain mooring system .....	- 45 -
Figure 19: GeniE FE-model of the FSU with hydrostatic 'dummy' load.....	- 46 -
Figure 20: Diffraction analysis in WADAM .....	- 48 -
Figure 21: Decay test example (Steen, 2012).....	- 50 -
Figure 22: Viscous damping coefficient pitch .....	- 51 -
Figure 23: Viscous damping coefficients heave .....	- 52 -
Figure 24: Numerical reconstruction of decay test 1250.....	- 54 -
Figure 25: Numerical reconstruction of decay test 1370.....	- 54 -
Figure 26: Numerical reconstruction of decay test 1380.....	- 55 -
Figure 27: Velocity profile in ocean basin during model test .....	- 56 -



Figure 28: Sensitivity test conducted on the numerical integration time step ..... - 61 -

Figure 29: Torsethaugen spectrum from MatLab and WAFO ..... - 62 -

Figure 30: Sensitivity test conducted on the OrcaFlex dividing period (environmental condition) ..... - 63 -

Figure 31: Viscous damping coefficients obtained from decay test in irregular waves ..... - 63 -

Figure 32: Test no 3021 FSU heave response 0 - 1000 sec. .... - 66 -

Figure 33: Test no 3021 FSU heave response 1000 - 2000 sec. .... - 66 -

Figure 34: Test no 3021 FSU heave response 2000 - 3000 sec. .... - 66 -

Figure 35: Test no 3021 FSU pitch response 0 - 1000 sec. .... - 67 -

Figure 36: Test no 3021 FSU pitch response 1000 - 2000 sec. .... - 67 -

Figure 37: Test no 3021 FSU pitch response 2000 - 3000 sec. .... - 67 -

Figure 38: Test no 3031 FSU surge response 0 - 1000 sec. .... - 68 -

Figure 39: Test no 3031 FSU heave response 0 - 1000 sec. .... - 68 -

Figure 40: Test no 3031 FSU pitch response 0 - 1000 sec. .... - 68 -

Figure 41: Test no 3411 FSU surge response 0 - 1000 sec. .... - 69 -

Figure 42: Test no 3411 FSU heave response 0 - 1000 sec. .... - 69 -

Figure 43: Test no 3411 FSU pitch response 0 - 1000 sec. .... - 69 -

Figure 44: Test no 3710 FSU surge response 0 - 1000 sec. .... - 70 -

Figure 45: Test no 3710 FSU heave response 0 - 1000 sec. .... - 70 -

Figure 46: Test no 3710 FSU pitch response 0 - 1000 sec. .... - 70 -

Figure 47: Power spectra of WF surge response from model test and SIMO/RIFLEX simulation ..... - 73 -

Figure 48: Power spectrum of WF surge response from OrcaFlex simulation ..... - 73 -

Figure 49: Power spectra of heave response from model test and SIMO/RIFLEX simulation.... - 74 -

Figure 50: Power spectrum heave response from OrcaFlex simulation ..... - 74 -

Figure 51: Power spectra of pitch response from model test and SIMO/RIFLEX simulation - 75 -

Figure 52: Power spectrum pitch response from OrcaFlex simulation..... - 75 -

Figure 53: Power spectra LF surge response from model test and SIMO/RIFLEX ..... - 76 -

Figure 54: Power spectrum LF surge response from OrcaFlex simulation ..... - 76 -



Figure 55: Numerical reconstruction of decay test 1950 (surge) .....	VII
Figure 56: Numerical reconstruction of decay test 1930 (heave) .....	VII
Figure 57: Numerical reconstruction decay test 1940 (pitch) .....	VIII
Figure 58: Decay test 1370 with applied viscous damping coefficients from section 5.5. ....	VIII
Figure 59: Decay test 1380 with applied viscous damping coefficients from section 5.5. ....	IX
Figure 60: Test no 5120 FSU surge response 0 - 1000 sec. ....	XIV
Figure 61: Test no 5120 FSU heave response 0 - 1000 sec. ....	XIV
Figure 62: Test no 5120 FSU pitch response 0 - 1000 sec. ....	XIV
Figure 63: Test no 5130 FSU surge response 0 - 1000 sec. ....	XV
Figure 64: Test no 5130 FSU heave response 0 - 1000 sec. ....	XV
Figure 65: Test no 5130 FSU surge response 0 - 1000 sec. ....	XV
Figure 66: Wave excitation coefficients surge .....	XVI
Figure 67: Wave excitation coefficients heave .....	XVI
Figure 68: Wave excitation coefficients pitch .....	XVII
Figure 69: Added mass surge .....	XVIII
Figure 70: Added mass heave .....	XVIII
Figure 71: Added mass pitch .....	XIX
Figure 72: Potential damping surge .....	XX
Figure 73: Potential damping heave .....	XX
Figure 74: Potential damping pitch .....	XXI
Figure 75: Mean wave drift coefficients .....	XXII
Figure 76: Definition of smoothing convolution (Muthanna, 2011) .....	XXV



## List of tables

Table 1: FSU particulars (Muthanna, 2011) .....	- 6 -
Table 2: Chain-polyester-chain system: mooring line composition (Muthanna, 2011) .....	- 42 -
Table 3: Polyester-chain-polyester mooring system: Coordinates and pretension (Muthanna, 2011).....	- 43 -
Table 4: Chain system: mooring line composition (Muthanna, 2011).....	- 43 -
Table 5: Chain mooring system: coordinates and pretension (Muthanna, 2011).....	- 44 -
Table 6: Viscous damping coefficients obtained from model decay tests .....	- 52 -
Table 7: Numerically reconstructed decay tests .....	- 53 -
Table 8: Environmental conditions implemented in the numerical simulation (Kendon, 2011)-	56 -
Table 9: Current only test and corresponding coefficient .....	- 57 -
Table 10: Wind only test and corresponding coefficient .....	- 57 -
Table 11: Numerically reconstructed irregular waves tests .....	- 64 -
Table 12: Final viscous damping coefficients .....	- 64 -
Table 13: Stiffness matrix used in diffraction analysis .....	I





## Nomenclature

FSU	Floating Storage Unit
PDQ	Production Drilling Quarter
QTF	Quadratic Transfer Function
FFT	Fast Fourier Transformation
IRF	Impulse Response Function
DOF	Degree of Freedom
CPU	Central Processing Unit
FE	Finite Element
WF	Wave frequency
LF	Low frequency
KC	Keulegan-Carpenter number
$a$	Fluid particle acceleration
$A$	Added mass /Projected area
$A_{wp}$	Water plane area
$B$	Damping
$C$	Hydrostatic stiffness
$C_d$	Drag coefficient
$C_M$	Mass coefficient
$D$	Diameter
$E$	Modulus of elasticity
$f$	Frequency
$F$	Force
$\bar{F}$	Mean force
$F^{sv}$	Slowly varying force
$g$	Acceleration of gravity
$G$	Center of gravity/Greens function
$h$	Water depth/Time increment length



$H_s$	Significant wave height
$I$	Moment of inertia
$k$	Wave number
$K$	Mooring line stiffness
$m$	mass/meter
$M$	Metacenter/Generalized mass
$n$	Unit vector
$p$	Pressure
$R_n$	Reynolds number
$S$	Energy
$S_b$	Submerged surface
$t$	Time
$T_H$	Horizontal tension
$T_n$	Natural period of oscillation
$T_p$	Peak period
$u$	Fluid particle velocity/displacement
$U$	Velocity
$V$	Volume displacement
$w$	Submerged weight
$\Delta$	Mass displacement
$\eta$	Rigid body displacement
$\dot{\eta}$	Rigid body velocity
$\ddot{\eta}$	Rigid body acceleration
$\lambda$	Wave length
$\varphi$	Velocity potential
$\omega$	Circular frequency
$\nabla$	Differential operator
$\zeta$	Wave amplitude
$\rho$	Density



$\nu$	Kinematic viscosity coefficient
$\xi$	Amplitude of motion
$\varepsilon$	Phase angle/Strains
$\beta$	Wave angle
$\sigma$	Stress
$\xi$	$\xi, \eta, \zeta$ coordinates
$\mathbf{i}, \mathbf{j}, \mathbf{k}$	unit vectors
$\mathbf{x}$	$x, y$ and $z$
$\mathbf{N}$	Interpolation polynomial vector
$\mathbf{v}$	Nodal degree of freedom vector
$\mathbf{m}$	Element mass matrix
$\mathbf{M}$	System mass matrix
$\mathbf{A}$	Added mass matrix
$\mathbf{b}$	Element damping matrix
$\mathbf{B}$	System damping matrix
$\mathbf{k}$	Element stiffness matrix
$\mathbf{K}$	System stiffness matrix
$\mathbf{K}_I$	Incremental stiffness matrix
$\mathbf{R}$	External load vector
$\mathbf{R}_{INT}$	Internal load vector
$\mathbf{r}$	System degree of freedom matrix
$\mathbf{a}$	Connectivity matrix
$\mathbf{U}$	Velocity vector



## 1 Introduction

The oil and gas industry is increasing its search for hydrocarbons in deep waters. These water depths can range from 1000-3000 meters. In deeper water, the effects on the floater motion from the mooring and riser systems increase significantly. Viscous damping, inertial mass, current loading and restoring effects from riser and mooring systems need to be adequately modeled in order to predict the system motion of response. Accurate prediction of the system motion of response is vital in the context of design verification of the complete system. The recommended method of numerical analysis of the dynamics of a moored structure, especially in deep waters, is by a coupled analysis approach (VERITAS, 2010). This is recognized by the dynamics of the floater, mooring lines and risers being solved simultaneously.

A decoupled separated approach to the analysis of moored structures has previously been used. In deep water, especially for low frequency translatory modes, this procedure has been described as complex, and possibly an inaccurate method for design verification (O.C. Astrup). In addition, the existing laboratories available for model testing of moored structures are challenged by the depth increase. Small scales used in model tests can introduce uncertainties related to measurements, and an accurate prediction of viscous effects is challenging due to the nature of scaling laws.

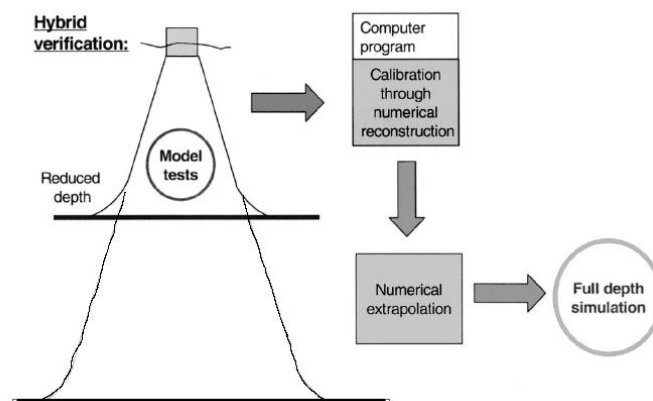


Figure 1: Hybrid verification procedure (Carl Trygve Stansberg, 2002)



In a hybrid verification procedure, both model tests and numerical simulations are utilized together in order to predict the system motion. This is done by running the model test with truncated mooring and riser systems in order to apply a reasonable model scale. The results obtained from the model tests are used to tune the numerical model. Once this is accomplished, i.e. there is compliance between the numerical model and the model test results, the mooring and riser systems are extrapolated. The possible inaccuracy of a decoupled numerical approach and the depth limitation of existing basin laboratories highlights the position of coupled analyses in design verification of moored offshore systems.

In this thesis, a coupled numerical simulation of a moored Sevan FSU (Floating Storage Unit) has been performed by the use of the software tool OrcaFlex. The results obtained from the OrcaFlex analyses are compared to results from a model test conducted on the moored FSU by Marintek.

In order to provide the reader of this paper an adequate understanding of the system which has been analyzed, chapter 2 contains a description of the FSU and mooring systems.

Loads on moored structures, and methods by which they can be determined, are examined in chapter three.

In chapter four, a few key subjects on global response analyses of moored structures are addressed and outlined.

The implementation and the assumptions made during the analyses performed in relation to this thesis are represented in chapter 5.

The FSU response obtained by the OrcaFlex analyses in irregular waves is presented in chapter 6 together with the corresponding model tests results, and results obtained from a coupled analyses performed by Marintek.

Comparison of power spectra obtained from a OrcaFlex time domain analysis and a corresponding model test is done in chapter 7. Uncertainties, conclusion and proposal for further work are outlined in chapter 8, 9 and 10.



## 2 System description of the moored FSU

The model tested in the Marintek basin was a Sevan hull with mooring lines. The test was conducted in 2011. The model scale applied during the test was 1:65, and the scaling was done according to Froude's scaling law (Muthanna, 2011).

The Sevan 1000 FSU (Floating Storage Unit) was intended to operate on the Mariner field in the UK sector of the North Sea. As the name implies it was planned to serve as a storage unit. The water depth at the Mariner field is approximately 108 meters. (Marine, 2011).



Figure 2: Model test of the FSU at the Marintek basin (Muthanna, 2011)

During the model test the moored FSU was subjected to four different environmental conditions, representing an operational condition and a 1, 100 and 1000 – year storm. Waves were generated according to Torsethaugen spectra (Muthanna, 2011). Wind was generated by fans, and the Marintek basin also holds a current generating system.



## 2.1 Coordinate system and rigid body modes

Throughout this thesis a global right-handed coordinate system  $(x,y,z)$  has been used.  $z$  is zero at the mean sea surface, and positive pointing upwards.

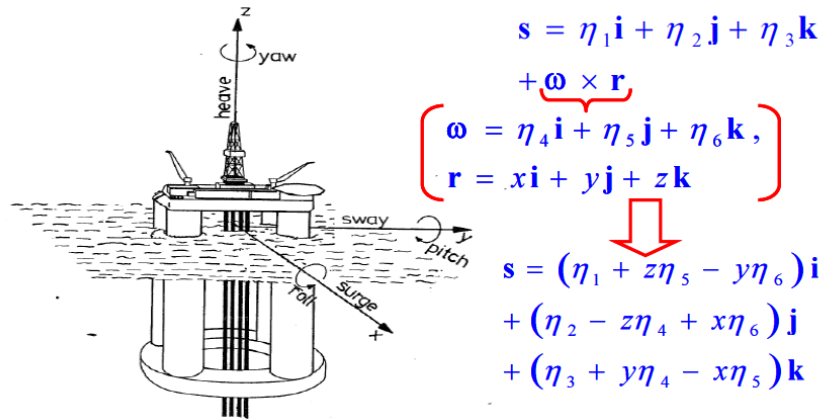


Figure 3: Coordinate system and rigid body modes of the FSU (Greco)

The direction of the waves, wind and current are given by degrees of their heading, i.e. waves propagating in the negative  $x$ -directions are heading 180 degrees.

## 2.2 The FSU

The Sevan FSU is a moncolumn structure with a main hull diameter of 85 meters. In the model tests the FSU was connected to a jacket PDQ (Production Drilling and Quarter) by a bridge with an approximate distance of 85 meters in calm conditions (Muthanna, 2011).

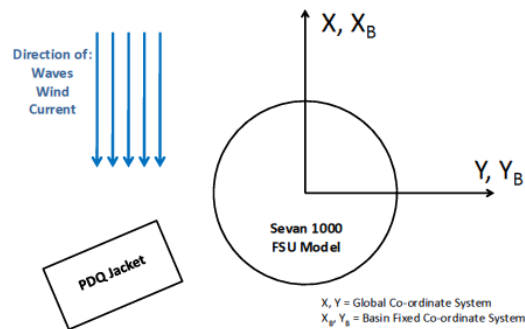


Figure 4: PDQ relative to the FSU during the model tests (Muthanna, 2011)

The PDQ was not included in the OrcaFlex analyses. As it was placed in the aft of the Sevan hull relative to the wave heading as shown in figure 2, it was assumed that the back-scattering of the waves from the legs of the PDQ was small, and would have little influence on the motion of the FSU. In addition, there was a riser connected between the PDQ and FSU during the model tests. This was also assumed not to influence the FSU motion in any significant way, and was not included in the OrcaFlex analyses.

The platform particulars in full scale are given in table 1:

Parameter	Unit	Dimensions
Diameter main hull cylinder	m	85.0
Diameter main deck	m	93.0
Diameter process deck	m	99
Area main deck	m <sup>2</sup>	6790
Diameter pontoon	m	105.0
Height pontoon	m	3.5
Elevation main deck	m	42.0
Elevation process deck	m	48.0
Elevation start flare	m	34.0
Radius of gyration in roll	m	28.2
Radius of gyration in pitch	m	28.2





Radius of gyration in yaw	m	41.5
Draught	m	30.0
Displacement	ton	184400
KG	m	22.5
GM	m	5.9
$I_{xx}$ excl. vertical comp.	$\text{ton}\times\text{m}^2$	145868012
$I_{yy}$ excl. vertical comp.	$\text{ton}\times\text{m}^2$	145868012
$I_{zz}$ excl. vertical comp.	$\text{ton}\times\text{m}^2$	315906120

Table 1: FSU particulars (Muthanna, 2011)

### 2.3 Mooring line systems

The FSU's response was tested to the series of sea states with two spread mooring setups:

- a 14 line chain-polyester-chain mooring system
- and an 18 line chain mooring system

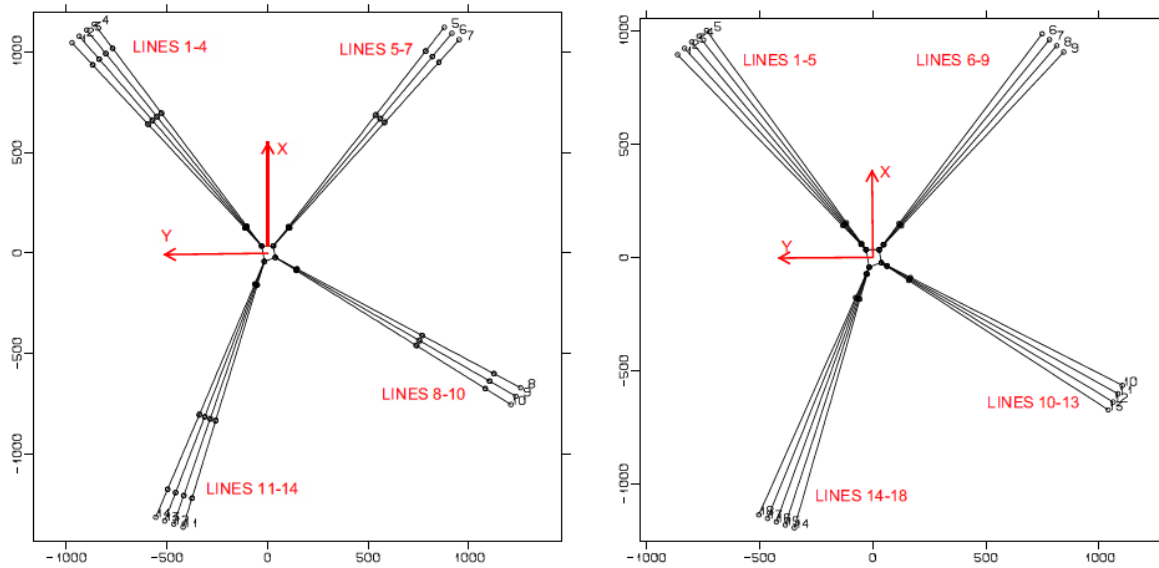


Figure 5: Mooring lines setup (Muthanna, 2011)



Left: 14 line chain-polyester-chain mooring system

Right: 18 line chain mooring system

Detailed information on the mooring lines is provided in chapter 5, Implementation of the OrcaFlex coupled analyses.



### 3 Loads on marine systems

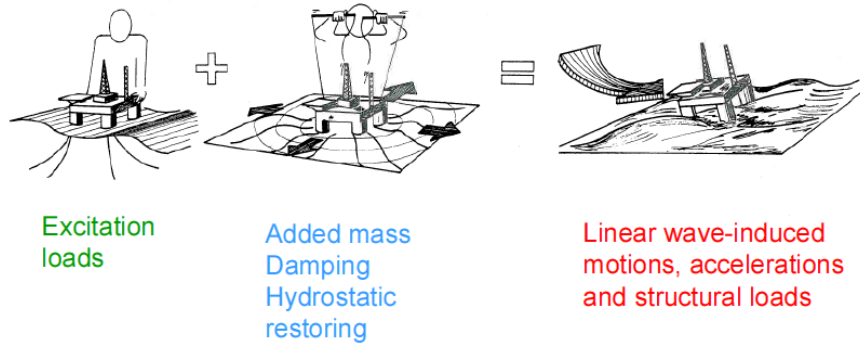


Figure 6: Wave excitation loads, added mass and damping (Greco)

Wave loads and wave induced motions on marine structures can to a large extent be expressed by linear wave theory, sometimes referred to as Airy theory. By linear superposition of the wave excitation, added mass, damping and restoring loads, the linear wave-induced motion can be described. Linear theory means that the velocity potential is proportional to the wave amplitude (Faltinsen, 1900).

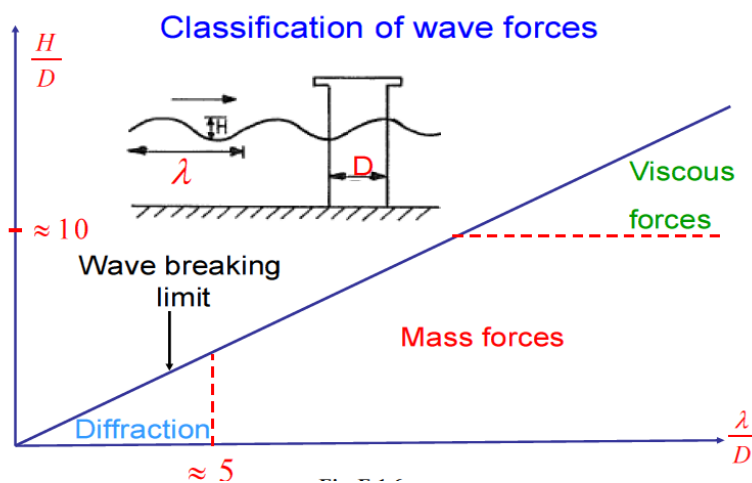


Figure 7: Relative importance of mass, viscous drag and diffraction forces on marine structures (Greco)

Second order motion of moored structures can be estimated by superimposing results from regular waves with different frequencies; hence the mean drift and difference frequency loads can be calculated by the linear (first order) velocity potential.



This chapter describes the assumptions of regular wave theory and how it can be used to calculate loads and motions on both large volume and slender marine structures. Figure 7 illustrates the importance of loads relative to the wave/ diameter ratio of a body subjected to waves. The water plane diameter of the FSU analyzed in this paper is 85 meters, while the diameters of the polyester rope or chain components are less than 0.5 meters.

### 3.1 Linear wave theory

Basic assumptions of linear wave theory are that fluid motion is irrotational, and sea water is incompressible and inviscid. The velocity potential  $\varphi$  is used to describe the fluid velocity vector  $\mathbf{U}(x, y, z, t) = (u, v, w)$  at time  $t$  at the point  $\mathbf{x} = (x, y, z)$  in a Cartesian coordinate system.

The velocity vector  $\mathbf{U}$  is expressed by

$$\mathbf{U} = \nabla\varphi \equiv \mathbf{i} \frac{\partial\varphi}{\partial x} + \mathbf{j} \frac{\partial\varphi}{\partial y} + \mathbf{k} \frac{\partial\varphi}{\partial z} \quad (0.1)$$

where  $\mathbf{i}, \mathbf{j}$  and  $\mathbf{k}$  are unit vectors along the  $x$ -,  $y$ - and  $z$ -axes. The assumptions of irrotational fluid is implemented when the vorticity vector

$$\boldsymbol{\omega} = \nabla \times \mathbf{U} = 0 \quad (0.2)$$

is zero everywhere in the fluid (no vorticities) (Newman, 1977). In order for the fluid to be incompressible the velocity potential must satisfy the Laplace equation

$$\nabla^2\varphi = \frac{\partial^2\varphi}{\partial x^2} + \frac{\partial^2\varphi}{\partial y^2} + \frac{\partial^2\varphi}{\partial z^2} = 0 \quad (0.3)$$

The linearized free-surface condition is given by

$$\frac{\partial^2\varphi}{\partial t^2} + g \frac{\partial\varphi}{\partial z} = 0 \text{ on } z = 0 \quad (0.4)$$



where  $\omega$  is the circular frequency of the velocity potential  $\varphi$ . The condition on the sea bottom must fulfill

$$\frac{\partial \varphi}{\partial z} = 0 \text{ on } z = -h \quad (0.5)$$

where  $h$  is the water depth. The latter equations ensure no flow through the sea bottom. The velocity potential for an irrotational, incompressible and inviscid fluid is found by solving the Laplace equation with boundary conditions. The linear velocity potential is expressed by

$$\varphi = \frac{g\zeta}{\omega} \frac{\cosh k(z+h)}{\cosh kh} \cos(\omega t - kx). \quad (0.6)$$

$z$  is zero at the mean water level and positive upwards.  $\zeta$  is the wave amplitude and  $\omega$  is the wave oscillation frequency.  $k$  is the wavenumber and the real root of the dispersion relationship.

$$k \tanh kh = \frac{\omega^2}{g} \quad (0.7)$$

The fluid pressure,  $p$ , is expressed by Bernoulli's equation. The  $z$ -axis is positive upwards.

$$p(x, t) = -\rho \left( \frac{\partial \varphi}{\partial t} + \frac{1}{2} \nabla \varphi \bullet \nabla \varphi + gz \right) \quad (0.8)$$

$\rho$  is the fluid density.

### 3.2 Wave excitation loads

The excitation loads are the forces and moments on the body when the structure is restrained from oscillating. The hydrodynamic loads are due to incident waves, and composed of Froude-Kriloff and diffraction forces and moments (Faltinsen, 1900). The Froud-Kriloff force is the result of the *undisturbed* wave pressure field. In order to gain an understanding of this component, one can imagine a body being replaced by an equivalent



volume of water. This water would have a mass  $\Delta$  and undergo an acceleration  $a$  like the particles in a propagating waves. The body is therefore exposed to a force equal to  $\Delta \cdot a$ .

The diffraction problem describes the wave scattering of the stationary body, and the forces and moments are results of the pressure being generated on the body surface by the scattering (Massie, 2001).

### **3.3 Added mass, damping and restoring loads**

The forces and moments on a body when it is forced to oscillate with the wave frequency are identified by added mass, damping and restoring terms (Faltinsen, 1900). There are no propagating waves. The forced motion of the structure generates a pressure field and resulting forces and moments.

The added mass term is an expression for the amount of water which oscillates when the structure is forced to oscillate. The surrounding fluid will oscillate with different fluid particle amplitudes throughout the fluid. The fluid particles will accelerate to varying degrees dependent on their position relative to the body, but the added mass is a weighted integration of this entire oscillating mass (Newman, 1977). The added mass term determines the inertial properties of a structure, but is a result of the generated pressure field.

There are different sources to damping of motion. In this thesis two sub-components will be discussed, namely potential and viscous damping. The potential damping is similar to the added mass resulting from the radiating waves emanating from the body when it is forced to oscillate. The potential damping is dependent on the body's ability to generate waves. The viscous damping is due to the separation of the flow as the fluid interacts with the body, and the resulting pressure this effects on a body. Although there is no precise limit on when the flow has separated, one can say that a flow has separated when vortices can be clearly observed in the fluid (Faltinsen, 1900). It is also clear that viscous effects are dependent on a number of parameters such as (Faltinsen, 1990):



- Reynolds number  $R_n = \frac{UD}{\nu}$  (U=characteristic free stream velocity, D = characteristic length of the body,  $\nu$  = kinematic viscosity coefficient)
- Roughness number  $= \frac{k}{D}$  (k =characteristic cross-sectional dimension of the roughness on the body surface)
- Keulegan-Carpenter number  $KC = \frac{UT}{D}$  (T=period of oscillation)
- Body form
- Free-surface effects
- Sea-floor effects

For the marine system described in chapter two, the restoring forces and moments can be obtained directly from the hull and mooring lines particulars. The hydrostatic stiffness of a monocolumn body like the FSU can be found accordingly (Faltinsen, 1990):

$$C_{33} = \rho g A_{wp} \quad (0.9)$$

$$C_{35} = C_{53} = -\rho g \iint_{A_{wp}} x ds \quad (0.10)$$

$$C_{55} = \rho g V (z_B - z_G) + \rho g \iint_{A_{wp}} x^2 ds = \rho g V \overline{GM} \quad (0.11)$$

where  $A_{wp}$  is the water plane area and  $\overline{GM}$  is the metacentric height relative to the center of gravity.  $V$  is the volume displacement.

The stiffness contribution from the mooring lines is dependent on the weight of the mooring lines, water depth, elasticity and pretension of the mooring system. If the catenary equation is valid, e.g. for a chain mooring system, then the horizontal stiffness of a moored structure can be expressed analytically by:



$$K_{11} = \frac{dT_H}{dx} = w \left[ \frac{-2}{\left(1 + 2\frac{a}{h}\right)^{\frac{1}{2}}} + \cosh^{-1}\left(1 + \frac{h}{a}\right) \right]^{-1} \quad (0.12)$$

where  $w$  is the submerged weight of the mooring.  $T_H$  is the horizontal mooring tension at the body and  $a = \frac{T_H}{w}$  (Faltinsen, 1900).

By determination of the added mass, damping and restoring loads, the equation of motion is expressed by

$$\sum_{k=1}^6 [(M_{jk} + A_{jk})\ddot{\eta}_k + B_{jk}\dot{\eta}_k + C_{jk}\eta_k] = F_j \quad (j=1, \dots, 6) \quad (0.13)$$

for a steady-state sinusoidal motion.  $M_{jk}$  and  $A_{jk}$  are the mass and added mass coefficients (moment of inertia and added moment of inertia for rotational degrees of freedom).  $B_{jk}$  are the damping coefficients and  $C_{jk}$  are the restoring coefficients.  $\ddot{\eta}$ ,  $\dot{\eta}$  and  $\eta$  are the body acceleration, velocity and displacement.  $F_j$  is the amplitude of the exciting forces and moments.  $F_1$ ,  $F_2$  and  $F_3$  are the force components in the  $x$ -,  $y$ - and  $z$ -directions known as surge, sway and heave.  $F_4$ ,  $F_5$  and  $F_6$  are the moments along the same axis and are named roll, pitch and yaw. The added mass and damping matrices in equation (0.13) will be of  $6 \times 6$  dimension and they are functions of body form, frequency of oscillation and forward speed. The sub index  $j$  and  $k$  expresses the force or moment in the  $j$ -direction due to rigid body motion in the  $k$ -direction. The coupling between surge and pitch, sway and roll and the coupled heave motion can be recognized from the vector multiplication in figure 3. Equation (0.13) can be solved by implicit time integration which will be further discussed in section 4.3.





### 3.4 Panel method for large volume structures

Panel methods are the most used techniques to calculate excitation loads and determine the added mass and potential damping of large volume structures like the FSU 1000. It is also known as the boundary integral equation method (IBEM) (Newman), and the method assumes:

- small fluid oscillation amplitudes of the fluid relative to the cross-sectional dimensions of the structure
- potential flow theory.
- a steady state response of the structure to the incoming waves

The linear first order problem can be decomposed into two sub problems:

- a diffraction problem
- a radiation problem.

The wave forces from the diffraction problem are termed wave excitation coefficients. The radiation problem expresses the body responding to wave frequencies in calm water. The wave forces from the radiation problem are presented in terms of added mass and potential damping according to section 3.3. The decomposition is expressed in the following way:

$$\varphi = \varphi_D + \varphi_R \quad (0.14)$$

where

$$\varphi_R = i\omega \sum_{k=1}^6 \xi_k \varphi_k \quad (0.15)$$

$$\varphi_D = \varphi_S + \varphi_I \quad (0.16)$$



$\varphi$  is the total potential.  $\varphi_k$  is the contribution to the potential from the  $k^{\text{th}}$  mode of motion (radiation).  $\xi_k$  is the amplitude of motion in each degree of freedom and  $\omega$  is the oscillatory frequency.  $\varphi_s$  and  $\varphi_t$  are the velocity potentials corresponding to the scattering of the wave and due to the incident undisturbed wave (Lee, 1995). Based on this superposition of potentials, functions that individually satisfy the Laplace equation may be added together to describe the flow field (Tuncer Cebeci, 2005).

The basis for the panel method is a form of Green's theorem where the velocity potential at any point in the fluid is represented by a distribution of singularities over the body surface. The singularities can be represented as sources with corresponding sinks.

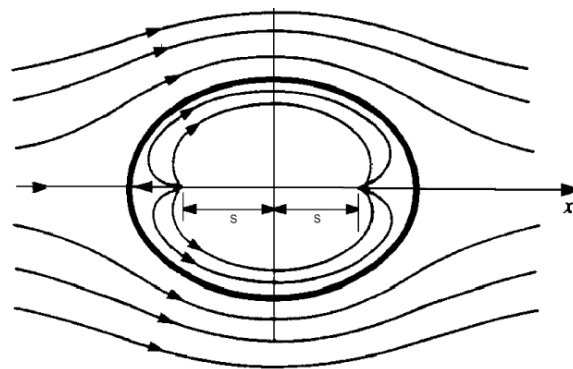


Figure 8: Source and sink illustration (Massie, 2001)

They are both usually referred to as sources independent of the direction of the flow. A positive source is a point from which flow radiates outward in all directions. Another way of representing the potential is by the potential formulation, where the source strength is known, and the dipole moment is set equal to the unknown potential (Newman). The unknown source strength or dipole moment leads to integral equations which are solved with corresponding boundary conditions. For the potential formulation the Green's theorem is used to represent the velocity potential  $\varphi$  (Newman):



$$\begin{pmatrix} 2\pi \\ 4\pi \end{pmatrix} \varphi(x) + \iint_{S_b} \varphi G_{n\xi} dS_\xi = \iint_{S_b} \varphi_n G dS_\xi \quad (0.17)$$

where the Green function  $G(x, \xi)$  represents the potential of an oscillatory source located at the point  $\mathbf{x} = \xi$  in the fluid domain. The coordinate system of the source point is defined by  $\xi = (\xi, \eta, \zeta)$ . The factors  $2\pi$  and  $4\pi$  are applied based on the location of the source relative to the submerged surface,  $S_b$ . Sub index  $n$  relates to the unit vector normal to the points on the body surface.

Equation (0.17) can be used to determine the radiation potential  $\varphi_R$  and the scattering potential  $\varphi_S$  (Newman). For the diffraction potential another integral equation is needed. The source formulation leads to other integral equations and utilizes the Green theorem in other forms than the potential formulation. The theory and the mathematics of the panel method rapidly become complicated and extensive. Further elaboration on the singularity formulation and linear and nonlinear solution procedure can be found in the literature, e.g. in the Wamit Theory Manual by C.-H. Lee. This section is on the other hand completed by a short summary of the low order panel method. The low order method is characterized by the assumption that the source strength and dipole moment are constant on each panel and that the panels used for the discretization are flat (Newman):

1. The velocity potential is represented by singularities on the body surface.
2. The body surface is approximated by a large number  $N$  of small quadrilateral panels
3. The source strength and dipole moment are assumed constant on each panel, giving a total of  $N$  unknowns.
4. In the source formulation the normal derivative of the potential is evaluated at the centroid of each panel, and set equal to the velocity at that point. In the potential formulation the potential itself is evaluated directly at the same points. This gives a total of  $N$  linear equations for the unknown source strengths.
5. The system of equations are solved by methods of linear algebra to determine the potential



6. The potential is used to calculate the pressure on each panel. The pressure is then integrated to compute the forces and moments on the body.

### 3.5 Morison's equation for estimating loads on slender structures

For objects with cross-sections which are small relative to the wave trajectory, free surface effects are not as significant as the oscillatory drag due to separation. Wave loads on relative small cross-sections like risers and mooring lines are calculated by the use of Morison's formula. Morrison's equation is based on potential flow theory and is the most frequently used method to calculate wave loads on circular cylindrical structures. The formula combines a viscous drag force with an inertial force proportional to acceleration. Morrison's equation represents an inertia force  $dF$  on a strip of length  $dz$  of a vertical rigid circular cylinder as

$$dF = \rho \frac{\pi D^2}{4} dz C_M a \quad (0.18)$$

Where  $\rho$  is the seawater density,  $D$  is the cross-section diameter,  $C_M$  is the mass coefficient and  $a$  is the undisturbed fluid acceleration at the midpoint of the strip. The mass coefficient,  $C_M$ , has to be empirically determined. If viscous effects are negligible, it is possible to show analytically that Morison's equation is the correct asymptotic solution for large  $\lambda/D$  – values (wavelength/diameter). The  $C_M$ -value should then be two for a circular cross-section (Faltinsen, 1900).

When viscous effects matter for offshore structures, the fluid flow will generally separate and generate a pressure difference that acts on the cylinder. In the Morison's equation, the viscous force  $dF$  on a strip  $dz$  is given by

$$dF = \rho \frac{\pi D}{2} dz C_D |u|u \quad (0.19)$$



Where  $u$  is the undisturbed fluid velocity normal to the cross-section. The drag coefficient, together with the mass coefficient, is dependent on parameters like Reynolds number, Keulegan-Carpenter number and surface roughness ratio, which also were described also in section 3.3.  $C_D$  is also determined empirically. When waves and current are acting simultaneously, the combined effect should be considered. The normal approach is to add vectorially the wave-induced velocity and the current velocity in the velocity term of Morison's equation.

Morison's equation can be modified in the case of a moving circular cylinder. By considering a vertical cylinder and denote the horizontal rigid body motion of a strip of length  $dz$  by  $\eta_1$ , one can write the horizontal hydrodynamic force on the cylinder as:

$$dF = \frac{1}{2} \rho C_D D dz (u - \dot{\eta}_1) |u - \dot{\eta}_1| + \rho C_M \frac{\pi D^2}{4} dz a - \rho (C_M - 1) \frac{\pi D^2}{4} dz \ddot{\eta}_1 \quad (0.20)$$

Dot stands for time derivative. The inertia term does not depend on the relative acceleration (Faltinsen, 1900). It should be noted that Morison's equation cannot predict the oscillatory forces due to vortex shedding in the lift direction, i.e. forces orthogonal to the wave propagation direction and in the cross-section plane.

### 3.6 Second order excitation and damping of floaters

Moored vessels in irregular waves are subjected to large first order wave forces and moments which are proportional to the wave height and contain the same frequencies as the waves. They are also exposed to smaller, second order mean and low frequency wave forces and moments proportional to the square of the wave height. There are also second-order sum frequency loads that are important for marine structures like TLP's (Tension Leg Platform) as it can excite high frequency natural modes of the system. In this thesis the

mean and low frequency effects will be most emphasized due to the model description in chapter 2.

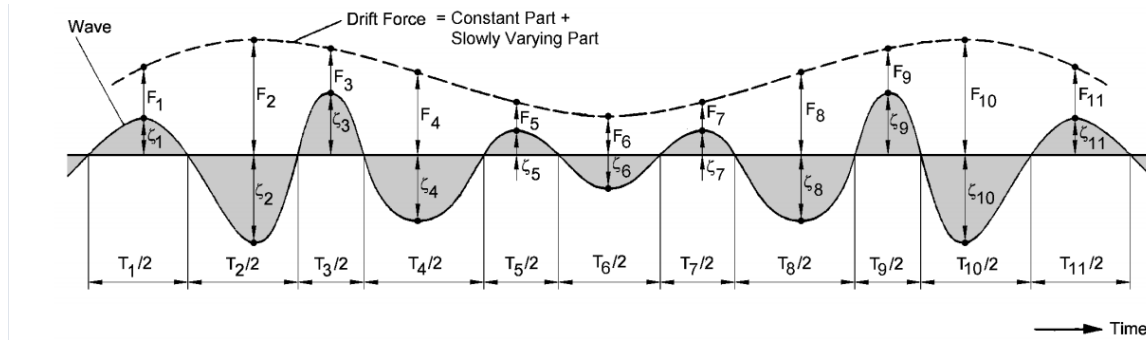


Figure 9: Wave drift forces (Massie, 2001)

An algebraic expression for mean, sum – and difference frequency effects can be illustrated by considering the quadratic velocity term in Bernoulli's equation(0.8):

$$-\frac{\rho}{2}[U_x^2 + U_y^2 + U_z^2] = -\frac{\rho}{2}|\nabla\phi|^2 \quad (0.21)$$

where the x-component of the velocity of two regular wave components can be written as

$$U_x = \zeta_1 \cos(\omega_1 t + \varepsilon_1) + \zeta_2 \cos(\omega_2 t + \varepsilon_2) \quad (0.22)$$

where  $\zeta$  is the wave amplitude,  $\omega$  the oscillating frequency and  $\varepsilon$  being the random phase angle. Equation (0.22) and (0.21) lead to the expression

$$-\frac{\rho}{2}U_x^2 = -\frac{\rho}{2} \left[ \frac{\zeta_1^2}{2} + \frac{\zeta_2^2}{2} + \frac{\zeta_1^2}{2} \cos(2\omega_1 t + 2\varepsilon_1) + \frac{\zeta_2^2}{2} \cos(2\omega_2 t + 2\varepsilon_2) + \zeta_1 \zeta_2 \cos[(\omega_1 - \omega_2)t + \varepsilon_1 - \varepsilon_2] + \zeta_1 \zeta_2 \cos[(\omega_1 + \omega_2)t + \varepsilon_1 + \varepsilon_2] \right] \quad (0.23)$$

which contains to a constant term  $-\frac{1}{2}\rho \left( \frac{\zeta_1^2}{2} + \frac{\zeta_2^2}{2} \right)$ , and a term oscillating with the

difference frequency  $(\omega_1 - \omega_2)$  and a sum frequency term  $(\omega_1 + \omega_2)$  (Faltinsen, 1990).



The horizontal mean and low frequency second order wave forces are also referred to as wave drift forces as they lead to a steady slow drift of a body in the direction of the propagating waves if the body is not restrained (Pinkster). Due to their nature the loads are most commonly represented by quadratic transfer functions (second order transfer functions). Although the drift forces can be relatively small in amplitude, they can excite large motions because the low frequency loads easily can coincide with the natural period of a moored structure 0(1-2 minutes), and the slow-drift damping is generally low (Pinkster). In the coming two sections a brief basis of the mean and slow-varying drift forces will be discussed.

The most important contribution to the mean wave drift for a surface piercing body in regular incident waves is the relative vertical motion between the waves and the body (Faltinsen, 1990). As the body is exposed to incident oscillating waves some of the body surface will be part of the time submerged in water and part of the time out of the water as the body oscillates in heave (Faltinsen, 1900). This motion leads to a non-zero mean pressure on the body, also in regular waves. Large volume structures can also disturb the propagating wave so the relative vertical motion differs along the waterline giving another contribution to the mean drift force. In order to calculate the mean wave load on a body it is not necessary to solve the second-order velocity problem. Although the loads are of second order, they are independent of the second order velocity potential (Faltinsen, 1900).

Irregular waves are the source of the slow-varying drift force which describes the wave loads occurring at the frequency  $\Delta\omega$  equal to the difference  $(\omega_j - \omega_k)$  of two wave frequencies  $(\omega_j, \omega_k)$ . This low frequency motion of the body is driven by difference frequencies in the sea state. The difference frequency term in equation (0.23) is from a given pair of wave components. In a defined sea state there will be  $N$  number of wave components, and each pair of wave components will contribute to low frequency wave load. The contribution from a given pair of wave components has a frequency equal to the difference in frequency between the frequencies of the wave components in the pair. Wave component pairs with equal frequencies, such as waves with self-paired wave components, give a constant (zero



frequency) contribution. The sum of all these contributions gives the mean wave drift load which was described in the latter section. In order to calculate the difference frequency loads ( $\omega_j - \omega_k$ ) the second-order velocity potential is generally needed (Pinkster), but simplifications can be introduced to reduce the extent of the calculations.

There are two different methods of calculating the mean drift forces and moments described in the literature and available in software tools. The methods are named direct pressure integration and conservation of momentum. The direct pressure integration takes hold in the quadratic term of Bernoulli's equation(0.8). The pressure is then integrated over the exact wetted surface. The other option, conservation of momentum is based on the conservation of momentum in the fluid over a surface (Faltinsen, 1900).

The conservation of momentum method can only be used to find translational mean drift forces, while the direct pressure integration can estimate the mean drift forces and moments for all six rigid body modes. The direct pressure integration is on the other hand dependent on finding the velocities obtained by differentiation of the potential on the body surface, and has been described as a possible source of inaccuracy by e.g. (Hermans, 1997).

### **3.6.1 Newman's approximation for difference frequencies loads**

The quadratic transfer function (QTF) of mean and low frequency wave loads  $F(\omega_1, \omega_2)$  is composed of two distinct parts. One dependent only on the quadratic products of the first-order wave fields, while the other term is analytically expressed by the second order incoming and diffraction potentials (Duan, 2007). In a full QTF matrix these terms are calculated and for the latter this implies solving the second-order velocity potential and implementation of a double summation over all wave components in the sea state  $(\omega_j, \omega_k)$ .

The calculations are computationally intensive.





By the use of Newman's approximation only the mean wave drift QTFs are used. The mean drift QTFs are the diagonal entries of a full QTF matrix, and are the product of  $(\omega_j - \omega_k = \Delta\omega = 0)$ . The off-diagonal wave drift QTFs where  $(\omega_j \neq \omega_k)$  are then approximated using mean values. This means that the low frequency excitation coefficients are approximated using the second order mean wave drift coefficients. As previously described the mean wave drift coefficients are independent of the second order potential, and in this way Newman's approximation circumvents the need for a full second order diffraction analysis. In (Faltinsen, 1990) the low frequency drift load is written

$$F_i^{SV} = \sum_{j=1}^N \sum_{k=1}^N \zeta_j \zeta_k \left[ QTF_{jk}^{ic} \cos \left\{ (\omega_k - \omega_j) t + (\varepsilon_k - \varepsilon_j) \right\} + QTF_{jk}^{is} \sin \left\{ (\omega_k - \omega_j) t + (\varepsilon_k - \varepsilon_j) \right\} \right] \quad (0.24)$$

where  $N$  is the number of wave components in the sea state,  $\zeta_i$  is the wave amplitude,  $\omega_i$  is the wave frequency and  $\varepsilon_i$  is the random phase angle.  $QTF_{jk}^{ic}$  and  $QTF_{jk}^{is}$  are real and imaginary quadratic transfer functions from the wave component pair of  $\omega_j$  and  $\omega_k$  for the difference frequency load (Faltinsen, 1990). The mean value of equation (0.24) occurs when  $k=j$  and there is no time dependence.

$$\bar{F}_i = \sum_{j=1}^N \zeta_j^2 QTF_{jj}^{ic} \quad (0.25)$$

Newman proposed that  $QTF_{jk}^{ic}$  and  $QTF_{jk}^{is}$  in equation (0.24) can be estimated by  $QTF_{jj}^{ic}$ ,  $QTF_{kk}^{ic}$ ,  $QTF_{jj}^{is}$  and  $QTF_{kk}^{is}$  so that the second-order velocity potential does not need to be calculated. Further the off-diagonal terms in the QTF matrix are given values accordingly;

$$QTF_{jk}^{ic} = QTF_{kj}^{ic} = \frac{1}{2} (QTF_{jj}^{ic} + QTF_{kk}^{ic}) \quad (0.26)$$

$$QTF_{jk}^{is} = QTF_{kj}^{is} = 0 \quad (0.27)$$

Although this implies that the second-order velocity potential does not need to be calculated, equation (0.24) is still time consuming. Newman also proposed to approximate



the double summation by the square of a single series, leading to  $N$  wave components being added instead of  $N^2$  at each time step. The formula is written in (Faltinsen, 1900) as

$$F_i^{SV} = 2 \left( \sum_{j=1}^N \zeta_j (QTF_{jj}^{ic})^2 \cos(\omega_j t + \varepsilon_j) \right)^2 \quad (0.28)$$

Newman's approximation can be poor in shallow water (Orcina). It is applicable for modes with sufficiently long natural periods, but questionable for other modes (Kendon, 2011).

Newman's approximation is the basis for the second order motion calculation in this thesis. The second order mean drift coefficients used for the analyses in this thesis can be found in Appendix J.

### 3.6.2 Damping of low frequency moored vessel motion

Damping of the slow-drift motion comprises (VERITAS, 2010):

- Wave drift damping
- Damping due to viscous loads on the body
- Damping due to drag forces on mooring lines and risers
- Damping due to variation of the wind velocity relative to the velocity of the structure

The wave drift damping force is defined as the increase in the second-order difference frequency force experienced by a body moving with a small forward velocity in waves (VERITAS, 2010). In a coupled analysis the damping contribution from the mooring lines and risers is included as the system equation of motion is solved simultaneously. If wind is present, its relative velocity to the slow drift velocity should be included in the simulation. There are both theoretically and empirically methods of estimating the slow-drift damping of a body. For column based structures in deep water a simplified method called Aranha's method is widely used.



$$B_i^{wave-drift} \approx k_0 \frac{\partial \bar{F}_i(\omega_0)}{\partial \omega_0} + \frac{4\omega_0}{g} \bar{F}_i(\omega_0) \quad (0.29)$$

(Hermans, 1997) where  $B_i$  is the wave drift damping coefficient,  $\bar{F}_i$  is the mean wave drift excitation, and  $k_0$  and  $\omega_0$  refers to the wave number and wave frequency. The damping terms are in other words calculated by means of differentiation of the QTF data. Aranha's method can also be generalized to cases of arbitrary wave direction and is also utilized to describe the effect of current on the wave drift damping. By the definition of encountering frequency,  $\omega_e$ , the effect of current on the vessels slow drift velocity can be accounted for by the following expression:

$$\omega_e = \omega_0 - \frac{\omega_0^2}{g} U \cos \beta \quad (0.30)$$

Where  $\beta$  is the incident wave angle referring to the x-axis and  $U$  is the current velocity relative to the vessels slow drift velocity (Sierevogel, 1997). Other methods for obtaining the wave drift damping coefficients and discussion of their accuracy can be found in articles listed in the bibliography.

### 3.7 Wind and current loads

There are several sources of the occurrence of current in the sea. The ocean circulation systems result in steady currents. The cyclic change in lunar and solar gravity causes tidal currents, and wind and fluid density differences are also sources of current. The tidal current can, in areas of restricted water depth, reach velocities of 5 m/s (Massie, 2001). More common tidal current velocities are in the order of 0-1 m/s.

The current velocity close to the surface is of course the area of most interest for floating structures. The current speed will in general decrease as  $z \rightarrow -h$ , but is also an important



parameter for the design of mooring and riser systems as it will affect certain variables e.g. stiffness properties and the static offset.

The forces and moments exerted by the current can be divided into the following parts (Massie, 2001):

- A viscous part due to friction between the structure and the fluid
- A potential part due to circulation around an object.

When Morrison's formula is applied on marine structures, the current velocity is added to the wave velocity as described in section 3.5. For other structures the loads due to current are still calculated as a drag force by the following formula

$$F = \frac{1}{2} \rho_{sea-water} C_d A U_c^2 \quad (0.31)$$

where  $A$  is the projected area normal to the current velocity  $U_c$ .  $C_d$  is the drag coefficient.

The change in velocity and direction of current is in general very slow, and current loads are in that way considered to be static. Wind loads on the other hand, have a stochastic nature. Wind can be characterized by large fluctuations in velocity and direction, and it affects the behavior of moored floating structures in two ways:

- The wind exerts a force on the part of the structure which is exposed to air. The forces are a result of the flow of air around the various parts of the air exposed structure.
- A second role of the wind gusts is that it generates waves and current.

The wind forces described in the first point above can be recognized as the direct part, and the force can be quantified by the use of the same formula as for the current. The wind speed should be modelled as a stochastic process according to its nature.

$$F = \frac{1}{2} \rho_{air} C_d A U_w^2 \quad (0.32)$$



## 4 Global analysis of moored floater motion

In this chapter a number of key subjects related to dynamic analyses of marine structures will be addressed.

### 4.1 Coupled analysis of marine systems

In this section two different approaches to describe the dynamics of moored structures will be described and discussed, namely the separated and coupled approach.

Traditionally the analysis has been carried out in two separate steps (Vugts, 1997):

1. Calculations of floater motions.
2. Dynamic response analysis of moorings and risers using the top end motions estimated in step 1. as excitation.

Coupled analysis on the other hand, is characterized by the floater motions, mooring and riser dynamics being calculated simultaneously. The two methods are illustrated in the figure:

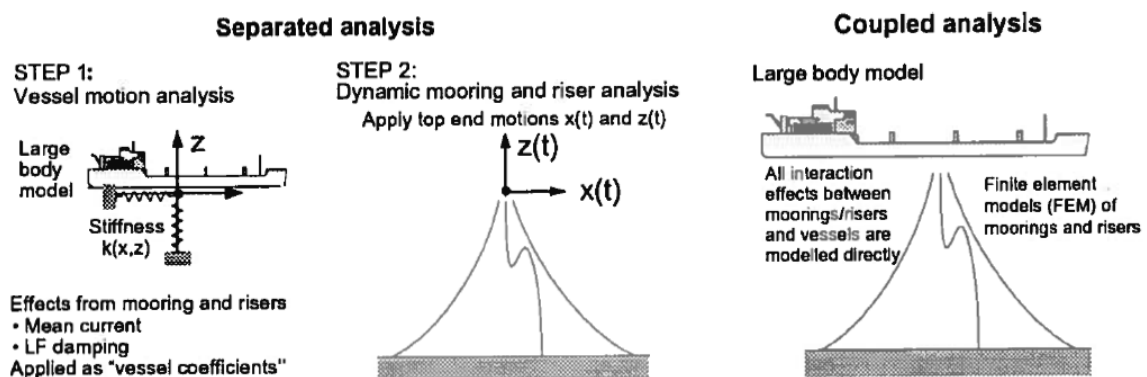


Figure 10: Separated and coupled analysis (Vugts, 1997)

In the separated two-step analysis the load effects from the mooring and risers are usually

modeled as nonlinear position dependent forces (stiffness). This leads to two main simplifications when the wave frequency and low frequency motion of the floating structure is analyzed:

1. The velocity dependent damping forces from the mooring lines and risers, which are important for accurate representation of the low frequency motion, are neglected or implemented in a coarse way by introducing a damping force that acts on the floater itself.
2. Current forces on the riser and mooring system are either neglected or implemented as a current force on the floater itself as in the latter simplification. The line tensions in the mooring system depend on an accurate representation of the static offset of the vessel, which is a result of the current forces exerted on the riser and mooring systems.

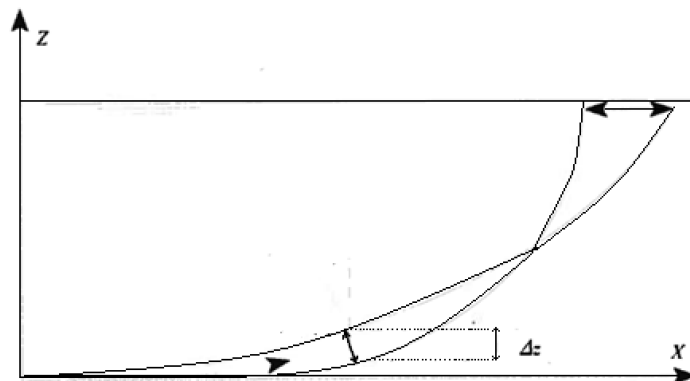


Figure 11: Damping normal to the mooring line due to vessel surge

The floater motion is calculated with the simplifications listed above. Once it has been conducted, the motion response is used as the top end excitation for the calculation of the riser and mooring system dynamics. The shortcomings of the procedure are especially apparent in deep water with strong current and many risers attached to the floater. The interaction between the underwater elements and the current forces is then pronounced, and the inertia related to the mooring and riser system is increased. The simplified mean and low frequency modeling in a separated method may be too inaccurate (Vugts, 1997).



The main objective of a coupled analysis is to determine the floater's mean position and dynamic response due to mooring lines and risers restoring, damping and inertia forces. This comprises current effects, mooring and riser stiffness, seafloor friction, damping forces (wave and low frequency) and inertia. In a coupled analysis, where the system equation of motion is solved simultaneously, the full interaction between mooring lines, risers and floater is taken into account, and accurate floater motion and dynamic loads in mooring lines and risers should be obtained. In addition to the improved accuracy of the coupled analysis compared to the separated approach, the importance of coupled analysis has also increased due to the increased offshore activity on deep waters. There is an increase of deep and ultra-deep offshore exploration, production and drilling activity, and existing laboratories have depth limitations which make it difficult to carry out model tests with complete systems for design verification of installations. Of course, this is also a matter of scaling, but small scales introduce uncertainties related to viscous effects (Astrup, 2004). It is well known that a correct scaling of viscous effects is dependent on Reynolds number, while correct scaling of gravitational forces is obtained with Froude's scaling.

This laboratory limitation emphasizes the importance of coupled analyses for design verification of deep water installations. A coupled numerical simulation can also be utilized together with a model test to encounter the depth limitation problem of laboratories. One option is to run a model test with a truncated mooring and riser systems. Once a model test has been conducted it can be numerically reconstructed and the mooring and riser systems can be extrapolated to full depth, enabling the complete system to be numerically simulated to express the system dynamics.

## **4.2 Time - and frequency domain representation of response**

For different applications of dynamic analyses, processes are represented in the time domain or the frequency domain. A spectrum is a way of expressing a Gaussian process and gives the intensity (energy) of a process as a function of frequency. From a spectrum it is possible to obtain the statistical properties of a Gaussian process such as extreme values,



standard deviation and zero crossing frequency. A spectrum describes the process in the frequency domain, and gives a complete statistical description. The frequency domain representation of a process assumes that the principle of linear superposition is valid, i.e. nonlinear processes cannot be analyzed in the frequency domain (Larsen, 2012). This will in general require a higher order dynamic analysis in the time domain. An article which describes a fully coupled analysis conducted in the frequency domain with linearized drag and statistical linearization of low frequency effects can be found in (Garrett, 2005).

In a time domain the realizations, e.g. response or wave elevation, are measured or represented in a given period of time. The realizations are a result of the underlying stochastic process. The same process can, during another given period of time, give other realizations and have other statistical properties. This implies that if one wish to determine the statistical properties of a process from time series, the duration of the time series need a sufficient length.

If the spectrum of a process is known, realizations in the time domain can be generated by the use of invers Fourier transformation. Conversely, if a time series of a process is available, the spectrum can be calculated by the use of Fourier transformations. Fast Fourier Transformation (FFT) is the most used algorithm to generate spectra from time series and vice versa (Larsen, 2012).



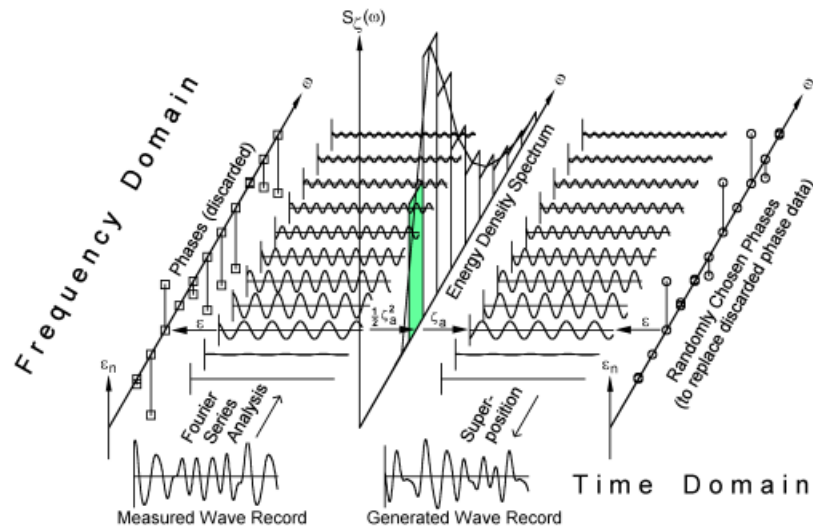


Figure 12: Frequency and time domain illustration (Massie, 2001)

One example of generating realizations from a spectrum can be studied through the simulation of irregular waves. In practice, linear wave theory is used to simulate irregular sea and to obtain statistical estimates of a sea state. By assessing the energy in a wave condition, the wave elevation of a long-crested irregular sea propagating along the positive x-axis can be written as the sum of a large number of wave components. Linear superposition yields:

$$\zeta = \sum_{j=1}^N \zeta_j \sin(\omega_j t - k_j x + \varepsilon_j) \quad (0.33)$$

where  $\zeta_j$  is the wave amplitude,  $\omega_j$  the circular frequency,  $k_j$  the wave number and  $\varepsilon_j$  is a random phase angle of wave component number  $j$ .

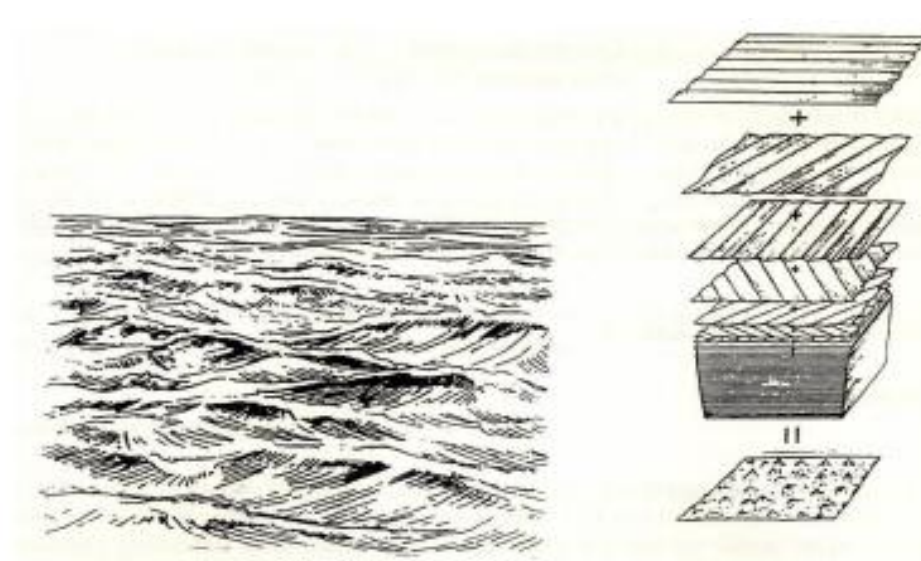


Figure 13: Simulation of irregular sea (Myrhaug)

The random phase angles  $\varepsilon_j$  are uniformly distributed between 0 and  $2\pi$  and constant with time. In software tools the  $\varepsilon_j$  are generated as pseudo random numbers and its start value is chosen by defining a seed number. The wave amplitude  $\zeta_j$  is expressed by the wave spectrum  $S(\omega)$ .

$$\frac{1}{2}\zeta_j^2 = S(\omega_j)\Delta\omega \quad (0.34)$$

$\Delta\omega$  is a constant difference between successive frequencies in the spectrum.

During the FSU model test at the Marintek basin, the wave maker generated irregular waves according to a Torsethaugen double peaked spectrum (Muthanna, 2011). The Torsethaugen spectrum has been developed based on measured spectra for Norwegian waters (Haltenbanken and Statfjord), and it allows for sea states where both wind generated waves and swells are present (VERITAS, 2010).



### 4.3 Implicit time integration: the generalized $\alpha$ -method

As described in section 3.3 the dynamic equation of motion is expressed by

$$(M + A)\ddot{\eta}_k + B\dot{\eta}_k + C\eta_k = F \quad (0.35)$$

for an uncoupled one degree of freedom. Equation (0.35) is an initial value problem and the solution is determined by the initial values. A time integration method for solving the dynamic equation of motion is a stepwise process where the simulation time is split into a number of time steps of equal length. Once the start values in the beginning of an interval are known, i.e. the displacement, velocity and acceleration, the solution at the end of the interval is found by assuming the motion of the system, i.e. by an iterative method. The result which is then obtained is applied as the initial value for the subsequent time step. In this way the motion of the total simulation time can be found. The accuracy of the obtained results is dependent on the size of the time increment (Sigbjörnsson). Short time steps will lead to more accurate results but implies longer simulation duration.

There are different algorithms describing how the acceleration  $\ddot{\eta}(t)$  varies over an interval, (Sigbjörnsson). What they have in common is that the displacement and velocity is found by integrating the acceleration twice:

$$\dot{\eta}_{k+1} = \dot{\eta}_k + \int_0^h \ddot{\eta}(t) dt \quad (0.36)$$

$$\eta_{k+1} = \eta_k + \int_0^h \dot{\eta}(t) dt \quad (0.37)$$

where the sub index  $k$  indicates the discrete time step, and  $h = \Delta t = t_{k+1} - t_k$  being the time increment. One algorithm, also used by OrcaFlex, is named the Generalized  $\alpha$ -Method. The solution for a discrete time step is found using:

$$\dot{\eta}_{k+1} = \dot{\eta}_k + h \left( (1 - \gamma_2) \ddot{\eta}_k + \gamma_2 \ddot{\eta}_{k+1} \right) \quad (0.38)$$



$$\eta_{k+1} = \eta_k + h^2 \left( \left( \frac{1}{2} - \beta_2 \right) \ddot{\eta}_k + \beta_2 \ddot{\eta}_{k+1} \right) \quad (0.39)$$

where  $\gamma_2$  and  $\beta_2$  are parameters used to control amplifications of high frequency numerical modes which are not of interest (Hulbert). Aside from these parameters one can identify (0.38) and (0.39) being (0.36) and (0.37) integrated over  $h$ . If  $\gamma_2$  and  $\beta_2$  are chosen correctly, Newmark methods can be discovered (Cesnik, 2006).

When the velocity and displacement are found, they are together with the assumed acceleration inserted in the dynamic equation of motion. If a preset tolerance level is exceeded in equation (0.35), a new acceleration is estimated together with corresponding velocity and displacement. If equation 4.3 is found in equilibrium, the process continues on to the next time step  $k$  with the obtained acceleration, velocity and displacement as the initial values.

The implicit integration scheme solves the equation of motion being solved at the end of each time step. Another option of integration method applied for dynamic analyses is the explicit integration method. This method solves for the acceleration vector in the beginning of each time step using forward Euler integration. In general this requires a much shorter time increment in order to be stable and accurate compared to the implicit method, and is generally not used for dynamic analyses of marine systems.

#### 4.4 Finite element formulation of marine systems

In dynamic analyses of offshore structures the finite element method can be utilized to model slender structures like risers and mooring lines, whilst the floater properties are commonly represented by a node. In a dynamic analysis the method generally includes the following steps (Sigbjörnsson):

1. Discretization. The system is divided into  $N$  number of elements.



2. Element analysis. Mass, damping and stiffness matrices and load vectors for each element is established.
3. System analysis. The mass, damping and stiffness matrices and load vector for the system is established based on the element matrices.
4. Solving the dynamic equation of motion.

Discretization involves the division of the system into  $N$  number of elements. The elements are connected through nodes which are placed at the element ends. The displacement, velocity and acceleration of the nodes are the unknowns and referred to as degrees of freedom (DOFs). The number of elements chosen to be included will affect both the accuracy of the results, and the CPU cost.

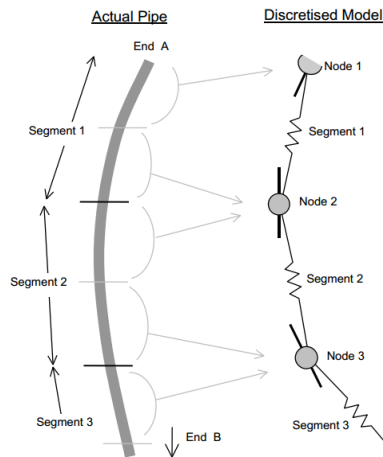


Figure 14: OrcaFlex discretization of pipe (Orcina)

When establishing the element analysis the displacement  $u(x, y, z)$  within an element is assumed to be represented by the nodal degrees of freedom  $\mathbf{v}$  and interpolation polynomial  $N_i$ .

$$u(x, y, z) = \mathbf{N}\mathbf{v} \quad (0.40)$$

where

$$\mathbf{N} = [N_1(x, y, z), N_2(x, y, z), \dots, N_n(x, y, z)] \quad (0.41)$$

and



$$\mathbf{v} = [v_1, v_2, \dots, v_n]^T \quad (0.42)$$

Bold letters indicates matrix formulation. The interpolation polynomials are determined such that  $N_i(x, y, z) = 1$  in the node that corresponds to  $v_i$ , but zero in all other nodes.

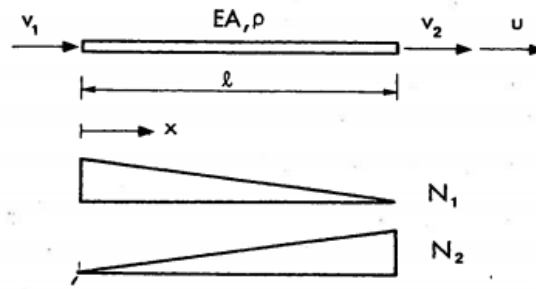


Figure 15: Interpolation polynomial 2D-bar (Sigbjörnsson)

By assuming kinematic compatibility the principle of virtual displacement can be utilized to determine the element stiffness.

$$\mathbf{k} = \int_V \mathbf{B}^T \mathbf{E} \mathbf{B} dV \quad (0.43)$$

For the bar element in figure 15 this yields:

$$\mathbf{k} = \int_0^l EA \mathbf{B}^T \mathbf{B} dx = \frac{EA}{l} \begin{bmatrix} 1 & -1 \\ -1 & 1 \end{bmatrix} \quad (0.44)$$

where  $\mathbf{E}$  is the modulus of elasticity as it is known from Hooke's law:  $\boldsymbol{\sigma} = \mathbf{E}\boldsymbol{\varepsilon}$ .  $\mathbf{B}$  is a matrix which represents the interpolation polynomials and the differential operator and has the form  $\mathbf{B} = \nabla \mathbf{N}$ .



The system nodal degrees of freedom are linked to the system degrees of freedom by a connectivity matrix such that  $\mathbf{v} = \mathbf{a}\mathbf{r}$ . The system stiffness matrix can be found through the relationship

$$\mathbf{K} = \sum_i \mathbf{a}_i^T \mathbf{k}_i \mathbf{a}_i \quad (0.45)$$

Iterative methods are commonly used in relation of finding the stiffness in non-linear structural analyses, and the most frequently used method is Newton-Raphson. In a non-linear problem, the stiffness matrix  $\mathbf{K}$  is itself a function of the system degrees of freedom  $\mathbf{r}$ . The non-linear relationship is expressed by the following equation:

$$\mathbf{K}(\mathbf{r})\mathbf{r} = \mathbf{R} \quad (0.46)$$

where  $\mathbf{R}$  is the load vector. The incremental stiffness has the following relationship (Moan, 2007):

$$\mathbf{K}_I(\mathbf{r}) = \frac{d}{d\mathbf{r}} (\mathbf{K}(\mathbf{r})\mathbf{r}) \quad (0.47)$$

Iterative methods treat the governing relations as a set of nonlinear equations and iterate within each increment until the unbalanced forces are smaller than a preset tolerance level. The incremental stiffness is found by the iterative process which can be illustrated by the following figure:

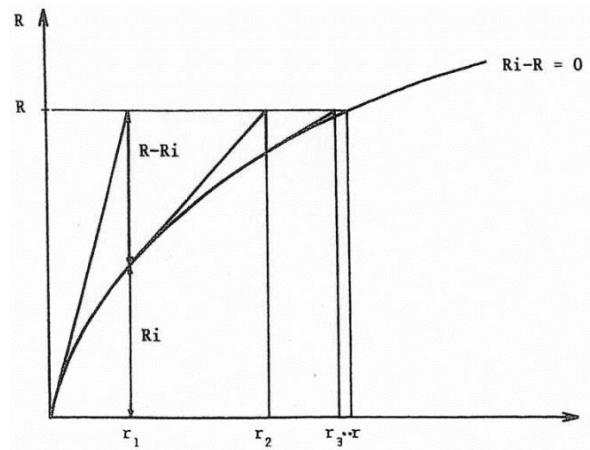


Figure 16: Newton-Raphson iteration (Moan, 2007)

Equilibrium is sought in the following expression (Moan, 2007):

$$\mathbf{r}_{n+1} - \mathbf{r}_n = \Delta \mathbf{r}_{n+1} = \mathbf{K}_I^{-1}(\mathbf{r}_n)(\mathbf{R} - \mathbf{R}_{int}) \quad (0.48)$$

where  $n$  refers to the steps in the iteration process and  $\mathbf{R}_{int}$  is the internal load vector.

There are two methods of describing the mass distribution of an element, namely by lumped and consistent mass formulation. In a consistent mass matrix, the same interpolation polynomials used to describe displacement are used to describe the mass distribution within an element. For element  $i$  this yields:

$$m_i = \int_{V_i} \rho \mathbf{N}^T \mathbf{N} dV \quad (0.49)$$

In a lumped mass model, the mass is concentrated in the element nodes.

For a bar with 2 DOFs in figure 15 it leads to

$$m_i = \frac{\rho A l}{2} \begin{bmatrix} 1 & \\ & 1 \end{bmatrix} \quad (0.50)$$

for element number  $i$ .





A lumped mass matrix cannot represent inertia related to rotation of the nodes, but has computational benefits compared to the consistent mass formulation. It requires less storage space, and it requires a lesser number of computational operations during dynamic analyses. The system mass matrix can also be found introducing compatibility such that:

$$\mathbf{M} = \sum_i \mathbf{a}_i^T \mathbf{m}_i \mathbf{a}_i \quad (0.51)$$

There are different mathematical methods to describe damping  $\mathbf{B}$ . Damping can in general be defined as the ability a construction or system has to dissipate kinetic energy (Sigbjörnsson). Linear and quadratic viscous damping have, together with potential damping, been described previously as properties of a vessel. The mooring line damping is typically expressed through Morison's equation, and the system damping matrix can analogous to the mass matrix be established by

$$\mathbf{B} = \sum_i \mathbf{a}_i^T \mathbf{b}_i \mathbf{a}_i \quad (0.52)$$

The linear system equation of motion can be expressed on matrix form as we know it from equation(0.13):

$$(\mathbf{M} + \mathbf{A})\ddot{\boldsymbol{\eta}} + \mathbf{B}\dot{\boldsymbol{\eta}} + \mathbf{K}\boldsymbol{\eta} = \mathbf{F} \quad (0.53)$$

where both the mooring lines and vessel properties are presented.



## **5 Implementation of the OrcaFlex coupled analyses**

The different steps, methods and assumptions for the implementation of the coupled OrcaFlex analyses will be introduced in this chapter.

In short, the mooring systems were built in OrcaFlex according to the information given in the Sevan Mariner Model Tests Report from Marintek. Based on the available information on the Sevan hull a FE – model was established in GeniE, and a radiation/diffraction analysis was conducted with the panel method software tool WADAM. The frequency dependent excitation load, added mass, damping and mean drift coefficients obtained from this analysis were imported directly to OrcaFlex and introduced as a vessel (node). The viscous damping coefficients were estimated based on the model test results from the Sevan Mariner Model Tests Report, and a system verification was completed by comparison of the OrcaFlex model to the offset and free decay tests conducted during the model tests.

Times series of the wave elevation and wind velocity recorded during the model tests were acquired through Marintek and introduced to OrcaFlex. Current was modeled in OrcaFlex based on the information given in the Sevan Mariner Model Tests Report. Time domain simulation with an implicit integration solver was then carried out and compared to results from the model tests and results obtained from a numerical simulation conducted by Marintek using the software tool SIMO/RIFLEX.

### **5.1 Basis for comparison to the OrcaFlex coupled analyses**

For clarification, the basis for comparison for the OrcaFlex numerical model should be outlined. The basis for comparison is primarily the results from the model test conducted on the moored FSU in 2011. Later, Marintek also performed a coupled numerical simulation of the moored FSU by the software tools WAMIT and RIFLEX/SIMO. Both these analyses, i.e. the model test and the numerical simulation, were presented in two reports named Sevan Mariner Model Test Report and SEVAN 1000 FSU –Numerical Simulation Final Report. The



FSU and mooring system particulars used in the WADAM/OrcaFlex analyses were obtained from the Sevan Mariner Model Test Report. Time series from the model tests of the FSU response during decay, offset and irregular wave tests were found in the SEVAN 1000 FSU – Numerical Simulation Report together with the RIFLEX/SIMO results. This implies that all the results obtained from the OrcaFlex analyses were plotted and compared to both the model tests and the RIFLEX/SIMO numerical simulations, enabling also the software tools to be compared. Finally, the names which were used by Marintek to describe the various model tests are kept the same also in this report.

## 5.2 Building the model in OrcaFlex

The FSU local coordinate system was located such that it coincided with the global OrcaFlex coordinate system. The mooring lines were modeled as pipes with zero inner diameters and zero bending stiffness. To convert the chain particulars to pipe dimensions, equivalent pipe diameters were calculated to keep the correct weight and density data.

Recommended drag coefficients for stud linked and stud less chains was though found in (VERITAS, 2010). The mooring line drag coefficients applied in the OrcaFlex model were the following:

- $C_d = 2.4$  for studless chain
- $C_d = 2.6$  for studlink chains
- $C_d = 1.5$  for fibre rope

The drag coefficients listed above corresponds to the nominal bar diameter of the chains (VERITAS, 2010) which also were used as drag diameter input for the OrcaFlex analyses (table 2 and 4).

In order to achieve approximately the same top tension as in the model test, the length of the top end segments of the mooring lines were either decreased or increased. The ‘winch’



length for both the OrcaFlex and SIMO/RIFLEX models varied from zero to two meters on the top chain segment

The length of the elements in the mooring lines was set to 0.5 meters for the mooring segments between the floater and touch down point on the seafloor. Segments laying on seafloor (also during dynamic analyses) were modeled with element length of 2 meters. A small friction coefficient of 0.1 was applied for these segments. This was an estimate based on an assumption that the seafloor friction at the Marintek basin also was small during the model tests. The mass coefficient of the mooring lines was set to  $C_M = 2$ .

OrcaFlex calculates the stiffness of the mooring lines with basis in an improved catenary equation, and utilizes an iterative method with basis in Newton-Raphson in order to find the system equilibrium.

The different line segment particulars, pretensions and coordinates for both mooring systems are given in the two following sections.

### 5.2.1 Chain-polyester-chain mooring system

As described in chapter 2 the FSU was tested with two different mooring systems. The primary system tested was a chain-polyester-chain system with the following composition:

Segment	Segment length [m]	Diameter [m]	Axial stiffness EA [kN]	Unit weight in water [kN/m]	Relative weight in water to dry weight
Anchor chain	150.0	0.161 stud less	$2.052 \times 10^6$	4.420	0.870
Link	1.0	0.161	$1.028 \times 10^6$	30.00	0.870
Lower polyester	400.0	0.262	$3.99 \times 10^5$	0.1220	0.270



rope					
Buoy with link	5.0	0.161	$1.026 \times 10^6$	-30.00	-1.000
Upper polyester rope	700.0	0.262	$3.99 \times 10^5$	0.1220	0.270
Link	1.0	0.161	$1.028 \times 10^6$	30.00	0.870
Top chain	125.0	0.161 stud less	$2.052 \times 10^6$	4.420	0.870

Table 2: Chain-polyester-chain system: mooring line composition (Muthanna, 2011)

The diameter of the chains refers to the nominal bar diameter. Coordinates and pretensions are given in table 3:

Line no.	Fairlead coordinates*		Anchor Coordinates		Pretension at fairlead [kN]		
	X [m]	Y [m]	X [m]	Y [m]	Model test	Riflex/SIMO	OrcaFlex
1	29.16	32.28	1036.53	979.41	1976.6	1965	1964
2	31.32	30.19	1068.80	943.56	1941.3	1930	1929
3	33.32	27.96	1099.82	906.60	1885.8	1877	1867
4	35.17	25.60	1129.52	868.59	2066.1	2049	2047
5	36.03	-24.37	1124.80	-875.77	1980.4	1965	1965
6	34.27	-26.80	1094.48	-913.23	1883.2	1874	1874
7	32.34	-29.09	1062.86	-949.59	1911.9	1900	1900
8	-20.44	-38.40	-673.95	-1255.87	1640.9	1634	1635
9	-23.04	-36.90	-716.09	-1232.51	1685.3	1680	1681
10	-25.52	-35.22	-757.40	-1207.69	1773.2	1766	1767
11	-41.80	12.03	-1358.50	429.85	2111.9	2097	2095
12	-40.88	14.88	-1343.59	475.73	2104.4	2088	2086
13	-39.75	17.66	1327.09	521.06	2201.5	2190	2188



14	-38.44	20.36	1309.02	565.78	1949.1	1942	1941
----	--------	-------	---------	--------	--------	------	------

Table 3: Polyester-chain-polyester mooring system: coordinates and pretension (Muthanna, 2011)

\*Fairlead z-coordinate is 7.5 meters above keel, or -22.5 meters from the mean free surface.

### 5.2.2 Chain mooring system

Analogous the composition of the alternative chain mooring scheme is given in table 4:

Segment	Segment length [m]	Diameter [m]	EA [kN]	Unit weight in water [kN/m]	Relative weight in water to dry weight
Anchor chain	1050.0	0.161 stud less	$2.052 \times 10^6$	4.420	0.870
Heavy chain	128.0	0.161 stud less + double 0.181 stud link	$2.052 \times 10^6$	17.40	0.870
Top chain	50.0	0.161 stud less	$2.052 \times 10^6$	4.420	0.870

Table 4: Chain system: mooring line composition (Muthanna, 2011)

Coordinates and pretensions are given accordingly:

Line no.	Fairlead coordinates*		Anchor Coordinates		Pretension at fairlead [kN]		
	X [m]	Y [m]	X [m]	Y [m]	Model test	Riflex/SIMO	OrcaFlex
1	29.16	32.28	880.43	862.19	2044	2061	2059
2	31.32	30.19	908.72	831.86	2125	2143	2111
3	33.32	27.96	935.93	800.57	1770	1791	1770
4	35.17	25.60	962.02	768.34	1847	1863	1836



5	36.85	23.11	986.97	735.22	1877	1894	1870
6	36.03	-24.37	983.33	-739.00	1771	1796	1763
7	34.27	-26.80	957.87	-771.59	1656	1676	1660
8	32.34	-29.09	931.28	-803.29	1802	1826	1795
9	30.26	-31.25	903.60	-834.03	1668	1687	1672
10	-17.74	-39.72	-563.82	-1092.81	1834	1833	1807
11	-20.44	-38.40	-600.34	-1073.39	1727	1726	1708
12	-23.04	-36.90	-636.16	-1052.70	1689	1686	1673
13	-25.52	-35.22	-671.24	-1030.78	1814	1813	1788
14	-42.53	9.12	-1178.94	353.28	1979	1956	1937
15	41.80	12.03	-1166.81	392.93	1879	1856	1829
16	-40.88	14.88	-1153.32	432.15	1949	1927	1908
17	-39.75	17.66	-1138.45	470.86	1926	1904	1886
18	-38.44	20.36	-1122.25	509.03	2111	2086	2055

Table 5: Chain mooring system: coordinates and pretension (Muthanna, 2011)

\*Fairlead z-coordinate is 7.5 meters above keel, or -22.5 meters from the mean free surface.

### 5.3 Verification of the mooring stiffness in the numerical model

Offset tests were conducted on both the mooring systems in order to verify the mooring stiffness. The hull was simply moved along the x-axis, away from its equilibrium position, and the corresponding restoring force was measured and plotted.

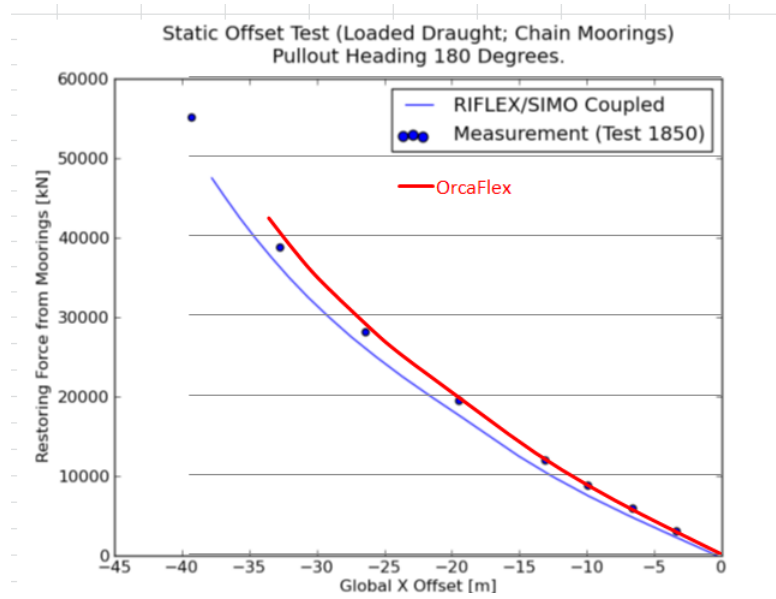


Figure 17: Static offset test chain mooring system

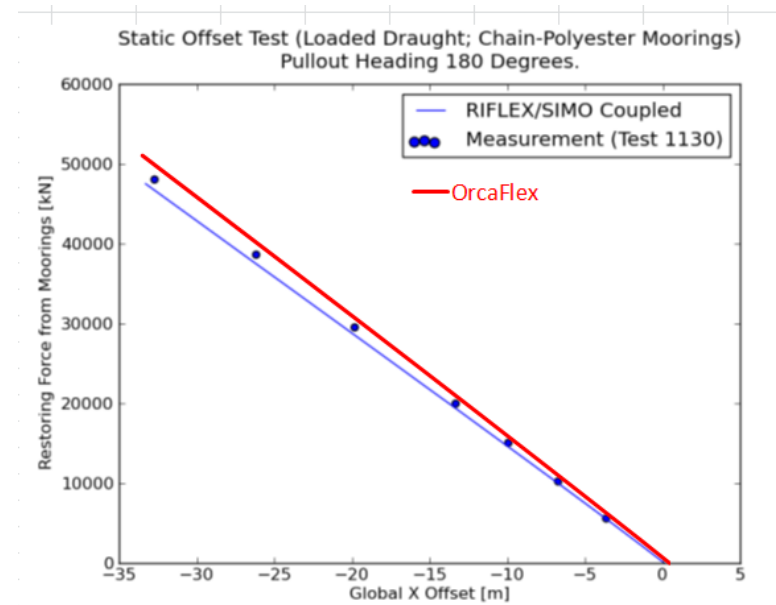


Figure 18: Static offset test chain-polyester-chain mooring system

Both mooring systems appear to represent correct horizontal stiffness compared to the model. The OrcaFlex mooring systems shows a weak over prediction of the mooring stiffness, while the SIMO/RIFLEX represents the opposite, a poor under prediction.





## 5.4 Diffraction analysis of the FSU by WADAM

WADAM is a 3-dimensional frequency domain panel code for first and second order diffraction analyses. In order to run a diffraction analysis of the FSU, a finite element (FE) model was created in the software tool GeniE. The main purpose of the establishment of the GeniE model was to define the FSU geometry and to generate a mesh and hence the panels used for the hydrodynamic calculations. By the introduction of a hydrostatic 'dummy' load the mean water level on the FSU was also defined.

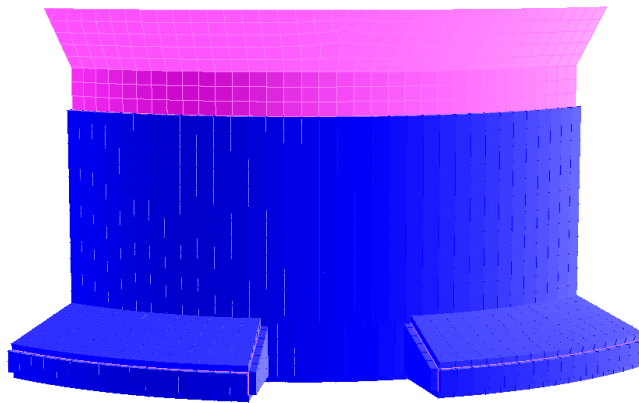


Figure 19: GeniE FE-model of the FSU with hydrostatic 'dummy' load

The FSU diameters were found in the Mariner FSU Concept Study report. The exact extent of the cutouts of the bilge keel where the fairleads were placed was though not found in the report. The extent of the cutouts was determined by a simple iterative process where the cutout extent was gradually changed and compared with the correct volume displacement of the FSU given in the Mariner FSU Concept Study report. The length of the cutouts was finally set to 20 meters.

As described in section 3.4 the velocity potential and/or source strength are assumed constant over each panel, and the results will depend on the size of the panels. The first order diffraction analysis of the FSU was carried out with varying mesh size. The mesh size on the final FE-model had an element size of 2 meters, leading to a total of 5284 panels defining the body. Although there is no documentation in this thesis on any sensitivity test,



different mesh sizes were tested, and convergence on the output parameters were found in such matter that the final mesh size was decided sufficient.

When the FE – model was imported to WADAM for the diffraction analysis, the mass properties of the FSU were introduced according to table 1. The stiffness contribution from the mooring lines was added accordingly to appendix A where the main assumptions are

$$K_{11} = 1300000 \text{ N / m} \text{ and } Z_{fairleads} = -22.5m$$

where  $K_{11}$  was an estimate based on the results represented in figure 17 and figure 18. The mooring stiffness in the chain and chain-polyester-chain systems are different, but in the context of a diffraction analysis, which assumes small fluid oscillations and steady state response the relatively small difference between the two values of mooring stiffness was assumed not to influence the output parameters in any significant way.  $K_{22}$  was for simplicity set equal to  $K_{11}$  in the establishment of the mooring stiffness matrix. This is a coarse simplification, but taken into account that all the OrcaFlex numerical simulations were run in the negative x-direction, it was assumed not to influence the OrcaFlex results.

The mean wave drift force is influenced by resonance responses (Kendon, 2011). For surge and sway, there is a local peak in the amplitude of the mean drift coefficients that corresponds to the natural heave period (approx. 17 seconds) of the system (Appendix J). This maxima is dependent on the level of eddy damping applied during the WADAM analysis. Eddy damping is a part of the viscous hull damping and it is correlated with vortex shedding. It is non-linear effect and takes the form

$$-Bu_r |u_r| \quad (0.54)$$

with  $u_r$  being the relative velocity between the body and fluid (Greco). During the WADAM analysis only a linear damping coefficient was included, and it was determined with basis in the decay tests conducted during the model tests. The level of relative damping,  $\frac{B}{B_{cr}}$ , was in the Sevan Mariner Model Test Report found to be approximately 0.08 for relatively large amplitudes during the heave decay test.



$$B_{cr} = 2 \cdot \sqrt{(M_{33} + A_{33}) \cdot C_{33}} \quad (0.55)$$

Eddy-making damping was introduced in heave as 8% of  $B_{cr}$  at 17 seconds and is listed in Appendix A. It is noted that this only affects the mean drift coefficients in the vicinity of 17 seconds, and in that way only should be recognizable in numerical simulations which contain waves of this period. Further, the amplitude of the mean wave drift coefficients for the total interval of periods calculated by WADAM were compared to an asymptotic limit for a circular water plane area given by (Pinkster):

$$\bar{F} = \frac{2}{3} \rho g r \quad (0.56)$$

which for the FSU yields:

$$\bar{F} = \frac{2}{3} \cdot 1025 \frac{\text{kg}}{\text{m}^3} \cdot 9.81 \frac{\text{m}}{\text{s}^2} \cdot 42.5 \text{m} = 285 \text{kN} / \text{m}^2 \quad (0.57)$$

The amplitude on the mean wave drift coefficients from the WADAM analysis (Appendix J) complies well with the result in equation(0.57).

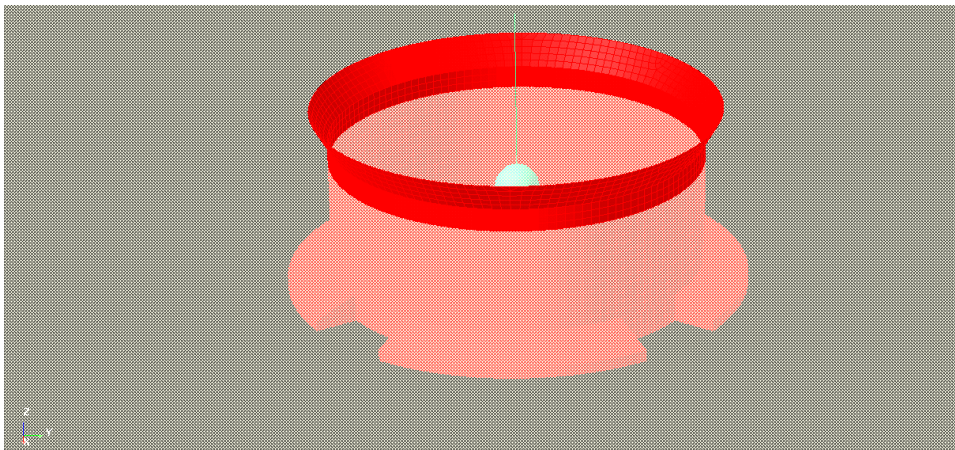


Figure 20: Diffraction analysis in WADAM

Results from the WADAM analysis included



1. Frequency and direction dependent first order wave excitation coefficients
2. Frequency dependent added mass coefficients
3. Frequency dependent potential damping coefficients
4. Frequency and direction dependent second order mean wave drift excitation coefficients

The results are presented in Appendix G-J.

## 5.5 Estimating the viscous damping of the FSU

Viscous damping coefficients were firstly established based on decay tests conducted during the model tests of the FSU. In a decay test, the model is restrained in a specified position, where it is not in equilibrium, and then released and free to oscillate. There are no excitation forces. It is normal to assume that the motion of an uncoupled one degree of freedom mode can be written as

$$(m+a)\ddot{\eta} + B^L\dot{\eta} + B^Q|\dot{\eta}|\dot{\eta} + c\eta = 0 \quad (0.58)$$

where  $B^L$  and  $B^Q$  are the linear and quadratic viscous damping coefficients. With basis in the free decay tests the damping coefficients were found based on the solution of a linear oscillating system and the technique of equivalent linearization. For each cycle of the oscillation the quadratic term is replaced by an equivalent linear term, which is required to contain the same energy as the quadratic term (Steen, 2012). In order to remove the uncertainty related to the inertia term, equation (0.58) can be divided by  $(m+a)$  which leads to the following equation:

$$\ddot{\eta} + p_1\dot{\eta} + p_2|\dot{\eta}|\dot{\eta} + p_3\eta = 0 \quad (0.59)$$

where

$$p_1 = \frac{B^L}{(m+a)} \quad (0.60)$$



$$p_2 = \frac{B^{\varrho}}{(m+a)} \tag{0.61}$$

$$p_3 = \frac{c}{(m+a)} \tag{0.62}$$

The linearized equation of motion is expressed by

$$\ddot{\eta} + p\dot{\eta} + p_3\eta = 0 \tag{0.63}$$

where

$$p = p_1 + \frac{16}{3} \frac{\eta_k}{T_n} p_2 \tag{0.64}$$

The last term in equation (0.64) is due to the linearization of the quadratic damping term and  $\frac{16}{3} \frac{\eta_k}{T_n}$  is an equivalent velocity.  $\eta_k$  is the amplitude of the  $k^{\text{th}}$  oscillation and  $T_n$  is the free damped oscillation period.

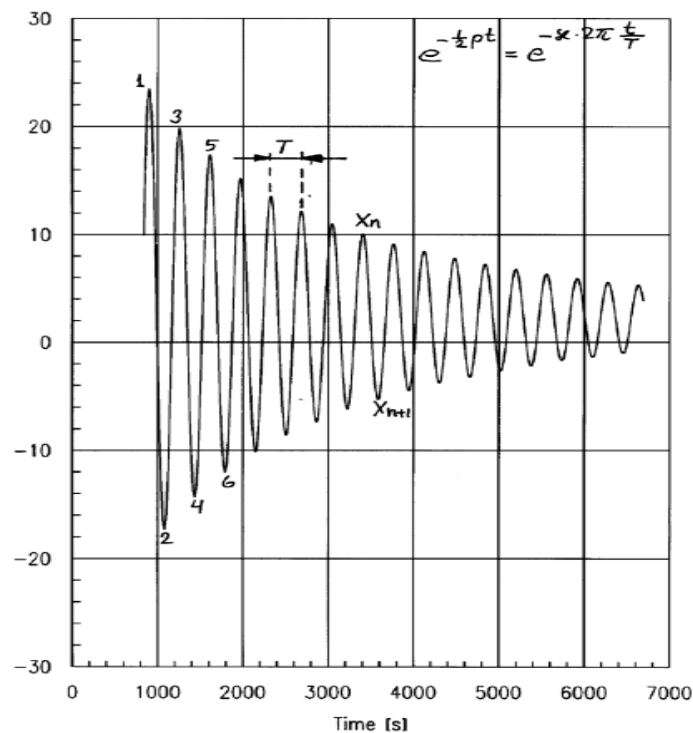


Figure 21: Decay test example (Steen, 2012)



Assuming the damping to be constant with respect to the amplitude of oscillation, the linear and quadratic damping coefficients can be determined from the relationship:

$$\frac{2}{T_n} \log\left(\frac{\eta_{k-1}}{\eta_{k+1}}\right) = p_1 + \frac{16}{3} \frac{\eta_k}{T_n} p_2 \quad (0.65)$$

There is one half period  $\frac{T_n}{2}$  between  $\eta_k$  and  $\eta_{k+1}$  for any  $k$ . By plotting the left hand side of equation (5.12) versus  $\frac{16}{3} \frac{\eta_k}{T_n}$  and fitting the points to a straight line by the least square method, the coefficients  $B^L$  and  $B^Q$  are found.  $p_1$  is the intersection with the vertical axis, and  $p_2$  is the slope of the curve.

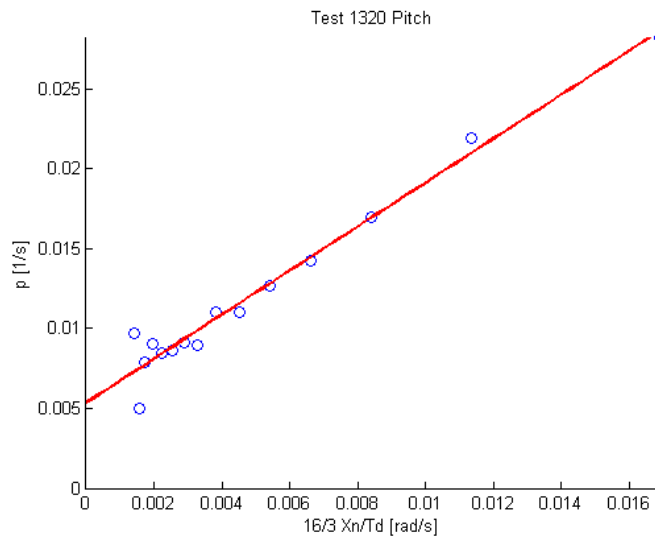


Figure 22: Viscous damping coefficient pitch

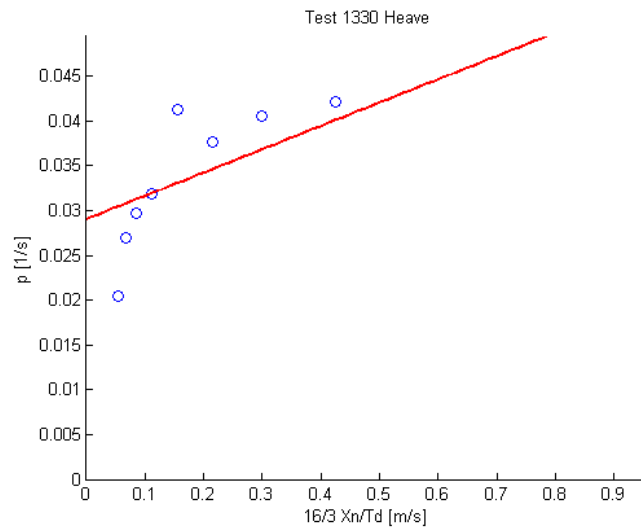


Figure 23: Viscous damping coefficients heave

Records of the measured oscillations from several model decay tests are represented in the Sevan Mariner Model Test Report. In the context of this report, two decay tests were analyzed in order to estimate the viscous damping of the FSU. These were decay tests performed without any mooring system, and the rigid body modes were heave and pitch. The added mass and added moment of inertia values used to find  $B^L$  and  $B^Q$  are those found in Appendix H, i.e. from the radiation analysis.

Test no	Motion	$T_d [s]$	$p_1$	$p_2$	$B^L$	$B^Q$
1320	Pitch	29.4	0.0053 [1/s]	1.3762 [1]	$6.52 \times 10^5$ [kNm/(rad/s)]	$1.68 \times 10^8$ [kNm/(rad/s) <sup>2</sup> ]
1330	Heave	16.8	0.029 [1/s]	0.026 [1/kg]	$1.11 \times 10^4$ [kN/(m/s)]	$9.95 \times 10^3$ [kN/(m/s) <sup>2</sup> ]

Table 6: Viscous damping coefficients obtained from decay model tests

The obtained viscous damping coefficients were used as initial values for the OrcaFlex numerical reconstruction of the model decay tests which are presented in the next section.



## 5.6 Numerical reconstruction of decay tests

A decay test describes the characteristics of a hull or a moored system, and its motion is described by equation(0.58). The natural frequency of oscillation of a system is dependent on the viscous damping, but it is dominated by the mass/stiffness ratio. This is especially apparent for systems with small viscous damping, or in decay tests where the velocities in general are low.

The undamped and uncoupled resonance periods can in general be written as:

$$T_{ni} = 2\pi \left( \frac{M_{ii} + A_{ii}}{C_{ii} + K_{ii}} \right) \quad (0.66)$$

where  $T_{ni}$  is the natural period of oscillation in motion mode  $i$ .  $K_{ii}$  is the mooring stiffness. The rate of amplitude decay during the model test and numerical simulation is due to the applied damping.

A total of six decay tests were numerically reconstructed:

Test no	Mode	Mooring system	$T_n$
1250	Surge	Chain-polyester-chain	88.2
1370	Heave	Chain-polyester-chain	16.7
1380	Pitch	Chain-polyester-chain	28.7
1950	Surge	Chain	116.5
1930	Heave	Chain	16.6
1940	Pitch	Chain	27.9

Table 7: Numerically reconstructed decay tests

The numerical reconstruction of the decay tests of the chain-polyester-chain mooring system are presented in the following section, while the corresponding tests for the chain mooring system can be found in Appendix C. Applied viscous damping coefficients during the numerical simulations are stated. The ‘tuning’ of the coefficients was done by empirically seeking a better fit between the model test and the OrcaFlex numerical simulation plotted in





the same graph. The decay test were, as previously stated, initiated with the viscous damping coefficients estimated in section 5.5. The results from these tests can also be found in Appendix C.

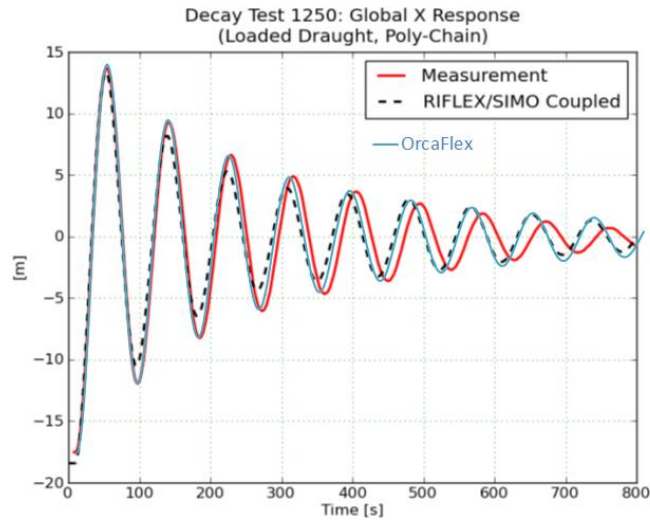


Figure 24: Numerical reconstruction of decay test 1250

Viscous damping coefficients applied in the numerical simulation:

$$B^L = 300kN / (m / s) \text{ and } B^Q = 0$$

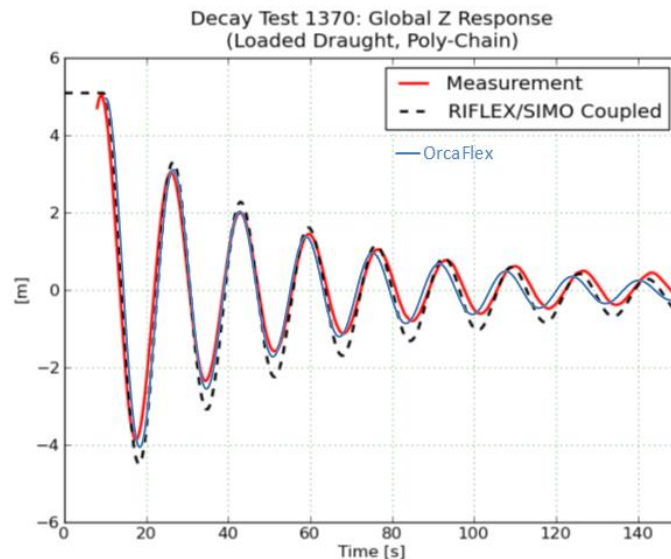


Figure 25: Numerical reconstruction of decay test 1370

Viscous damping coefficients applied in the numerical simulation:

$$B^L = 3000kN / (m / s) \text{ and } B^Q = 6000kN / (m / s)^2$$

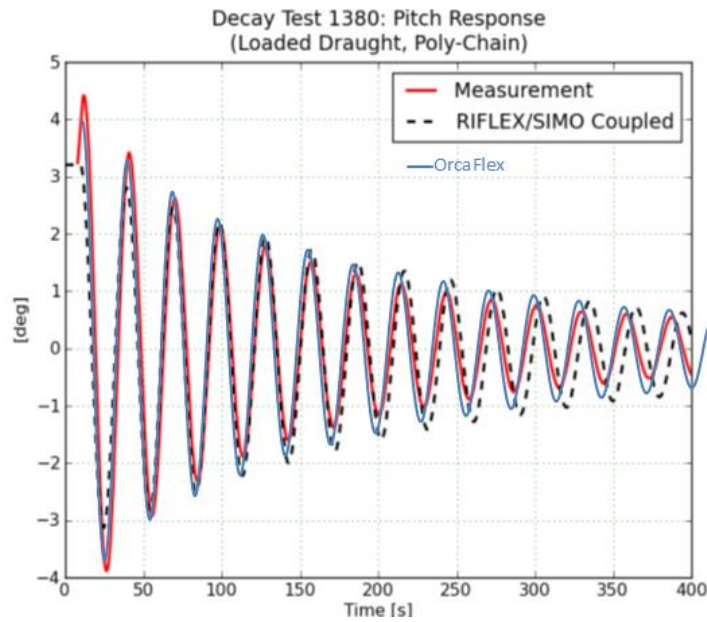


Figure 26: Numerical reconstruction of decay test 1380

Viscous damping coefficients applied in the numerical simulation:

$$B^L = 7.75 \times 10^5 \text{ kN} / (\text{rad} / \text{s}) \text{ and } B^Q = 2 \times 10^8 \text{ kN} / (\text{rad} / \text{s})^2$$

The numerical simulations of the decay tests did to a large extent confirm that the mass/stiffness ratio of the system was correct. The viscous damping coefficients applied in the numerical reconstruction of decay test number 1380 (pitch) have good compliance with the coefficients estimated in section 5.5., while the viscous heave coefficients gave poor compliance in test 1370. It can be recognized in figure 23 that the procedure of linearization of the heave damping gave scattered points, and that the determination of  $p_1$  and  $p_2$  necessarily led to more uncertain values than if the scattering was less significant.

## 5.7 Introducing loads in OrcaFlex

The moored FSU was subjected to four environmental conditions, representing an operational condition and a 1, 100 and 1000 – year storm:



Environment no	Condition	$H_S$ [m]	$T_P$ [s]	$V_{current}$ [m/s]	$V_{wind}$ [m/s]	$\lambda$ [m]
1	Operational	7.5	12	0.5	20	224
2	1 year storm	9.5	12	0.88	28	224
3	100 year storm	14	15.8	0.88	32	370
4	1000 year storm	17.5	17.6	0.88	32	441

Table 8: Environmental conditions implemented in the numerical simulation (Kendon, 2011)

Both the wind, current and the waves had the same heading of 180 degrees. In the following sections the introduction of the different loads to OrcaFlex will be outlined.

### 5.7.1 Current load in OrcaFlex

The current profile in the OrcaFlex numerical model was established based on measurements done during the model test.

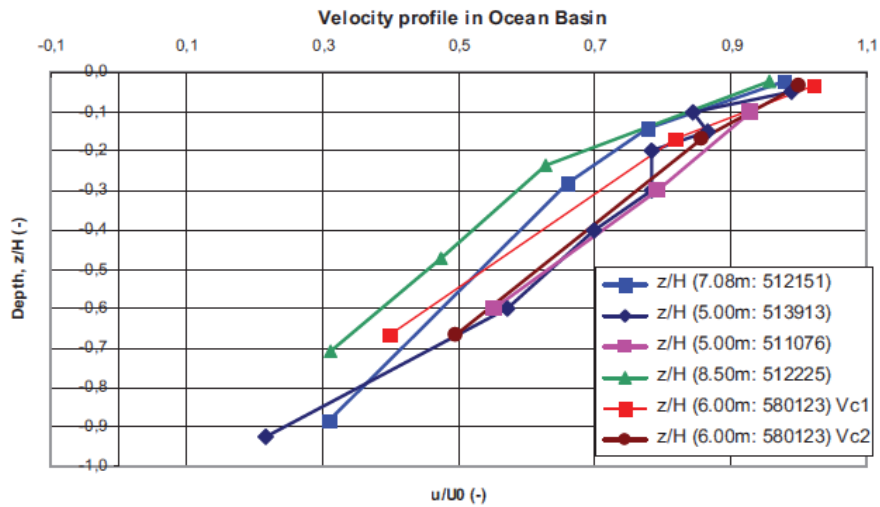


Figure 27: Velocity profile in ocean basin during model test

Based on figure 27, a linear velocity profile was applied during the numerical simulations.

$$V_C = V_C|_{z=0} (1+z/h) \quad (0.67)$$

where  $z=-h$  at the seabed, and  $V_C|_{z=0}$  is the specified surface current.



The current force per unit velocity squared of free-stream current was obtained from a model test with ‘current only’. The results are given in table 9:

Test no.	Draught L [m]	$V_C^{Z=0}$ [m/s]	$F/(V_C^{Z=SWL})^2$ [kN/(m/s) <sup>2</sup> ]
1415	30	0.88	765

Table 9: Current only test and corresponding coefficient (Muthanna, 2011)

OrcaFlex takes current velocity, drag coefficient and projected area as inputs. The projected area of the submerged hull is approximately  $85 \times 30 = 2550 \text{m}^2$  leading the  $C_d$  input to be

$$C_d = \frac{765000 \text{N}/(\text{m/s})^2}{\frac{1}{2} \times 1025 \frac{\text{kg}}{\text{m}^3} \times 2550 \text{m}^2} = -0.6 \quad (0.68)$$

The distance from the sea-level to the current force center was set to 15 meters which is half the draught.

### 5.7.2 Wind load in OrcaFlex

The wind generated by fans during the model tests was based on a NPD (Norwegian Petroleum Directorate) spectrum formulation. The wind coefficient,  $C$ , in table 10 is obtained from a ‘wind only’ test, and refers to an elevation level of 10 meters above the sea water surface.

The following data was collected from the Sevan 1000 FSU Numerical Simulations Report.

Test no.	Draught L [m]	$V_w^{Z=10m}$	$C$ [kN/(m/s) <sup>2</sup> ]
1415	30	0.88	1.37

Table 10: Wind only test and corresponding coefficient (Muthanna, 2011)

As OrcaFlex takes wind velocity, projected area and drag coefficient as inputs, the wind coefficient  $C$  was converted accordingly:



$$1.37 = \frac{F_w}{V_w} = \frac{1}{2} \times \rho_{air} \times A \times C_w \left[ \frac{kN}{\left(\frac{m}{s}\right)^2} \right] \quad (0.69)$$

leading to

$$A \times C_w = \frac{C}{\frac{1}{2} \times \rho_{air}} = \frac{1370 \frac{N}{(m/s)^2}}{\frac{1}{2} \times 1.3 \frac{kg}{m^3}} = 2107.7 \times C_w \left[ m^2 \right] \quad (0.70)$$

For simplicity, the projected area of the FSU was set to  $2107.7m^2$ , and the drag coefficient for the wind load was set to  $C_w = -1$ .

The wind time series which were recorded during the model tests were imported to OrcaFlex and used to drive the numerical simulation. The center of the wind generated pressure force was set to  $z = 15$  meters.

### 5.7.3 Import time series of wave elevation to OrcaFlex

As for the wind, time series of the wave elevation recorded during the model tests were imported to OrcaFlex. This enabled the results obtained from the OrcaFlex numerical simulations to be directly compared to the model test results and the SIMO/RIFLEX results.

In short, OrcaFlex uses a FFT (Fast Fourier Transform) to transform the wave time series into a number of frequency components. Each component is then used to define a single Airy wave. These waves are then combined to represent the wave elevation and kinematics at all points during the simulation time (Orcina). When the time history wave is modeled by superposition of these Airy waves and the wave components have the periods, amplitudes and phases that match the Fourier components, the wave conditions from the model tests were regenerated.



Due to the FFT, the number of samples  $N$  used to represent a given period of time need to be a power of two, and  $N$  number of samples produces  $N/2$  components. The  $N$  number of wave components used to regenerate the wave condition strongly affects the duration of the simulation. This is further discussed on in chapter 7 and 8.

#### 5.7.4 Second order wave excitation and damping in OrcaFlex

The mean drift coefficients obtained from the diffraction analysis described in section 5.4 were the basis for the prediction of the second order motion of the FSU. OrcaFlex utilizes Newman's approximation in order to establish the off diagonal entries of the full QTF matrix. Newman's original approximation was based on arithmetic mean values (equation(0.26)) in order to approximate the off diagonal values, while OrcaFlex uses a geometric mean value approach (Orcina).

OrcaFlex calculates the FSU wave drift damping based on Aranha's simplified method expressed in equation(0.29). Orcina, founders of OrcaFlex, states that their version includes developments done by both Molin and Malenica *et al* in order to be applicable for all water depths and to accommodate for encounter effects expressed in equation(0.30). The velocity used in the calculations is the vessels low frequency velocity relative to the current and wind velocity.

Once the mean drift coefficients from the diffraction analysis are imported to OrcaFlex, the QTF matrix is established based on Newman's approximation. The slow drift damping of the vessel is incorporation in this QTF matrix by OrcaFlex. In the context of second order motion this means that importing the mean drift coefficients to OrcaFlex is all the user is able to do through the standard OrcaFlex user interface. This is further discussed in chapter 8.

The slow drift damping contribution from the mooring lines (figure 11) is accounted for through the Morison elements.



## 5.8 Irregular wave tests OrcaFlex

To account for the frequency-dependent added mass and damping in the time domain, OrcaFlex calculates the Impulse Response Function for the vessel and applies the IRF at each time step using a convolution integral to account for history effects (Orcina).

For the six degrees of freedom, and at each time step in the simulation, the total added mass and damping load on the vessel is given by:

$$F(t) = -A(\infty)\ddot{\eta}(t) + \int_0^{T_c} IRF(s)\dot{\eta}(t-s)ds \quad (0.71)$$

where  $\ddot{\eta}$  and  $\dot{\eta}$  is the vessel acceleration and velocity,  $T_c$  is a cutoff time, and  $s$  is a time lag integration variable.  $T_c$  was during the irregular wave simulations kept on a value of 25 seconds. The IRF is calculated by:

$$IRF(t) = 4 \int_0^{\infty} B(f) \cos(2\pi ft) df \quad (0.72)$$

$B(f)$  is frequency dependent potential damping coefficients imported from the diffraction analysis. The infinite-frequency added mass describes the vessel's instantaneous response to acceleration, and is also estimated with basis in the added mass values imported from the diffraction analysis.

Orcaflex' implicit integration was used to solve the system equation of motion. For implicit integration OrcaFlex uses a Generalized- $\alpha$  integration scheme. It is second-order accurate and unconditionally stable (Orcina). The accelerations, velocities and displacements were found by this iterative method which also is described in section 4.3.

A sensitivity test was conducted on the time increment value. The OrcaFlex results were found converging towards the model tests results all the way down to a time increment of 0.05 seconds, hence this was the time step used for the OrcaFlex time series being compared to the model test.

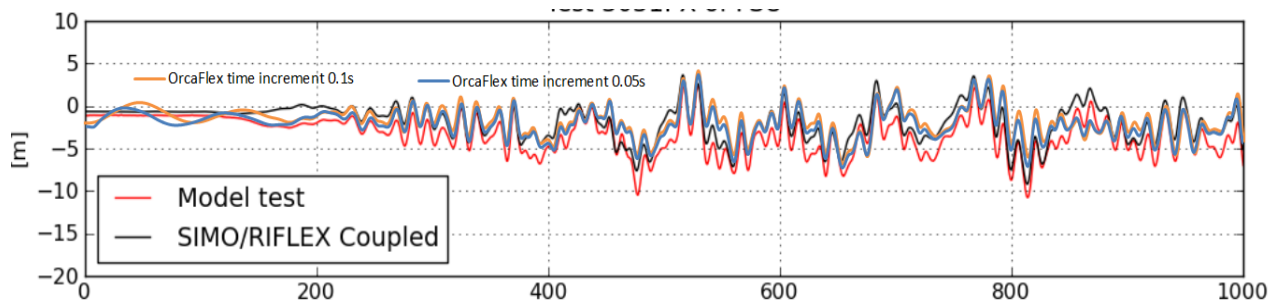


Figure 28: Sensitivity test conducted on the numerical integration time step

In addition, there were two other parameters that needed adjustment based on results from the OrcaFlex time series. This comprises the dividing period and the pitch viscous damping coefficients. The moored FSU motion consists of both wave -and low frequency motion, and the OrcaFlex user must define a dividing period which is used to filter the vessel motion into its low frequency and wave frequency components. This is because the different loads depend on whether the FSU motion is of first or second order during the analyses (Orcina). The dividing period should in general be well above the highest period of the significant wave frequency response of the vessel motion, and well below the lowest period of significant slow drift vessel response (Orcina). The determination of the dividing period turned out to influence on the calculated vessel response when the system was subjected to the different environmental condition. As several environmental conditions were analyzed, and due to the fact that the simulation durations were long, more information on this topic was sought. Orcina software support suggested that one can give an initial dividing period based on mean values. I.e. if a system has a natural damped period of oscillation  $T_n$  and is subjected to waves with a peak period of  $T_p$ , the dividing period can be estimated by the following:

$$T_{dividing} = \frac{1}{\frac{1}{2} \left( \frac{1}{T_e} + \frac{1}{T_p} \right)} [s]$$





Orcina also recommended to run a sensitivity study on the diving period. This was done together with studies of the corresponding Torsethaugen spectra of the wave generated during the model tests.

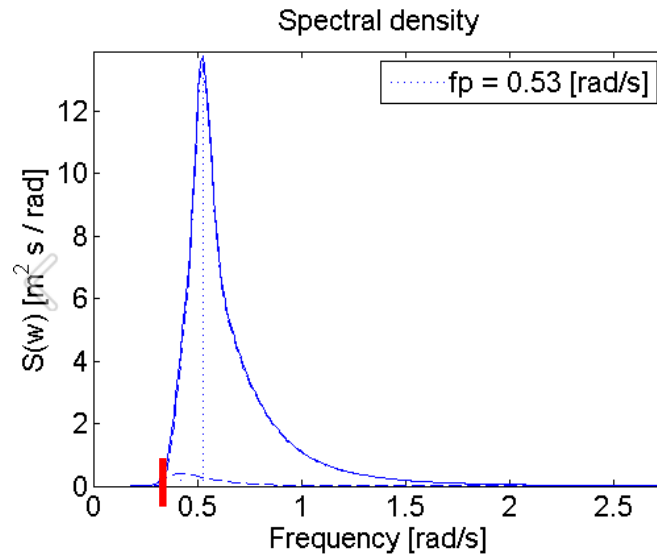


Figure 29: Torsethaugen spectrum from MatLab and WAFO

Figure 29 was established by the use of MatLab and WAFO (Wave Analysis for Fatigue and Oceanography) and illustrates a Torsethaugen spectrum corresponding to the operational condition listed in table 8. This was done for the all the four different sea states in order to obtain an estimate of the longest wave periods of the sea states and hence the wave frequent FSU response. In this case the highest  $\omega$  can be approximated to be 0.33, i.e. wave periods should be expected to reach

$$T = \frac{2\pi}{\omega} = \frac{2\pi}{0.33} \approx 21s$$

This procedure was carried out for all four environmental conditions. Together with sensitivity tests of the dividing periods in the time domain this lead to dividing periods of 23, 23, 25 and 27 for the respectively to conditions.

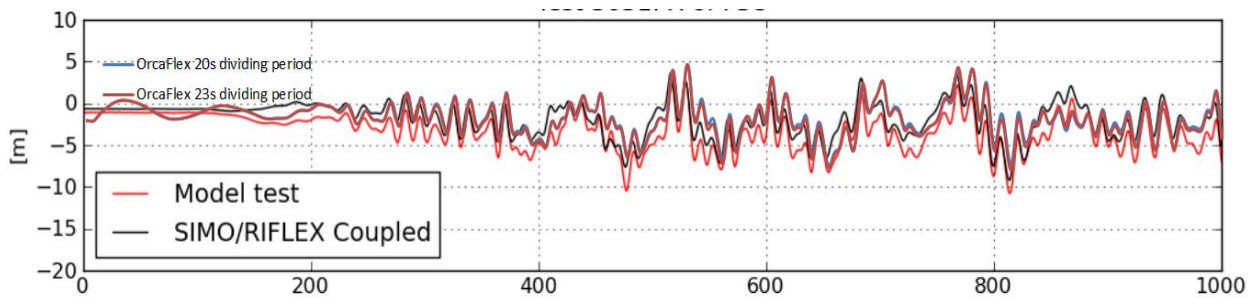


Figure 30: Sensitivity test conducted on the OrcaFlex dividing period (environmental condition)

Viscous effects can be divided into viscous effects due to the pressure distribution around the hull, and skin friction effects (Faltinsen, 1990). The first term is recognized by the making of eddies, and referred to as eddy-making damping. It is also known to be of greater values in waves than in calm water (Kendon, 2011). Viscous damping coefficients obtained from numerical reconstruction of the decay tests may not necessarily express the correct viscous damping in waves.

Applying the pitch viscous damping coefficients obtained from the decay tests gave the following results during irregular wave test number 3411 in pitch:

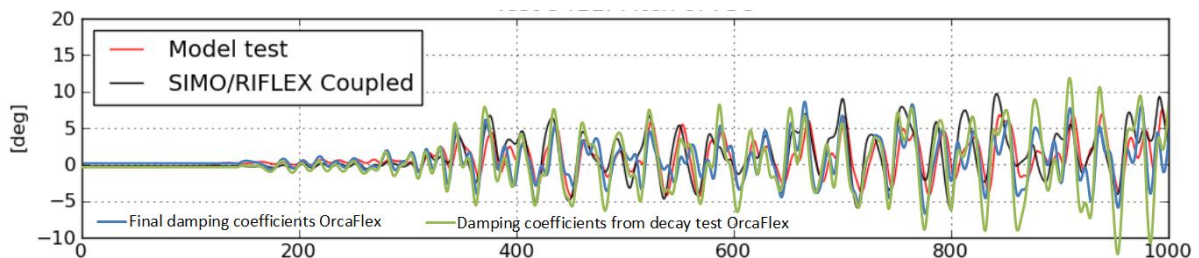


Figure 31: Viscous damping coefficients obtained from decay test in irregular waves

The consequence of the chosen viscous damping coefficients became evident when the FSU response in pitch exceeded approximately  $\pm 5$  degrees.



## 6 Results from numerical simulations with irregular waves

The following model tests were numerically reconstructed in OrcaFlex:

Test no	Draught	Mooring system	Environment
3021	Loaded	Chain-polyester-chain	Environment 1
3031	Loaded	Chain-polyester-chain	Environment 2
3411	Loaded	Chain-polyester-chain	Environment 3
3710	Loaded	Chain-polyester-chain	Environment 4
5120	Loaded	Chain	Environment 1
5130	Loaded	Chain	Environment 3

Table 11: Numerically reconstructed irregular waves tests

The final viscous damping applied during the OrcaFlex simulations were:

	$B^L [kN / (m / s)]$	$B^Q [kN / (m / s)^2]$
Surge	300	0
Heave	$3 \times 10^3$	$6 \times 10^3$
Pitch	$2 \times 10^6$	$4 \times 10^8$

Table 12: Final viscous damping coefficients

Current was calculated as a static load in the OrcaFlex analyses. This implies that the FSU has a static offset at the start of the OrcaFlex analyses. Wind is assumed to excite oscillations of the FSU in the start of the analyses. It is believed that the current was slowly built up to its steady velocity during the model tests, and that the RIFLEX/SIMO simulation was conducted with ramping of the current in the dynamic analyses. It is assumed that this encountered the motion observed in the OrcaFlex analyses at the early stages of the numerical simulation.



## 6.1 Test 3021

### FSU response surge

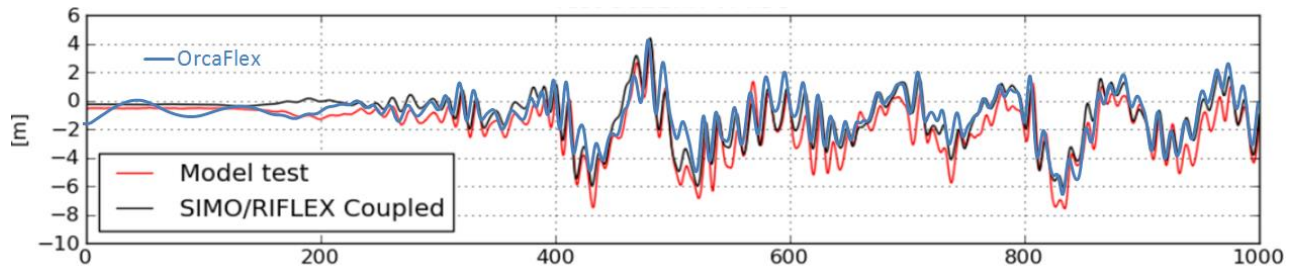


Figure 31: Test no 3021 FSU surge response 0 - 1000 sec.

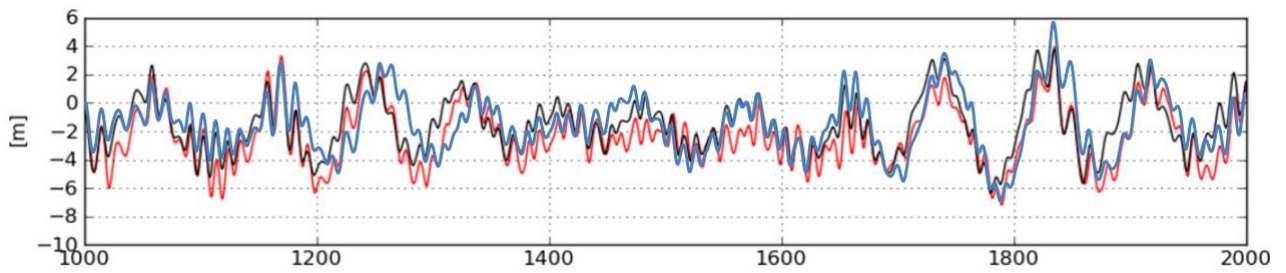


Figure 32: Test no 3021 FSU surge response 1000 - 2000 sec.

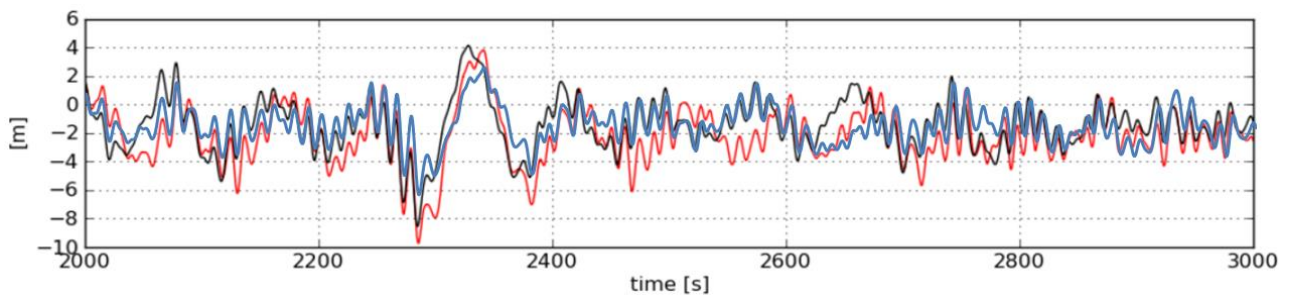


Figure 33: Test no 3021 FSU surge response 2000 - 3000 sec.



### FSU response heave

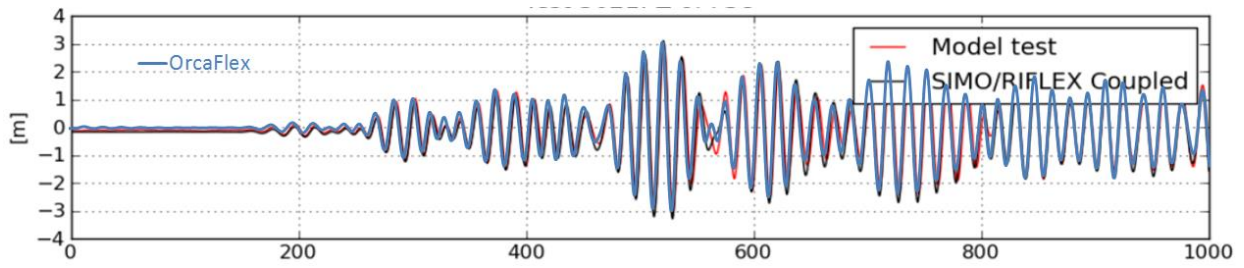


Figure 32: Test no 3021 FSU heave response 0 - 1000 sec.

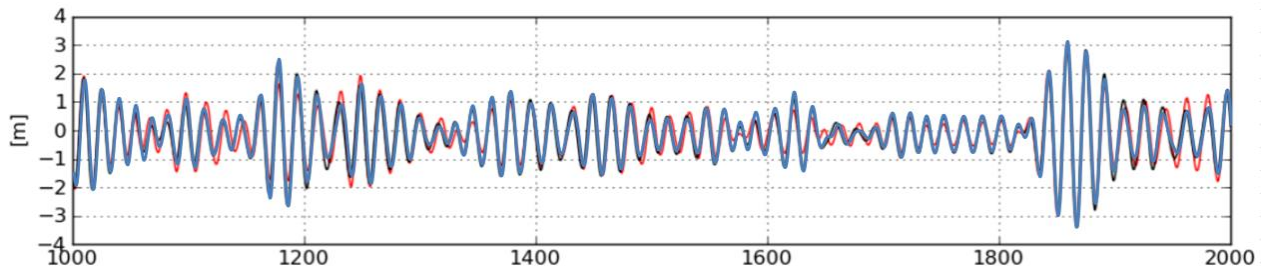


Figure 33: Test no 3021 FSU heave response 1000 - 2000 sec.

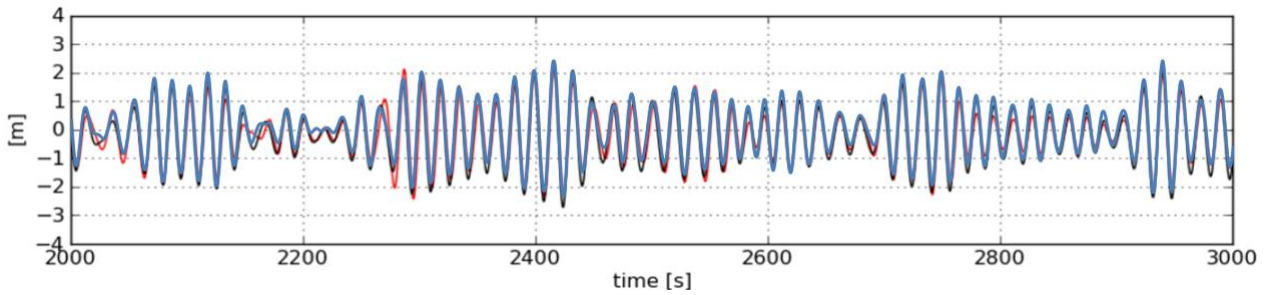


Figure 34: Test no 3021 FSU heave response 2000 - 3000 sec.



### FSU response pitch

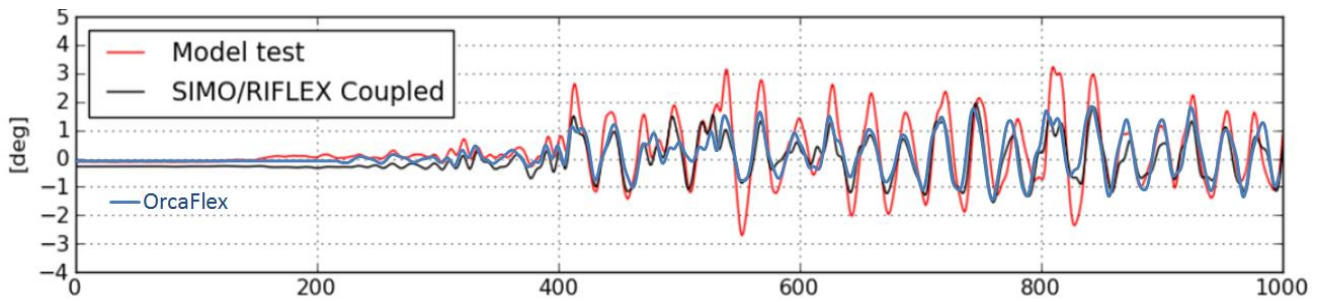


Figure 35: Test no 3021 FSU pitch response 0 - 1000 sec.

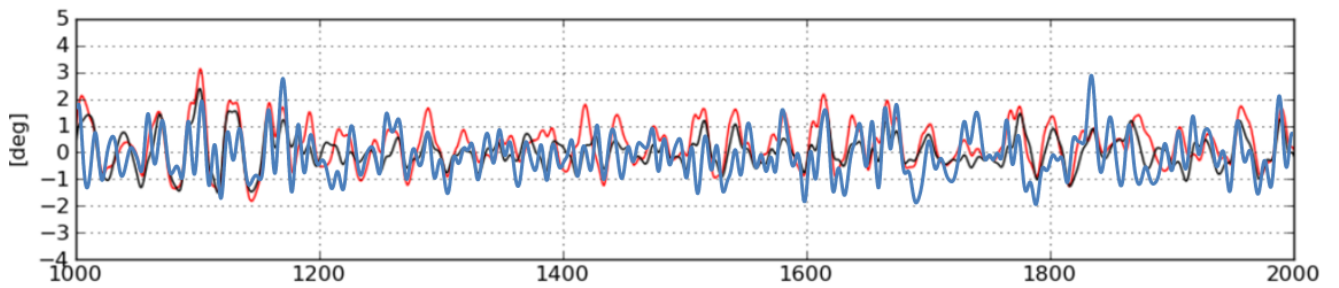


Figure 36: Test no 3021 FSU pitch response 1000 - 2000 sec

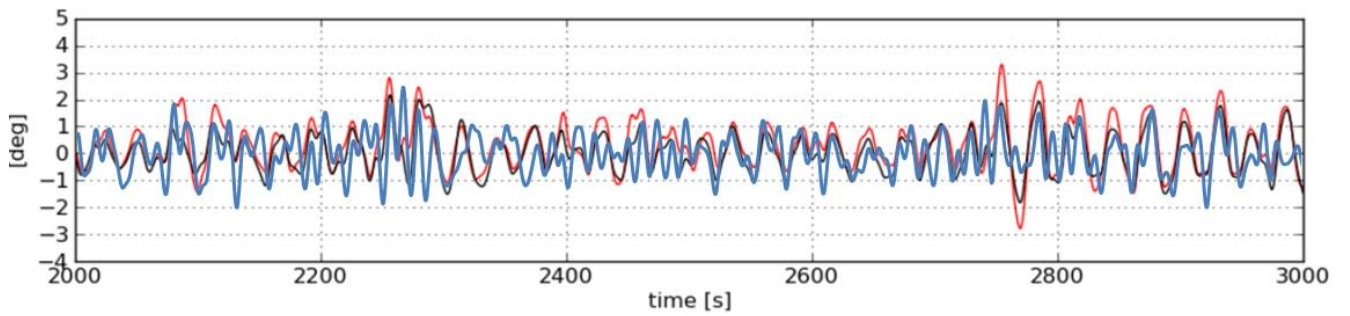


Figure 37: Test no 3021 FSU pitch response 2000 - 3000 sec



## 6.2 Test 3031

### FSU response surge

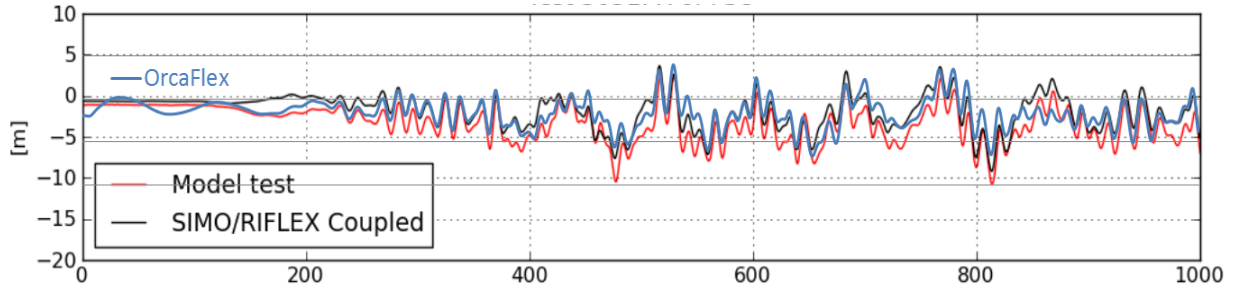


Figure 38: Test no 3031 FSU surge response 0 - 1000 sec.

### FSU response heave

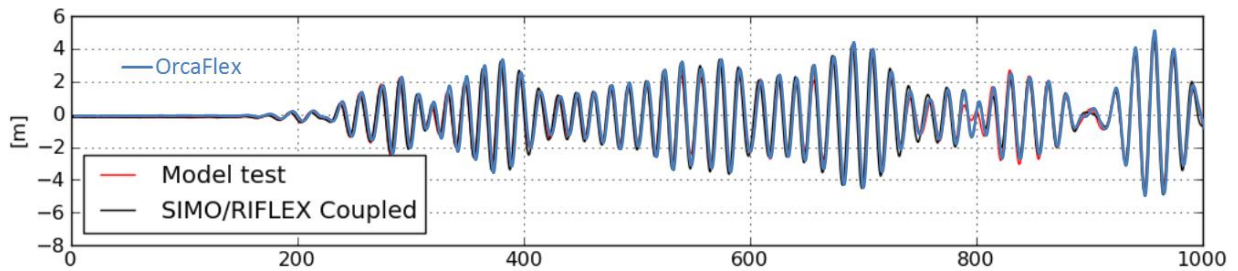


Figure 39: Test no 3031 FSU heave response 0 - 1000 sec.

### FSU response pitch

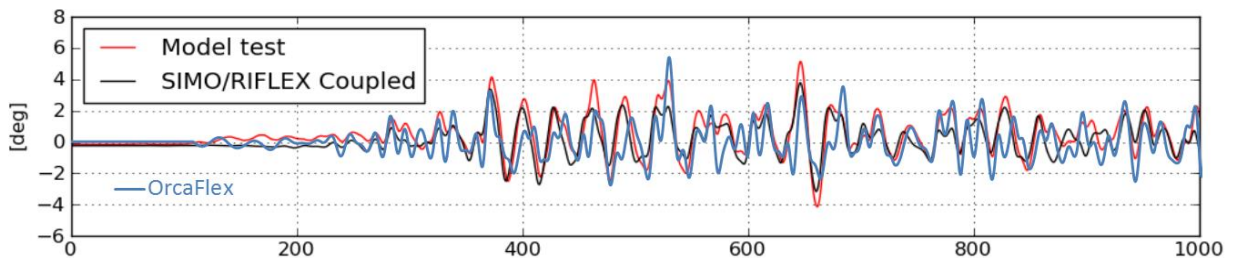


Figure 40: Test no 3031 FSU pitch response 0 - 1000 sec.



### 6.3 Test 3411

#### FSU response surge

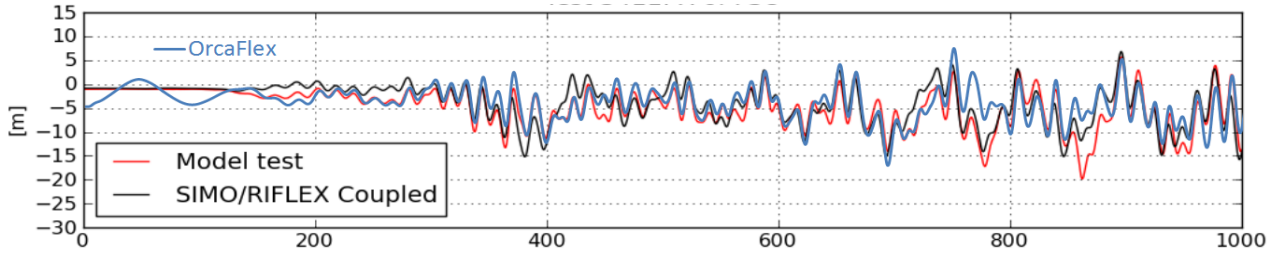


Figure 41: Test no 3411 FSU surge response 0 - 1000 sec.

#### FSU response heave

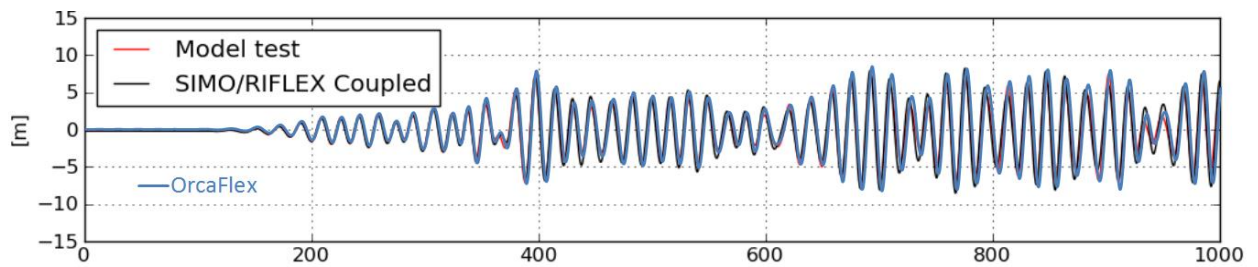


Figure 42: Test no 3411 FSU heave response 0 - 1000 sec.

#### FSU response pitch

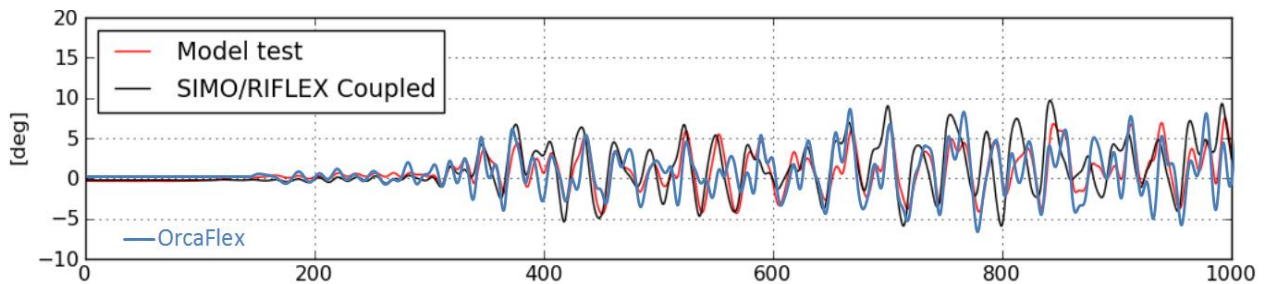


Figure 43: Test no 3411 FSU pitch response 0 - 1000 sec.





## 6.4 Test 3710

### FSU response surge

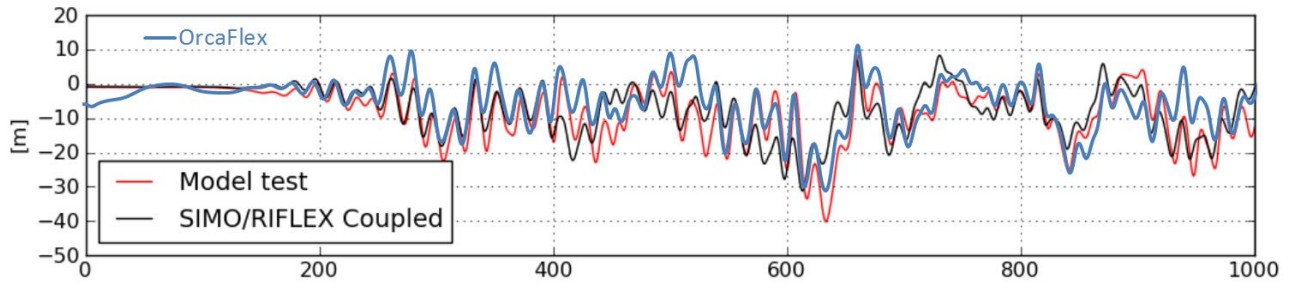


Figure 44: Test no 3710 FSU surge response 0 - 1000 sec.

### FSU response heave

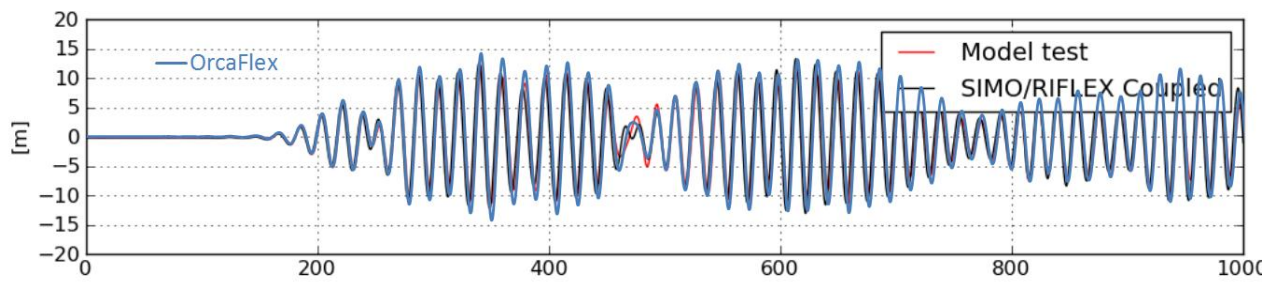


Figure 45: Test no 3710 FSU heave response 0 - 1000 sec.

### FSU response pitch

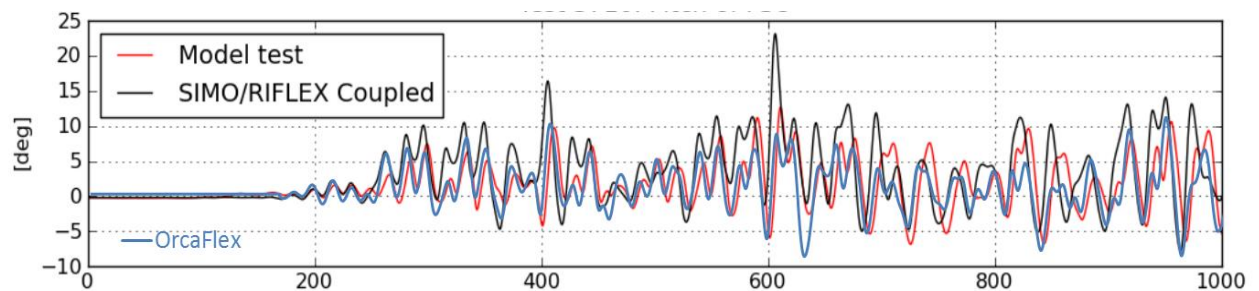


Figure 46: Test no 3710 FSU pitch response 0 - 1000 sec.



Test number 5120 and 5130 have the same trends as the simulations plotted above. The results can be found in Appendix F.

Test 3021, which has a real time length of 3000 seconds, had a simulation duration of approximately 12 days (!). The computer which was available for the OrcaFlex analyses was a 2 core 2.93 GHz laptop with 4 GB memory. The diving period, the viscous damping coefficients in pitch and the integration time increment were all either adjusted based on previously obtained results from the time series, or tested in order to ensure convergence. These are all reasons why the length of the OrcaFlex analyses is shorter than desired.



## 7 Comparison of power spectra

Unfortunately, the real time length of the results presented in the latter chapter is limited. The wave frequency response (first order) of the FSU from the OrcaFlex analyses looks to have acceptable compliance to both the model test and RIFLEX/SIMO results. Test 3021 reveals that the low frequency surge response obtained from the OrcaFlex analysis expresses good accordance to the low frequency phase and period of the model test and RIFLEX/SIMO results. The low frequency response amplitude can on the other hand seem to be slightly under predicted. In order to evaluate this more thoroughly, and in a context of predicting extreme events of the system, longer simulation lengths are needed.

The regeneration of the waves recorded during the model tests turned out to be very CPU-costly. In order to examine the OrcaFlex model more thoroughly, a 12 000 seconds analysis was carried out with waves generated from a Torsethaugen spectrum provided by the OrcaFlex software. I.e. the wave history which was recorded during the model test was not regenerated, but the operational environmental condition was established based on spectra formulation. This reduced the simulation time significantly, but the OrcaFlex time series was no longer directly comparable to the model test or RIFLEX/SIMO time series.

A Fast Fourier Transform was conducted on the resulting OrcaFlex time series in order to calculate the power spectra of the FSU response. There are different techniques applied to smooth the raw spectra in order to become continuous and to express the correct amount of energy and stochastic properties as it should. Marintek, responsible for both the model test report and the RIFLEX/SIMO report utilizes a Gaussian-shaped frequency window convolution to smooth the raw spectra (Appendix L). This was performed on the raw spectra obtained from the OrcaFlex time series, and compared to both the model test and the SIMO/RIFLEX power spectra. Test number 3021, containing the operational environmental condition, was used as the basis for power spectra comparison.

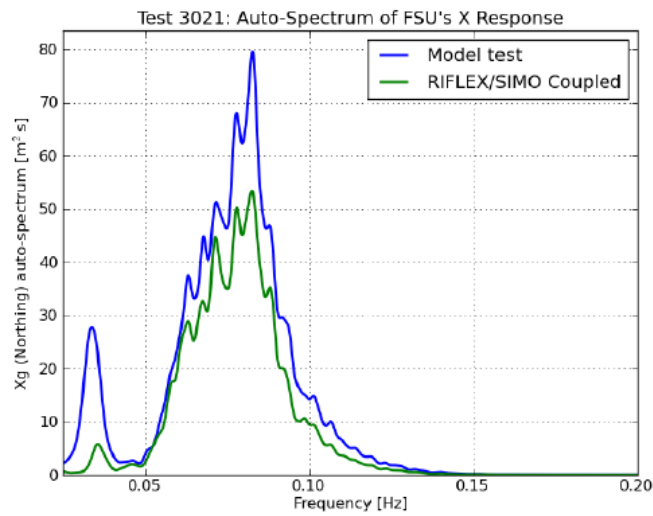


Figure 47: Power spectra of WF surge response from model test and SIMO/RIFLEX simulation

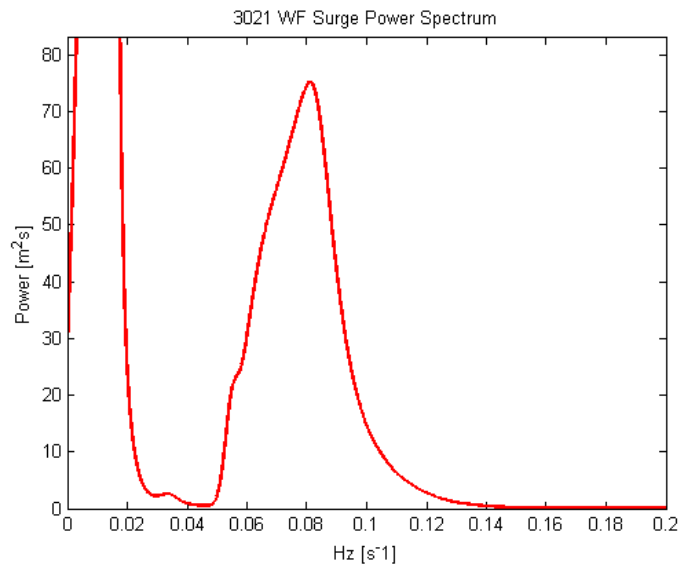


Figure 48: Power spectrum of WF surge response from OrcaFlex simulation

The power spectra of the wave frequency (WF) surge response all have peaks at a frequency of approximately  $0.08 \text{ s}^{-1}$  and a corresponding amplitude can be recognized at approximately  $75 \text{ m}^2 \text{ s}$ . Low frequency motion was not filtered away in figure 48 which represents the OrcaFlex results.

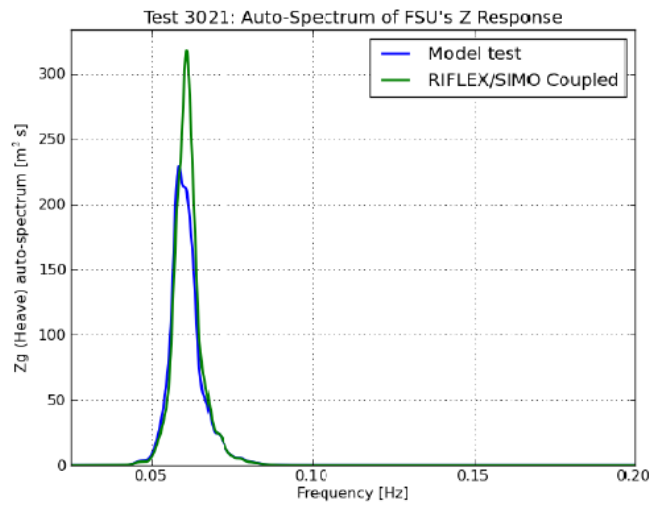


Figure 49: Power spectra of heave response from model test and SIMO/RIFLEX simulation

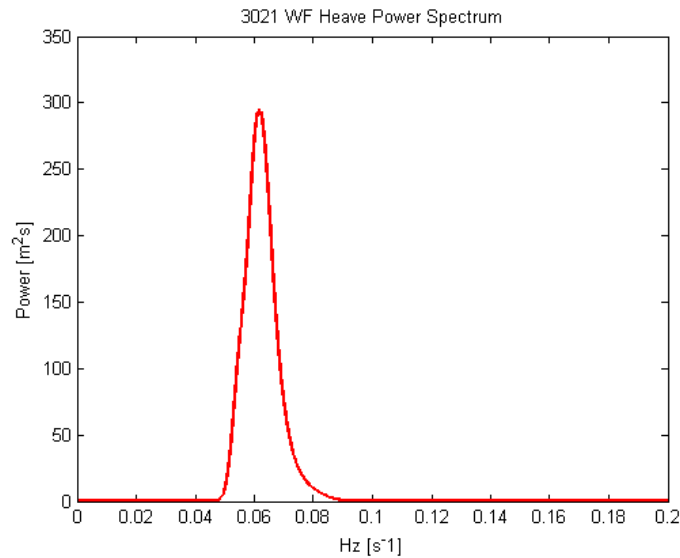


Figure 50: Power spectrum heave response from OrcaFlex simulation

Both the amplitudes and frequencies of the heave response power spectrum obtained from the OrcaFlex analysis coincides well with the model test results. From the response time series in chapter six it can be seen that heave also is the mode with the best compliance to both the model test and the RIFLEX/SIMO simulation.

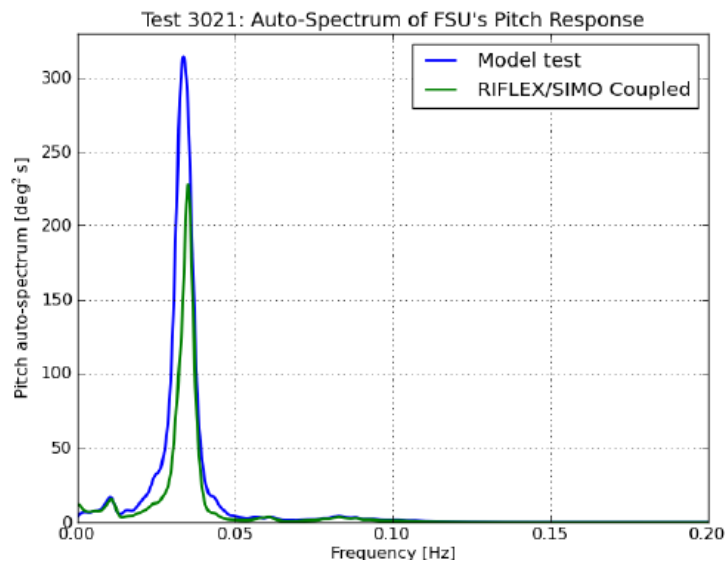


Figure 51: Power spectra of pitch response from model test and SIMO/RIFLEX simulation

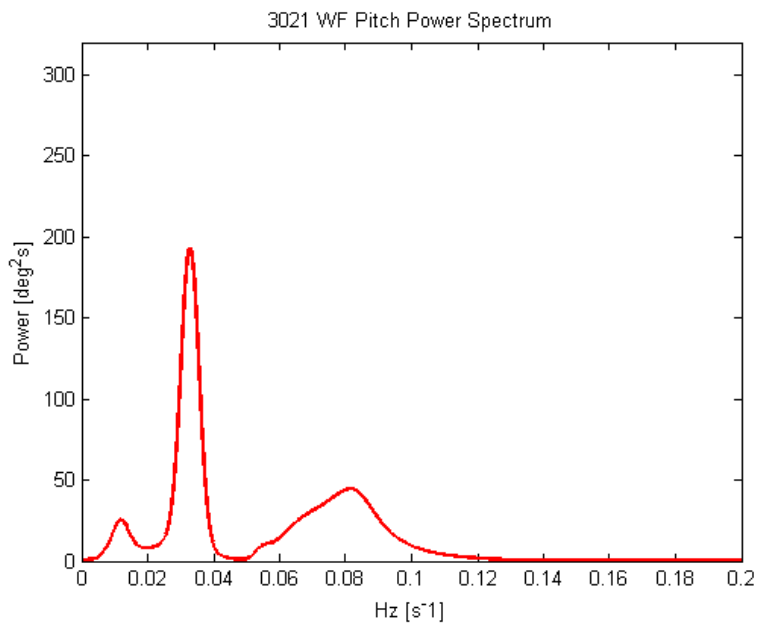


Figure 52: Power spectrum pitch response from OrcaFlex simulation

The power spectrum obtained from the OrcaFlex simulation shows a peak at approximately  $0.03 \text{ s}^{-1}$ . The amplitude of the spectrum, i.e. the corresponding energy at this frequency, shows an under prediction of the OrcaFlex results compared to model test, but coincides well with the SIMO/RIFLEX result. The source of the energy observed at  $0.08 \text{ s}^{-1}$  is unknown.

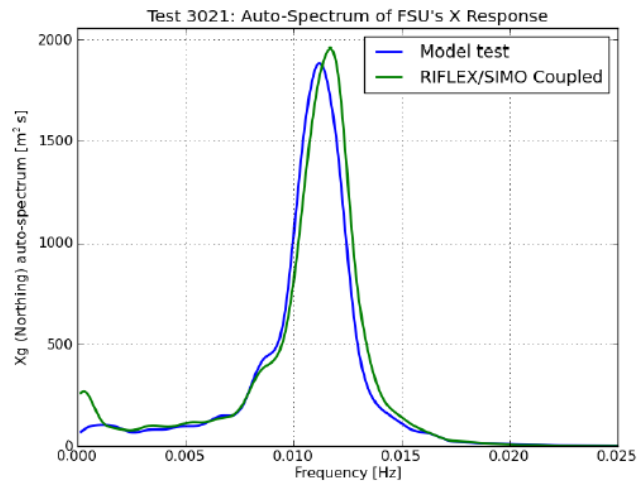


Figure 53: Power spectra LF surge response from model test and SIMO/RIFLEX

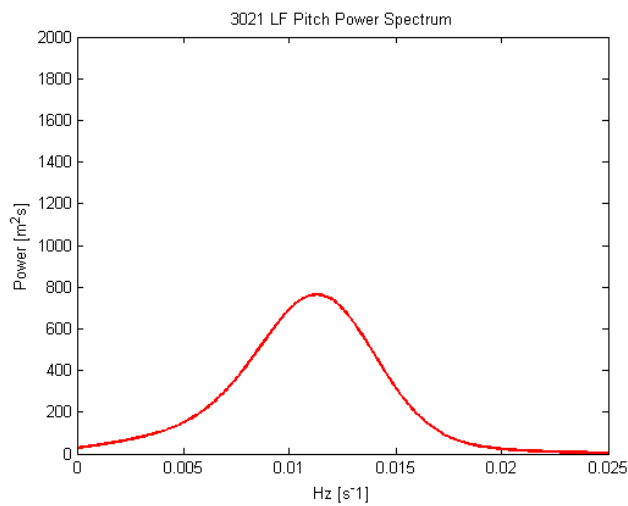


Figure 54: Power spectrum LF surge response from OrcaFlex simulation

The energy peak of the low frequency surge response of the FSU can in all three spectra be recognized at a frequency of approximately  $0.011 \text{ s}^{-1}$ . This corresponds well with the damped natural period of the system from decay test number 1250, which is approximately 89 seconds.

The energy level at this frequency in the OrcaFlex spectrum is on the other side not in accordance with the energy obtained from the model test and RIFLEX/SIMO simulation.



## 8 Uncertainties related to parameters used in the analyses

The implementation of the different analyses carried out in this report contains both assumptions and uncertainties that should be evaluated.

### 8.1 Mooring systems

The mooring line loads were calculated with Morison's equation, and drag coefficients independent of Reynolds number were applied. The accuracy of this procedure is unknown. The choice of  $C_M = 2$  is not well argued, but the inertia related to the mooring lines in a water depth of 108 meters was assumed to be small compared to the hull, and this was not further investigated.

The stiffness of the mooring systems, illustrated in figure 17 and 18, show a small over prediction of the OrcaFlex mooring stiffness compared to the model tests. The differences are small relative to amplitude of the stiffness. Taking into account that the low frequency excitation force in general may be low, this could influence the amplitude of low frequency response.

The mooring lines were assumed to have constant modulus of elasticity during the coupled analyses. The outcome of this assumption was believed not to influence the results presented in this report.

### 8.2 Diffraction analysis

Firstly, the cut out radius of the FSU bilge keel was estimated. In particular, the added mass and damping coefficients in heave and pitch are influenced by the bilge keel geometry. The process described in sections 5.4, where the cut out length is estimated based on the volume displacement can be inaccurate taking into account that quadrilateral elements used for the FE-model are flat, i.e. the volume displacement is likely to be under predicted. The





pitch and heave added mass and potential damping coefficients of the FSU were on the other hand compared to WAMIT results presented in the SEVAN 1000 FSU – Numerical Simulation Report. Through visual inspection the WAMIT and WADAM coefficients had good compliance. The compliance was also believed to verify that the stiffness matrix applied during the diffraction analysis was acceptable. Results obtained in chapter 6 and 7 also verify that the OrcaFlex wave frequency responses have good compliance to the model test and RIFLEX/SIMO results.

The implementation of the eddy-making viscous damping during the diffraction analysis was based on results from the model tests. Eddy-making damping is a non-linear damping effect, and only a linear coefficient was applied during the analysis. As previously stated, the damping was only added in the resonant period of heave, i.e. approximately 17 second. The influence of the level of eddy-making should in other words be most recognizable in test 3710, as environmental condition number four had a  $T_p$  of 17.6 seconds. The OrcaFlex results do not seem to differ more in test 3710 than in other irregular wave tests compared to the model test and RIFLEX/SIMO simulation. The mean wave drift coefficients obtained from the diffraction analysis were also compared to the mean wave drift coefficients estimated in the SEVAN 1000 FSU – Numerical Simulation Report, and the comparison showed good accordance.

### **8.3 Viscous effects**

The viscous damping coefficients estimated for pitch in section 5.5 gave satisfactory results in the numerical reconstruction of decay test 1380, but during the irregular wave tests these coefficients had to be adjusted in order to give better accordance to the model test results. For the pitch viscous damping coefficients this can be interpreted to underpin the fact the eddy-making damping is larger in waves than in calm water. It can be observed from the time series that the final viscous damping coefficients seem to under predict the pitch response in test number 3021, while the opposite looks to occur in test 3710. The reason for



this was not explored, but these amplitudes are assumed to be influenced by other factors, e.g. the local KC-number, bilge keel geometry and higher order effects.

The viscous damping coefficients for heave obtained in section 5.5 turned out to over predict the damping. One can easily see that the points plotted in figure 23 (decay test 1330 heave) are scattered, and that this will influence the regression done to obtain the damping coefficients for the heave motion. (Faltinsen, 1990) addresses the challenges of finding a straight line by the least square method and explains that this can be a problem if the damping force has a large KC-number dependence and if the oscillating system is not lightly damped. The reason is that the maximum velocity can change significantly for each subsequent oscillation period, leading to the  $p_1$  and  $p_2$  obtained being inaccurate. Regardless of this, the final viscous damping coefficients for heave applied in the OrcaFlex analyses gave good compliance to the model test during irregular wave tests.

The viscous damping coefficients of the FSU in surge were simply determined with basis in the numerical reconstruction of decay test number 1250. In order to determine the viscous damping coefficients in surge of a hull like the FSU, it could be beneficial to run a model test with regular waves in order to examine the first order motion of the FSU without the difference frequency effects being present.

#### **8.4 Second order motion obtained by the OrcaFlex analyses**

The final dividing periods used in the OrcaFlex numerical simulations were 23, 23, 25 and 27 seconds. The wave frequent response of the FSU was assumed to have frequencies close to the wave frequencies of the corresponding wave spectrum.

There is still uncertainty related to whether the dividing periods used in the OrcaFlex analyses are optimal or not, but figure 30, together with the input from Orcina, were assumed to support these choices.



The OrcaFlex analyses clearly represent a slow-drift motion of the FSU which phase corresponds to the model tests and SIMO/RIFLEX results. The amplitude of the low frequency motion is determined by the second order excitation load, and the stiffness, damping and inertial properties of the system. The low frequency damping coefficients calculated by OrcaFlex are inaccessible through the standard user interface. They are, however, implemented in the analyses through the modification of the QTF matrix established by Newman's approximation. This was described in section 5.7.4.

Whether Newman's approximation and the OrcaFlex method of estimating the slow drift damping are good estimations for the prediction of a Sevan hull's second order motion, is a comprehensive question. It is also hard to state how well the OrcaFlex analyses predict the low frequency motion of the FSU based on the short real time lengths of the simulation performed in relation with this thesis.

It is interesting that also RIFLEX/SIMO utilizes Newman's approximation in order to estimate the second order difference frequency excitation of the FSU. In the SEVAN 1000 FSU – Numerical Simulation Report it can also be found that Aranha's method was the basis for the establishment of the low frequency damping coefficients of the FSU in the RIFLEX/SIMO simulations. It is also stated in the report that the coefficients are adjusted in order to account for current effects and later adjusted again in order to obtain a better compliance with the model test results. The extent of these RIFLEX/SIMO adjustments remains unknown, but taking into consideration that both Newman's and Aranha's methods are *approximations*, it would be beneficial if these coefficients were available through the user interface of OrcaFlex.

## **8.5 Power spectra calculation**

There are uncertainties related to the transformation of the OrcaFlex time series to the power spectra. This comprises the energy calculations performed in MatLab (Appendix K), the filtering of the motion (dividing period) and to the smoothing of the raw spectra.



Marintek did share their smoothing convolution, but still it is obvious from chapter 7 that there are differences in the applied smoothing technique applied on the OrcaFlex time series and the model test and RIFLEX/SIMO results. How this influences the results, especially the amplitude of the power spectra, remains unknown.

It is also unknown, for the author, how well the wave making system in the Marintek basin generated waves that corresponds to the operational Torsethaugen spectrum which is stated to be the input for the wave making system (Muthanna, 2011). This is a relevant topic because the power spectra from the model tests and RIFLEX/SIMO simulations were obtained from the exact same wave history record. The power spectra from the OrcaFlex analysis were as previously described obtained from an analysis where a Torsethaugen spectrum provided by OrcaFlex was used to drive the numerical simulation.



## 9 Summary and conclusion

One of the main challenges during the work with this thesis has been the great CPU-cost of the coupled analyses when the model test wave and wind history were incorporated in the OrcaFlex analyses. As previously stated, a number of parameters needed adjustment based on the time series results, and these processes became very time consuming. Looking back at the scope of the work, it could have been more reasonable to focus on only one mooring system, and/or fewer environmental conditions. In the early stages of the analyses, a time series of 12 000 seconds of the recorded wave elevation was imported to OrcaFlex. An attempt of starting the dynamic simulation was done, but the calculations did not progress. I.e. for long real time simulation higher capacity hardware is needed.

Viscous effects are not accounted for by potential theory. In order to determine the viscous damping coefficients for a hull like the Sevan FSU, data of model test response in waves are required as basis for comparison. Experiences gained from the work with this report imply that numerical methods based on decay tests only soon become incorrect.

The second order slow drift motion of moored structures like the FSU is an important parameter in the design verification of a system. In order to predict the extreme events of the slow drift motion it is common practice to conduct several simulations of 3 hours. Based on the result presented in this report it is hard to give a precise comment on how the slow-drift motion was predicted by the OrcaFlex analyses compared to both the model test and the RIFLEX/SIMO simulations. Based on interpretation of the limited time series in chapter 6, it appears as though the coupled analyses performed in OrcaFlex under predict the amplitude of the slow drift response of the FSU compared to the model test. Results from the RIFLEX/SIMO simulations look to obtain slightly better compliance with the model test results, but does on the other hand obtain an almost identical power spectrum of the low frequency response compared to the model test. The latter statement should however not be greatly emphasized as there are considerable uncertainties related to the power spectra calculations described in section 8.5.



The most likely sources of the OrcaFlex deviation compared to the model test results are believed to be one or more of the following:

- The system modeling in OrcaFlex was somehow inaccurate or different from the model test.
- Under prediction of the mean wave drift excitation coefficients obtained from WADAM
- Over prediction of the slow drift damping by the method incorporated in OrcaFlex



## **10 Proposal for further work**

There are a number of parameters, effects, and methods of calculation that can be further investigated in the context of a coupled analysis.

Based on the topic of this thesis, and based on the personal experiences gained during the work with OrcaFlex, the following points must be listed:

- Gain more knowledge on how OrcaFlex filters the vessel response, and how this influences the algorithms used to calculate the resulting vessel response during dynamic analyses.
- Conduct a more thorough study of the observations done by Aranha. A better understanding of these observations could result in more knowledge on when the method is applicable, and of its limitations.

Disregarding these 'personal' steps, one of the main objectives of a coupled analysis is to predict the low frequency motion of moored structures. In order to predict extreme events, and to gain a better basis for evaluating the OrcaFlex numerical model, the FSU response should be simulated for a longer real time period.



## 11 Bibliography

**Astrup, Ole Chr.** *DeepC Coupled Analysis Tool* . 2004.

**Carl Trygve Stansberg, Harald Ormberg & Ola Oritsland.** *Challenges in Deep Water Experiments: Hybrid Approach*. 2002.

**Cesnik, Christopher M. Shearer and Carlos E.S.** *Modified Generalized  $\alpha$ - Method for Integrating Governing Equation of Very Flexible Aircraft*. 2006.

**Faltinsen, O.M. 1900.** *SEA LOADS ON SHIPS AND OFFSHORE STRUCTURES*. s.l. : Cambridge University Press, 1900.

**Garrett, D.L.** *Coupled Analysis of Floating Production Systems* . 2005.

**Greco, Marilena.** *Lecture Notes TMR 4215: Sea Loads*.

**Hermans, Aad J.** *Low-frequency second-order wave drift forces and damping*. 1997.

**Hulbert, J. Chung & G. M.** *A Time Integration Algorithm for Structural Dynamics With Improved Numerical Dissipation: The Generalized-Alpha Method*.

**Kendon, Timothy.** *Sevan 1000 FSU - Numerical Simultaions Final Report*. s.l. : Norsk Marinteknisk Forskningsinstitut AS , 2011.

**Larsen, Carl M.** *Marin Dynamikk*. 2012.

**Lee, C.-H.** *Wamit theory manual*. s.l. : Cambridge, 1995.

**Marine, Sevan.** *Model Test Specification*. 2011.

**Massie, J.M.J. Journée and W.W.** *OFFSHORE HYDROMECHANICS DELFT UNIVERSITY OF TECHNOLOGY*. 2001.

**Moan.** *Nonlinear analysis Addendum to TMR4305* . 2007.

**Muthanna, Chittiappa.** *Sevan Mariner Model Tests Report*. 2011.





**Myrhaug, Dag.** *Marin Dynamikk.*

**Newman, C.-H. Lee & J.N.** *Computation of wave effects using the panel method.*

**Newman, J.N.** *Marine Hydrodynamics.* 1977.

**O.C. Astrup, A. Nestegård, M. Ronæs and N. Sødahl.** *Coupled Analysis Strategies for Deepwater Spar Platforms.*

**Orcina.** *OrcaFlex Manual Version 9.6 .*

**Pettersen, Bjørnar.** *Hydrodyamikk .* 2007.

**Pinkster, J.A.** *Low frequency second order wave exciting forces on floating structures.*

**Sierevogel, Aad J Hermans & Lisette M.** *A discussion on the second-order wave forces and wave drift damping.* 1997.

**Sigbjörnsson, Ivar Langen og Ragnar.** *DYNAMISK ANALYSE AV KONSTRUKSJONER.*

**Steen, Sverre.** *Experimental Methods in Marine Hydrodynamics.* 2012.

**Tuncer Cebeci, Jian P. Shao, Fassi Kafyeke & Eric Laurendeau.** *Computational Fluid Dynamics for Engineers.* 2005.

**VERITAS, DET NORSKE.** *POSITION MOORING DNV-OS-301.* 2010.

**VERITAS, DET NORSKE.** *ENVIRONMENTAL CONDITIONS AND ENVIRONMENTAL LOADS.* s.l. : DNV, OCTOBER 2010.

**Vugts, J.H. 1997.** *Behaviour of offshore structures.* 1997.



## Appendices

### Appendix A - Input WADAM analysis

#### MOORING SYSTEM STIFFNESS

K11=K22      1300000 [N/m]

Z\_fairlead      -22,5 [m]

K24              29250000 [Nm/m]

K15              -29250000 [Nm/m]

K44              658125000 [Nm<sup>2</sup>/m]

K55              658125000 [Nm<sup>2</sup>/m]

K66              100000000 [Nm<sup>2</sup>/m]

	1	2	3	4	5	6
1	1,30E+06	0,00E+00	0,00E+00	0,00E+00	2,93E+07	0,00E+00
2	0,00E+00	1,30E+06	0,00E+00	2,93E+07	0,00E+00	0,00E+00
3	0,00E+00	0,00E+00	0,00E+00	0,00E+00	0,00E+00	0,00E+00
4	0,00E+00	2,93E+07	0,00E+00	6,58E+08	0,00E+00	0,00E+00
5	2,93E+07	0,00E+00	0,00E+00	0,00E+00	6,58E+08	0,00E+00
6	0,00E+00	0,00E+00	0,00E+00	0,00E+00	0,00E+00	1,00E+08

Table 13: Stiffness matrix used in diffraction analysis

#### EDDY MAKING DAMPING

$$A_{33} = 1.95 \times 10^8 \text{ kg (from diffraction analysis)}$$

$$M_{33} = 1.844 \times 10^8 \text{ kg (from FSU particulars)}$$

$$C_{33} = 5.7 \times 10^7 \frac{N}{m} \text{ (from FSU particulars and equation 3.9)}$$



$$B_{cr} = 2 \cdot \sqrt{(1.844 \times 10^8 + 1.95 \times 10^8) \text{kg} \cdot 5.7 \times 10^7 \frac{\text{N}}{\text{m}}} = 295 \times 10^6 \text{N} \cdot \frac{\text{s}}{\text{m}}$$

$$B_{33} = 0.08 B_{cr} = 23600 \text{kN} \frac{\text{s}}{\text{m}}$$



## Appendix B- Estimation of viscous damping coefficients

### DAMPING PITCH LOADED TEST 1320

```
%% Input from Sevan Mariner Model Tests Report %%
```

```
T_d = 29.41; % [s] Mean period from Marintek report
M = 184400000; % [kg] Mass from Sevan report
gyr_rad = 28.2; % [m] Radius gyration pitch from Sevan
report

GM_loaded = 5.9; % [m] GM from Sevan report
g = 9.81; % [m/s^2]
dens_w = 1025; % [kg/m^3]
vol_disp = 179902; % [m^3] Volume displacement from Sevan
report

C55 = g*dens_w*vol_disp*GM_loaded; % [Nm/rad]
A55 = 117000000000; % [kg*m^2] Value from radiation analysis

Tn5= 2*pi*sqrt((M*gyr_rad^2 + A55)/C55); % Natural undamped oscillation period

Xn= [5.334 3.5903 2.6523 2.0906 1.7084 1.4285 1.21 1.0390 0.9081 0.8010...
      0.7059 0.6215 0.544 0.4949 0.4498] * (pi/180); % [rad]

Xn_m1= [-4.3326 -3.0562 -2.3417 -1.8825 -1.5566 -1.3170 -1.1158 -0.973...
        -0.8493 -0.7517 -0.6634 -0.5815 -0.5134 -0.4771 -0.4189]*(pi/180); % [rad]

horizontal_vector = 16/3 * Xn/T_d;

d = log(abs(Xn_m1)./Xn);

p= -4*pi/T_d .* d./sqrt(pi^2 + d.^2);
```

```
%% plotting measured points %%
```



```
scatter(horizontal_vector,p);
xlim([0,max(horizontal_vector)]);
ylim([0,max(p)]);
ylabel(' p [1/s] ');
xlabel(' 16/3 Xn/Td [rad/s] ');
coeff = polyfit(horizontal_vector,p,1);
title('Test 1320 Pitch')

% Coefficients from least square test %

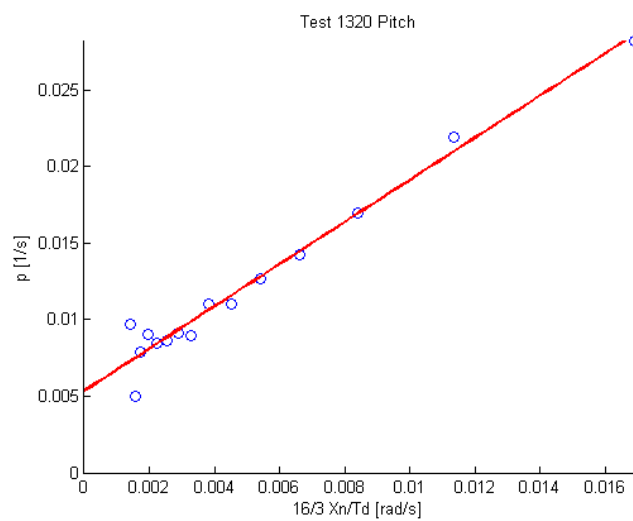
p1 = coeff(2) % [1/s]
p2 = coeff(1) % [1]
```

```
%% plotting ax+b %%
```

```
hold on
x=linspace(0,max(p));
y=p1+p2*x;
plot(x,y,'r','linewidth',2);
```

```
%% damping coefficients %%
```

```
B_linear = p1 * (A55 + M*gyr_rad)/1000 % [kNm/(rad/s)]
B_quadratic = p2 * (A55 + M*gyr_rad)/1000 % [kNm/(rad/s)^2]
```





### DAMPING HEAVE LOADED TEST 1330

```
%% Input from Sevan Mariner Model Tests Report %%

T_d = 16.8; % [s] Mean period from Marintek report
M = 184400000; % [kg] Mass from Sevan report

GM_loaded = 5.9; % [m] GM from Sevan report
g = 9.81; % [m/s^2]
dens_w = 1025; % [kg/m^3]
area_water = 5674.5; % [m^2] Waterline area from Sevan report

C33 = g*dens_w*area_water; % [N/m]
A33 = 198000000; % [kg] Value from radiation analysis

Tn3= 2*pi*sqrt((M + A33)/C33); % Natural undamped oscillation period

Xn= [3.0238 2.0016 1.3414 0.94092 0.67698 0.48705 0.3523 0.26856 0.21290...
     0.17146]; % [m]

Xn_m1= [-2.4677 -1.6256 -1.1232 -0.79325 -0.57795 -0.40938 -0.30816 ...
        -0.23704 -0.19004 -0.15731]; % [m]

horizontal_vector = 16/3 * Xn/T_d;

d = log(abs(Xn_m1)./Xn);

p= -4*pi/T_d .* d./sqrt(pi^2 + d.^2);

%% plotting measured points %%

scatter(horizontal_vector,p);
xlim([0,max(horizontal_vector)]);
ylim([0,max(p)]);
ylabel(' p [1/s] ');
xlabel(' 16/3 Xn/Td [m/s] ');
coeff = polyfit(horizontal_vector,p,1);
title('Test 1330 Heave')
```



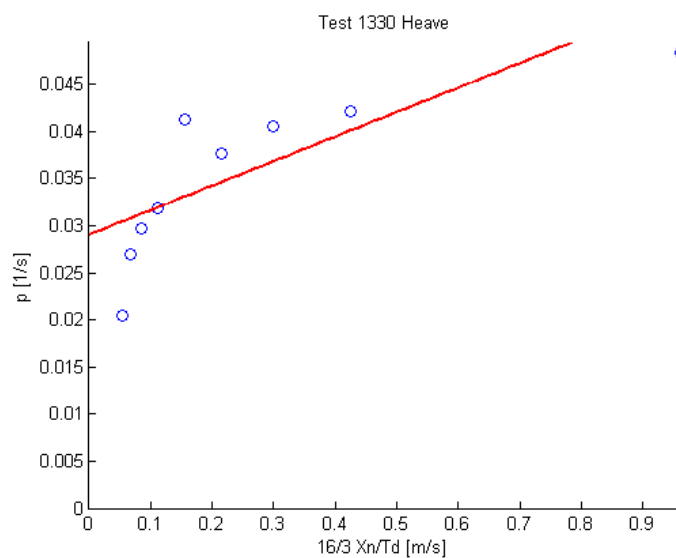
```
p1 = coeff(2) % [1/s]
p2 = coeff(1) % [1/m]
```

```
%% plotting ax+b %%
```

```
hold on
x=linspace(0,max(horizontal_vector));
y=p1+p2*x;
plot(x,y,'r','linewidth',2);
```

```
%% damping coefficients %%
```

```
B_linear = p1 * (A33 + M)/1000 % [kN/(m/s)]
B_quadratic = p2 * (A33 + M)/1000 % [kN/(m/s)^2]
```





## Appendix C- Decay tests chain mooring system

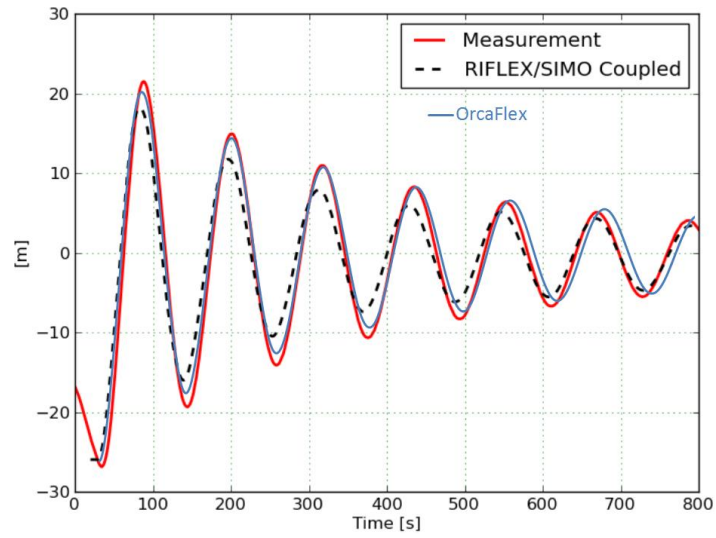


Figure 55: Numerical reconstruction of decay test 1950 (surge)

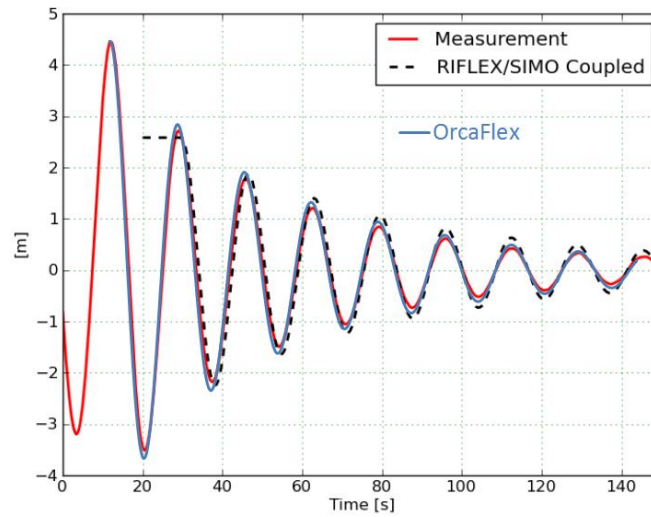


Figure 56: Numerical reconstruction of decay test 1930 (heave)



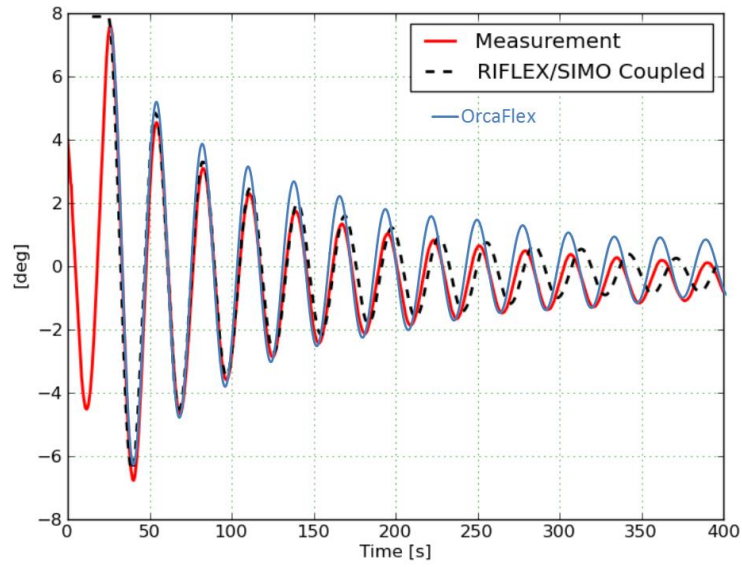


Figure 57: Numerical reconstruction decay test 1940 (pitch)

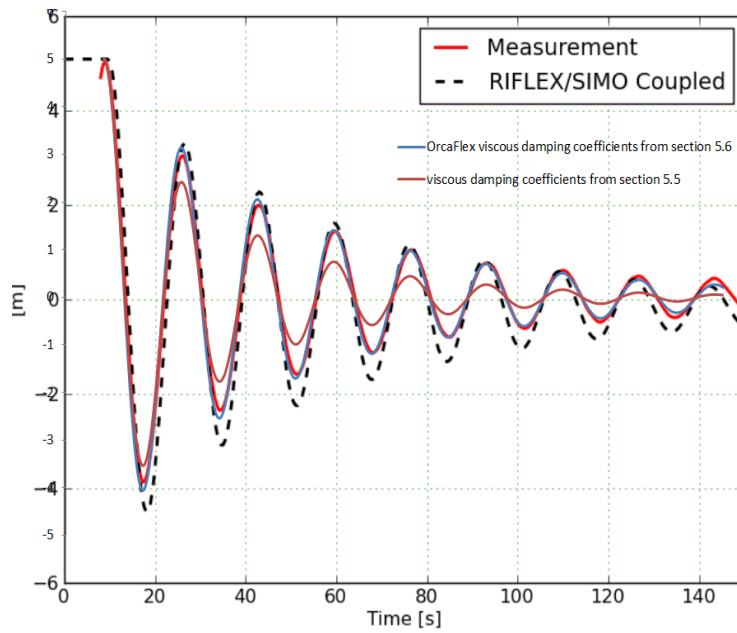


Figure 58: Decay test 1370 with applied viscous damping coefficients from section 5.5.

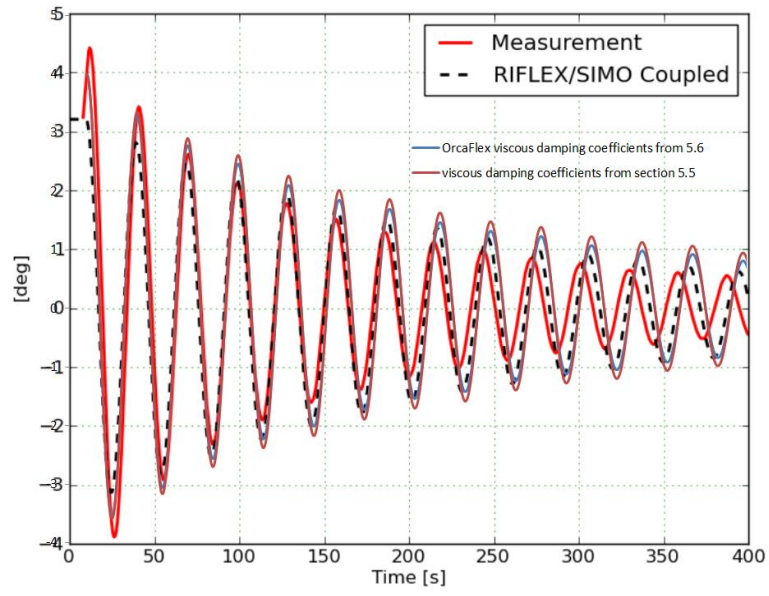


Figure 59: Decay test 1380 with applied viscous damping coefficients from section 5.5.



## Appendix D- Orcina support on system stiffness

Erik,

Indeed, our default static iteration method, called 'Line Search' on the line data form, is based on the Newton-Raphson method. If you want full details, our line search is based on the Numerical Recipes line search algorithm, which improves on the basic Newton-Raphson method to achieve better global convergence properties. I'm sure you have heard of the book, so that's the best reference I can provide.

I feel that I should mention that the OrcaFlex line full statics calculation is more sophisticated than a typical catenary calculation, including effects such as seabed contact and drag from current.

I hope that this is enough information. Do let us know if you need anything else.  
Regards,

Colin Lewis.  
Orcina Limited,  
Daltongate, Ulverston, Cumbria,  
LA12 7AJ, UK  
Tel: +44 (0)1229 584 742  
Fax: +44 (0)1229 587 191  
Email: [orcina@orcina.com](mailto:orcina@orcina.com)  
Web: [www.orcina.com](http://www.orcina.com)

<erikbha@stud.ntnu.no> 03/06/2013 10:24 >>>

Hi Colin.

Thank you very much for the answer.

I have, however, just one quicker question.

I'm searching for information on how the system stiffness is found in OrcaFlex. My model consists of a vessel and mooring lines. I've read in the manual that OrcaFlex uses the catenary equation and an iterative method to find the system equilibrium (statics).

What kind of algorithm is used in this iterative process? Does it have basis in e.g. Newton-Raphson or similar processes?

If you have the time it would be appreciated.

Regards,

Erik



## Appendix E- Orcina support on dividing period

Hi Erik,

Setting Dividing Period

As you have realised, this is not straightforward when the low frequency and wave frequency responses are close together. There are a couple of options, which I've outlined below, using your case with 12s wave period, 90s second order period.

Firstly, a simplified (rule of thumb) approach could be to simply use the mean of the frequencies (this was originally proposed by one of my colleagues in the software team):

Dividing Freq. =  $(LF + WF) / 2 = 0.5 * [(1/12) + (1/90)] = 0.047\text{Hz}$   
=> Dividing Period = 21s

This is pretty close to your proposed value.

Alternatively, since OrcaFlex uses a low-pass filter, there may be another approach. If you take a look at the graphs of filter performance in the OrcaFlex help page VIV Toolbox | Time Domain Models | Time Domain Models (the same filter is used for the VIV tools :-)), you can see that responses with periods longer than the dividing period are passed through, while responses with period shorter than the dividing period are attenuated. In other words, the filter allows the low frequency motions to pass through and the wave frequency motions are filtered out. Knowing this, it is possible to choose to set the dividing period closer to the lowest resonant period. This is generally OK because we know that periods a only bit longer than the dividing period will be passed through almost unaltered.

For example, ignoring phase lag (which may be less important for a system with irregular waves anyway), we can see that the filtered amplitude is almost 1 for periods twice the dividing period; for periods three times the dividing period we have almost the full response passing through unfiltered. If we were happy to have the lowest resonant period (90s) being twice the filter period then this would imply a dividing period of 45s, If we were happier to have the lowest resonant period (90s) being three times the dividing period, then this would imply a dividing period of 30s. Both options are produce longer filter periods than your current dividing period. This has the advantage of hopefully allowing more of the wave frequency motions to be adequately filtered out (which may be



important if you have many wave components with periods  
>> significantly longer than 12s).

>>

I would probably take one case of interest and perform a brief  
sensitivity study on dividing period - try a few different values  
and see how much difference it makes.

Best Regards,  
Sarah

Sarah Ellwood  
Orcina Limited,  
Daltongate, Ulverston, Cumbria,  
LA12 7AJ, UK  
Tel: +44 (0)1229 584 742  
Fax: +44 (0)1229 587 191  
Email: [orcina@orcina.com](mailto:orcina@orcina.com)

Web: [www.orcina.com](http://www.orcina.com)

Hi Sarah.

I have done several time domain analyses of the moored vessel  
that I'm working on. I have used a 'Time history' wave type, which  
enables me to compare my OrcaFlex results directly to model test  
results. This is very CPU-costly, so the length of these simulations is  
limited. Due to this, I'm running the moored structure with wave type  
'Torsethaugen spectrum', with parameters that corresponds to the sea  
state which was used during the model tests. Further I'm extracting  
the resulting time series and converting them to power spectra. In  
this context, I wish to analyze the primary x and low frequency x  
separately.

This is an available option in the OrcaFlex 'Select Results'. The  
power spectra I get from this procedure do not comply with what I want to find. In  
this context

I once again wonder how the 'Dividing period should be determined. I  
realize that this determines the 'filtering' of wave and low frequency  
X-motion. So far I have tried out the following reasoning, e.g.:

    Tp seastate : 12s  
    Dividing period : 20s

The damped period of oscillation of my system in surge is  
approximately 90 seconds.



Is there any theory/tips that exceed the OrcaFlex manual that you can share?

Regards

Erik Byholt Hanssen

<erikbha@stud.ntnu.no> 02-May-13 10:00



## Appendix F- Irregular wave tests chain mooring system

### 5120 SURGE

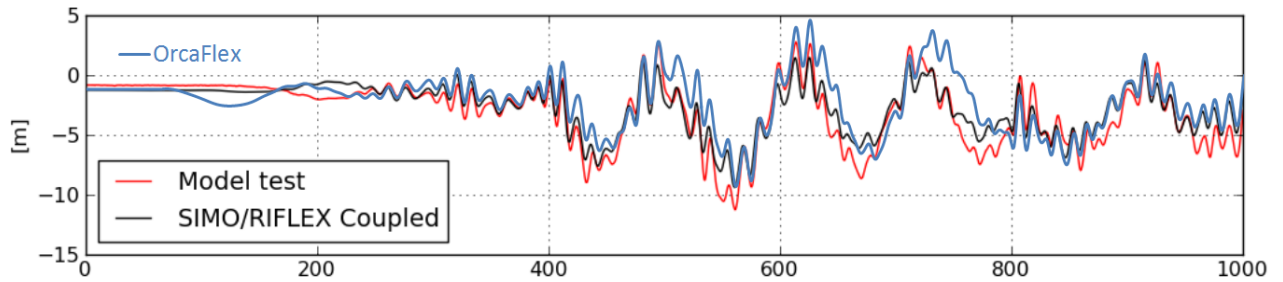


Figure 60: Test no 5120 FSU surge response 0 - 1000 sec.

### 5120 HEAVE

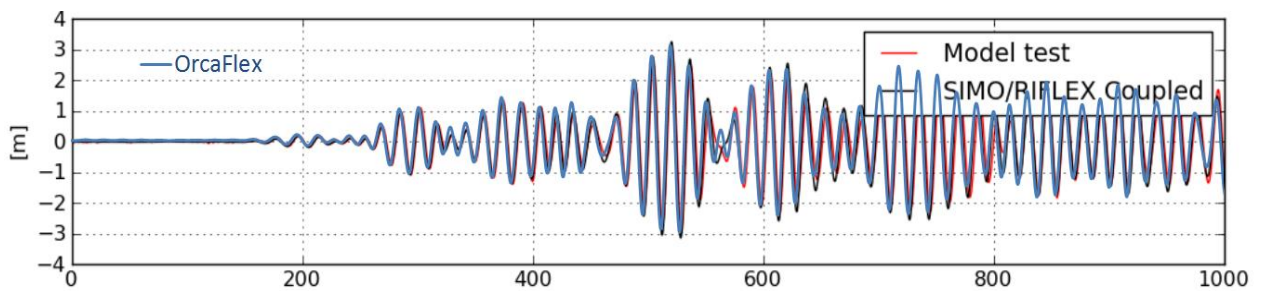


Figure 61: Test no 5120 FSU heave response 0 - 1000 sec.

### 5120 PITCH

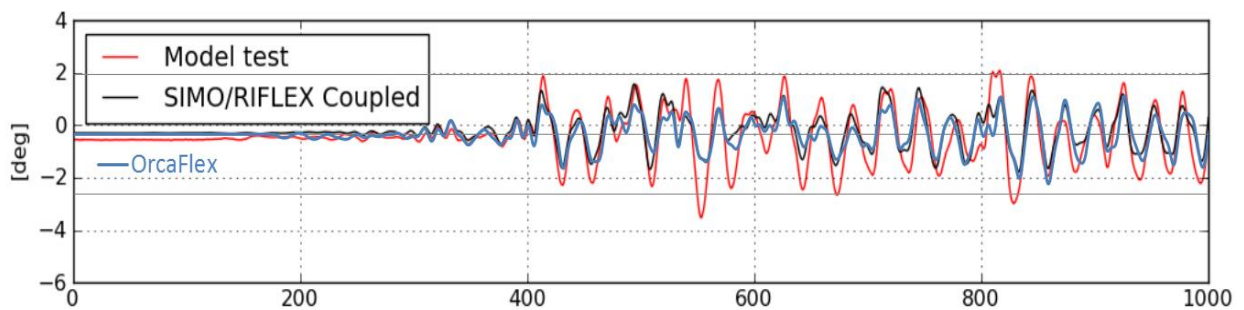


Figure 62: Test no 5120 FSU pitch response 0 - 1000 sec.



### 5130 SURGE

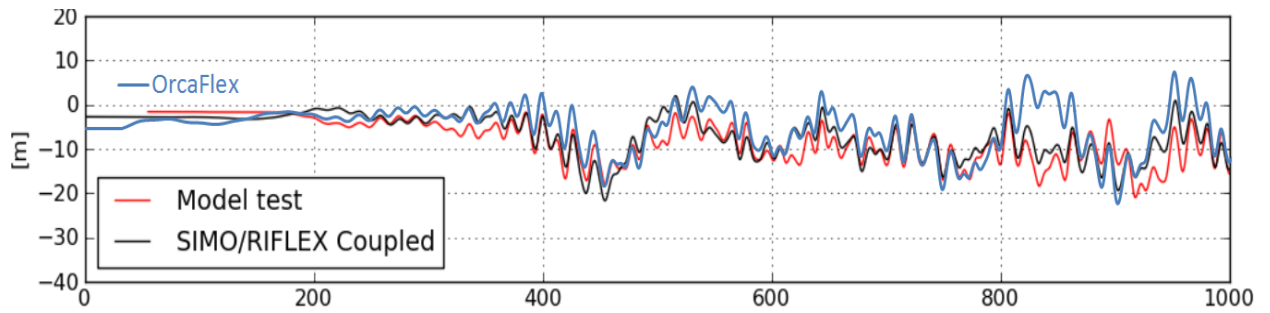


Figure 63: Test no 5130 FSU surge response 0 - 1000 sec.

### 5130 HEAVE

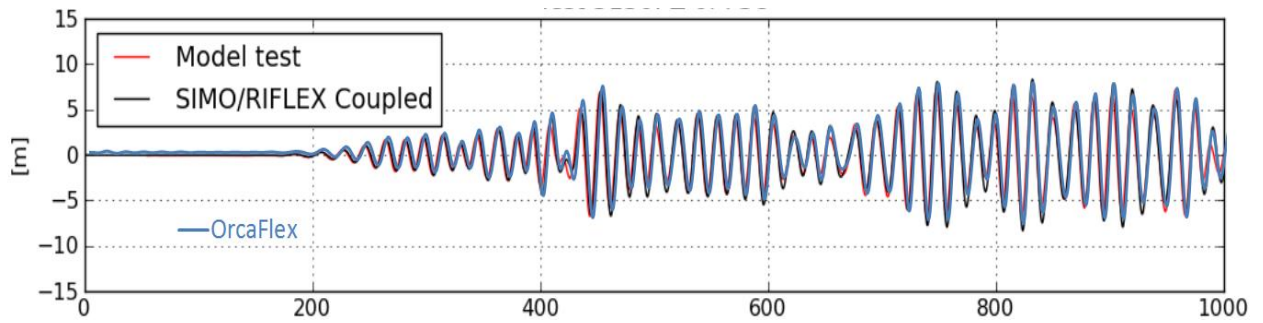


Figure 64: Test no 5130 FSU heave response 0 - 1000 sec.

### 5130 PITCH

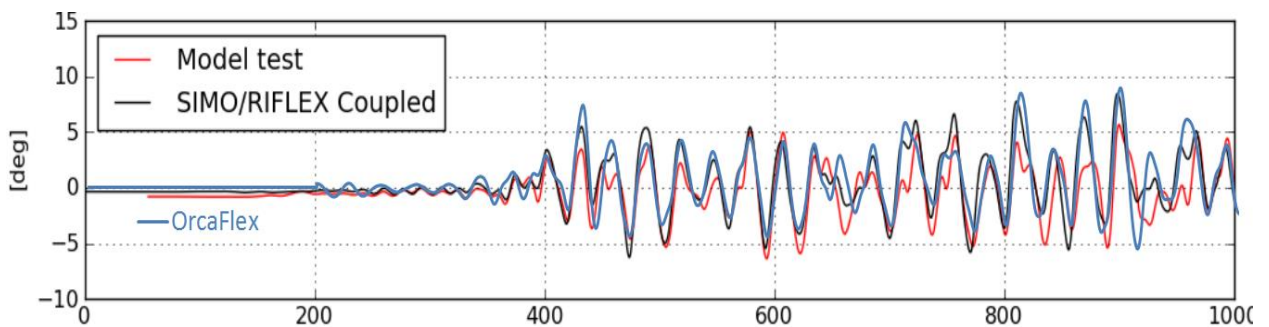


Figure 65: Test no 5130 FSU surge response 0 - 1000 sec





## Appendix G - Wave excitation coefficients FSU 1000

SESAM POSTRESP 6.2-04

22 MAR 2015

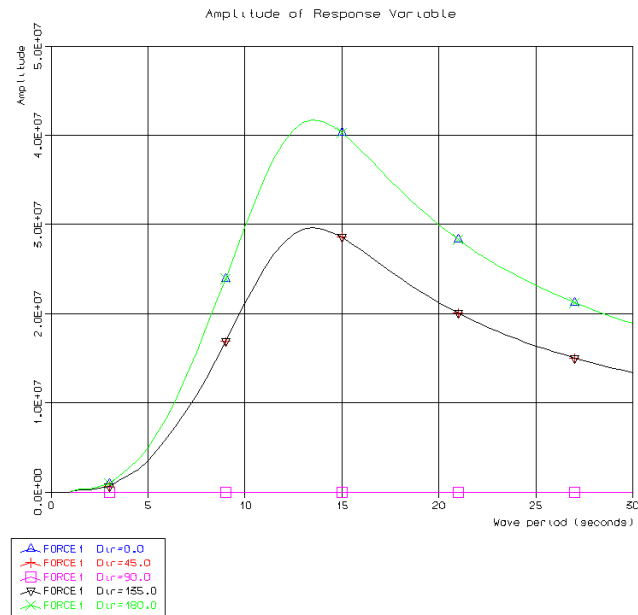


Figure 66: Wave excitation coefficients surge

unit of ordinate [N/m]

SESAM POSTRESP 6.2-04

22 MAR 2015

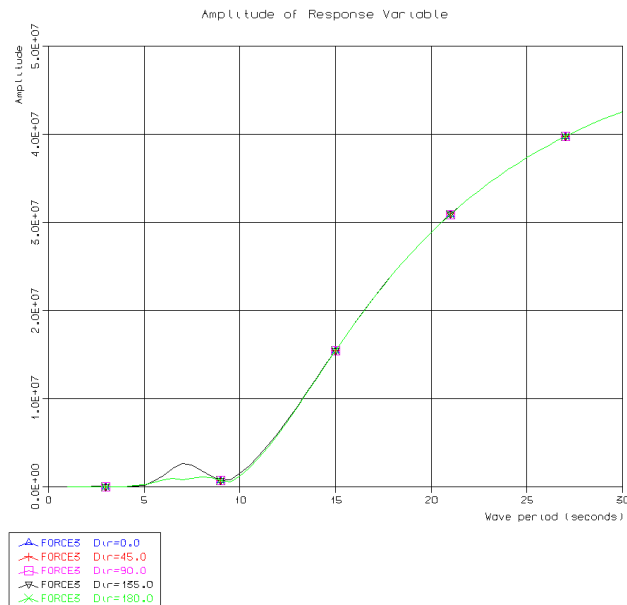


Figure 67: Wave excitation coefficients heave

unit of ordinate [N/m]

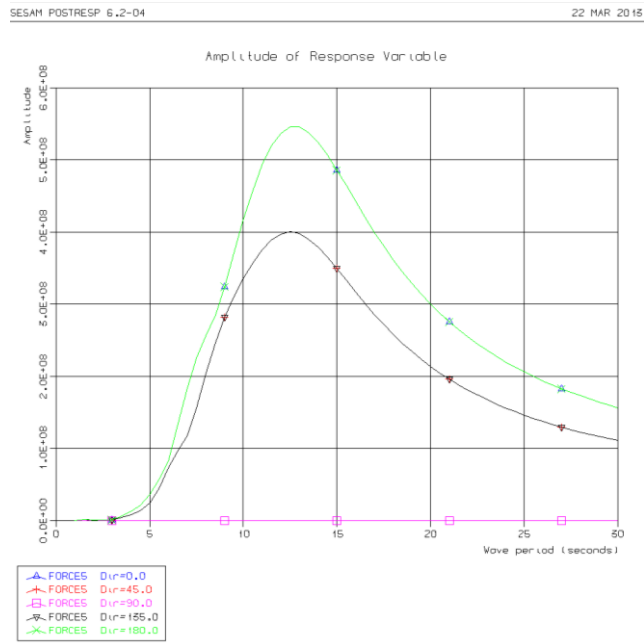


Figure 68: Wave excitation coefficients pitch

unit of ordinate [Nm/m]



## Appendix H- Added mass FSU 1000

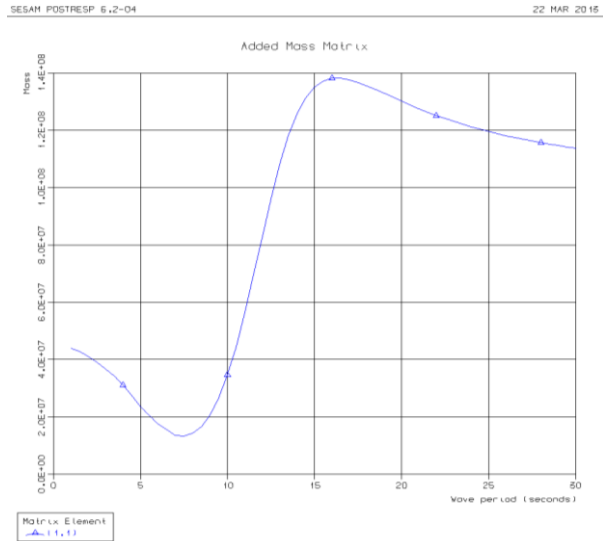


Figure 69: Added mass surge

unit of ordinate [kg]

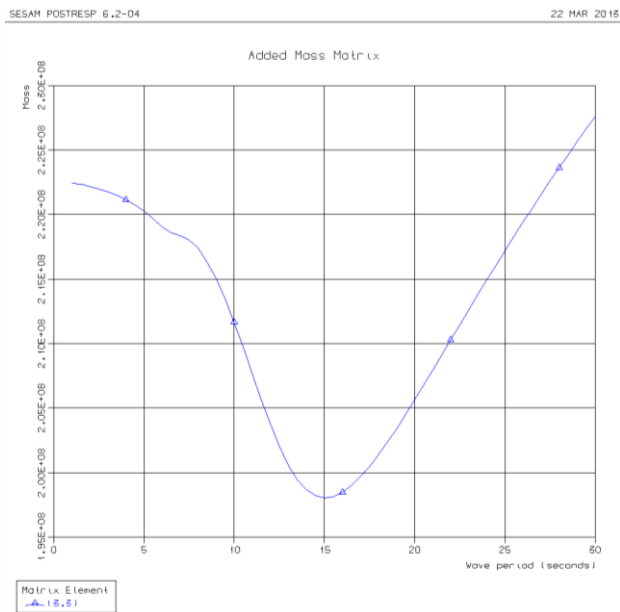
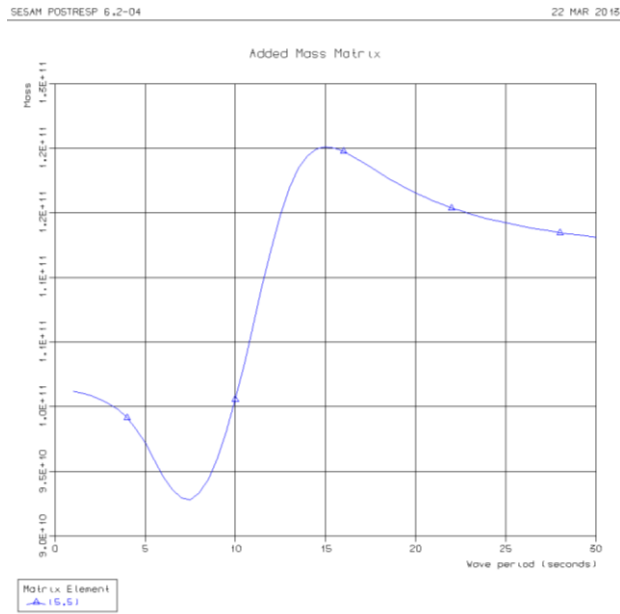


Figure 70: Added mass heave

unit of ordinate [kg]



**Figure 71: Added mass pitch**

unit of ordinate [kg x m<sup>2</sup>]



## Appendix I - Potential damping FSU 1000

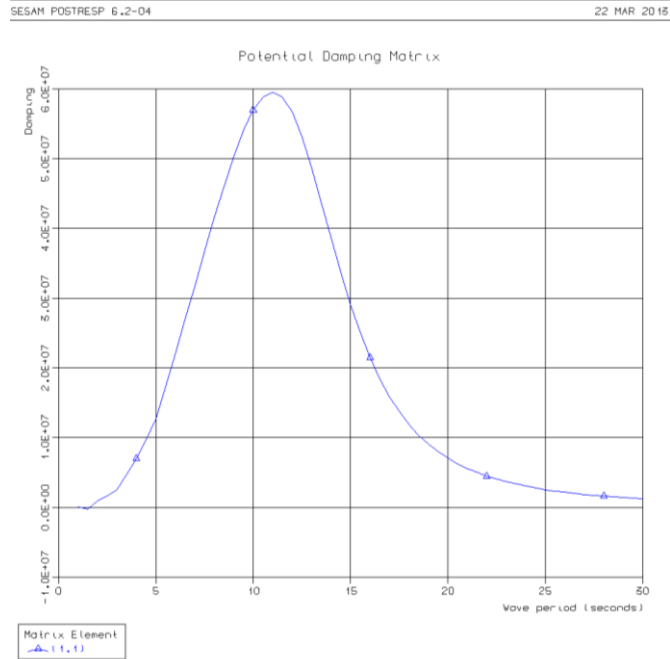


Figure 72: Potential damping surge

unit of ordinate [N/(m/s)]

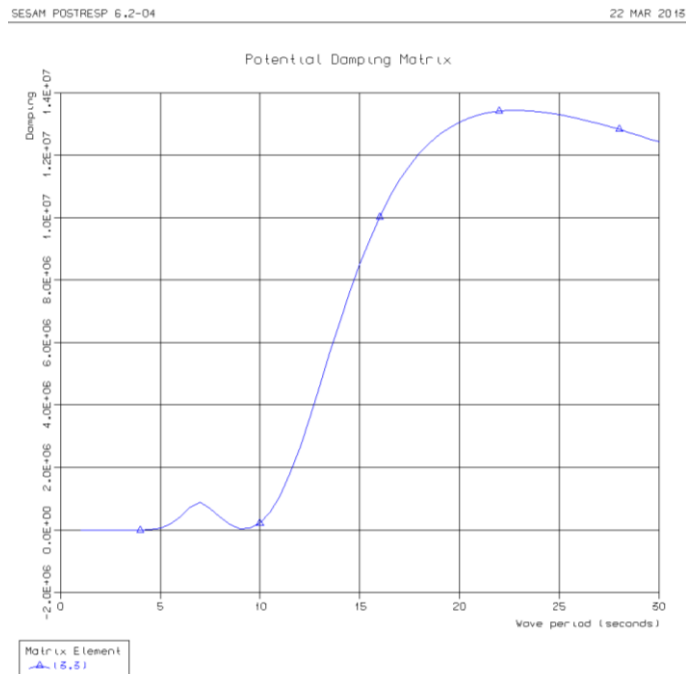


Figure 73: Potential damping heave

unit of ordinate [N/(m/s)]

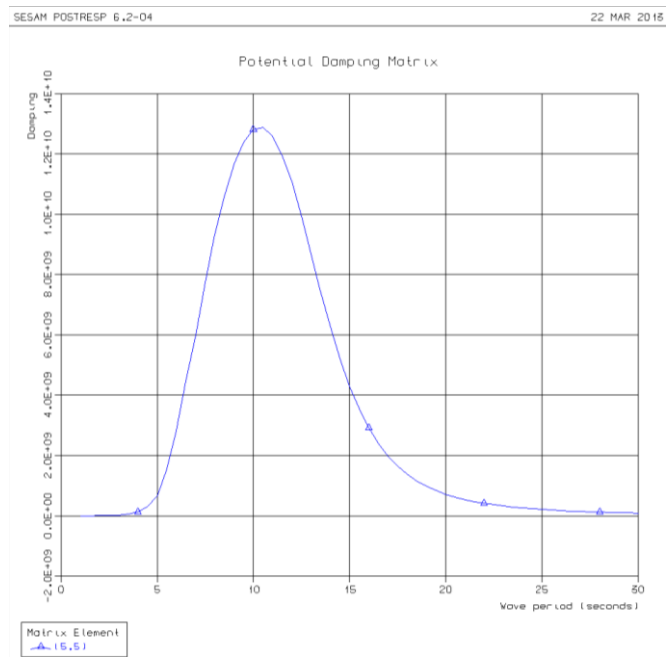


Figure 74: Potential damping pitch

unit of ordinate [Nm/(rad/s)]



## Appendix J- Mean wave drift coefficients FSU 1000

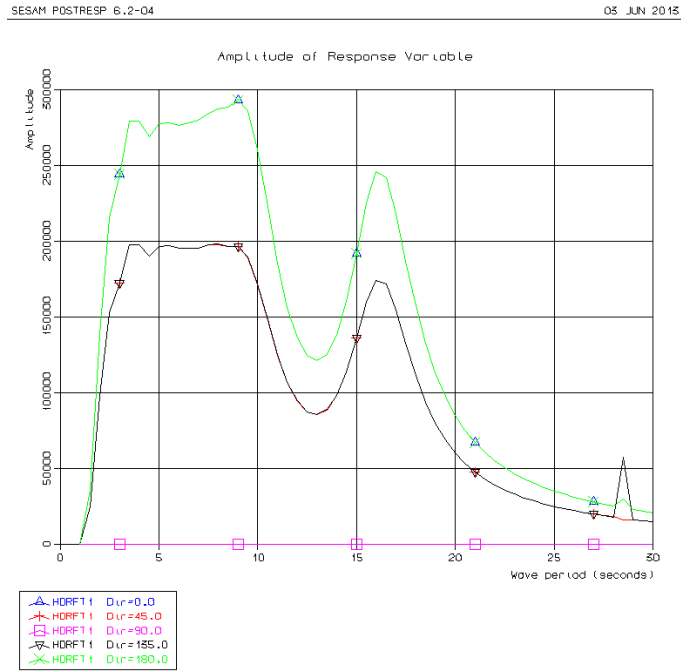


Figure 75: Mean wave drift coefficients

unit of ordinate [N/m<sup>2</sup>]



## Appendix K – Converting time series to Gaussian-shaped power spectra

```
% INPUT FROM ORCAFLEX      %
```

```
load 3021;                    %loading OrcaFlex results
r=heave3021_0_12000;        %the matrix
a=heave3021_0_12000(:,2);   %vector with realizations
a=detrend(a)                 %detrend vector
N=length(a);                %number of points
t=heave3021_0_12000(:,1);   %vector with time
T=max(t)-min(t);            %total simulation time
df=0.5*(1/T);               %frequency range
freq=[0:N/2-1]/T;           %vector of frequencies
Fs=10;                      %samples pr unit time
```

```
% FFT AND PLOT OF RAW SPECTRUM AND GAUSSIANSMOOTH      %
```

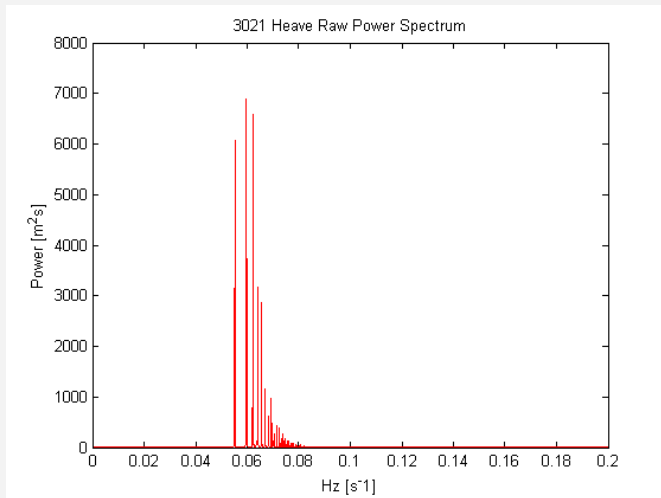
```
fft_a=fft(a) ;               %fast fourier transform of signal

power=(fft_a(1:N/2).*conj(fft_a(1:N/2)))/(N/2)^2/df;

                                %finding the power up to N/2 (Nyquist)

figure(1)                      %plotting the unsmoothed spectrum
plot(freq,power,'r')
xlim([0 0.2])
ylim([0 8000])
ylabel('Power [m^2s]')
xlabel('Hz [s^-1]')
title('3021 Heave Raw Power Spectrum')
```

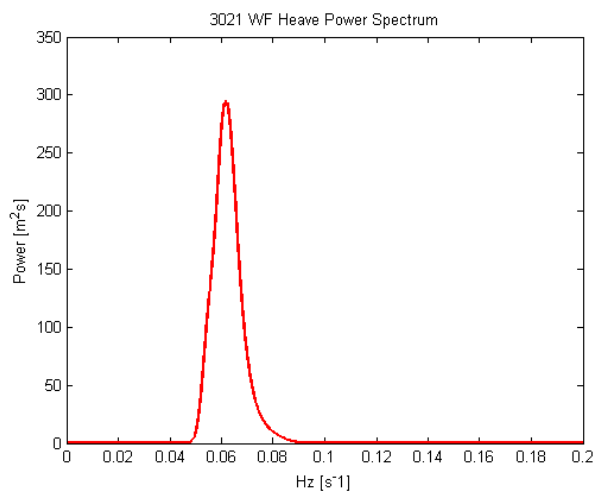




```
rad=2*pi*freq'; % convert [1/s] -> [rad/s] input to
gaussianSmooth

ss=gaussianSmooth(power',rad,0.015); % gaussianSmooth, technique shared by
% Marintek

figure(2) % plotting gaussianSmooth spectrum
plot(freq,ss,'r','linewidth',2)
hold on
xlim([0 0.25])
ylim([0 325])
ylabel('Power [m^2s]')
xlabel('Hz [s^-1]')
title('3021 Heave Power Spectrum')
```





## Appendix L – Smoothing convolution of raw power spectra

The convolution of Gaussian-shaped frequency window smoothing of a raw spectrum was shared by Marintek. The MatLab GaussianSmooth function utilized in the latter Appendix was also shared by Marintek, and the underlying theory is presented in the following:

$S(\omega)$  is the raw spectrum and the smoothed spectrum  $S_s(\omega)$ . The following Gaussian bell function is utilized:

$$G(\omega) = \frac{1}{\sqrt{2\pi}\sigma} e^{-\frac{\omega^2}{2\sigma^2}}$$

as a moving weighted average of the raw spectrum  $S(\omega)$ :

$$S_s(\omega) = \int_{-\infty}^{\infty} S(\omega)G(\omega - \omega)d\omega$$

in the frequency domain. The Fourier transform reads:

$$S_s(\tau) = \int_{-\infty}^{\infty} \left( \int_{-\infty}^{\infty} S(\omega)G(\omega - \omega)d\omega \right) e^{-i\omega\tau} d\omega d\omega$$

Introducing  $\omega' = \omega - \omega$  and  $\omega' = \omega$

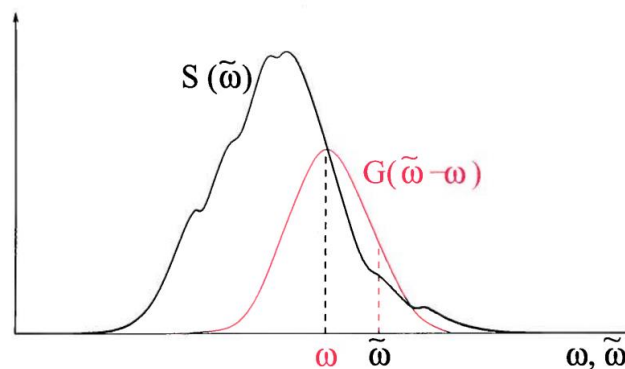


Figure 76: Definition of smoothing convolution (Muthanna, 2011)



Yields:

$$S_s(\tau) = \int_{-\infty}^{\infty} \left( \int_{-\infty}^{\infty} S(\omega') G(\omega') \right) e^{-i(\omega' - \omega' \tau)} d\omega' d\omega'$$

$$= \int_{-\infty}^{\infty} S(\omega') e^{-i\omega' \tau} d\omega' \int_{-\infty}^{\infty} G(\omega') e^{i\omega' \tau} d\omega'$$

Using symmetry property  $G(\omega') = G(-\omega')$  yields:

$$S_s(\tau) = \int_{-\infty}^{\infty} S(\omega') e^{-i\omega' \tau} d\omega' \int_{-\infty}^{\infty} G(\omega') e^{-i\omega' \tau} d\omega' = S_s(\tau) G(\tau)$$

where the Fourier transform of the Gaussian bell function  $G(\tau)$  is defined as:

$$G(\tau) = \int_{-\infty}^{\infty} G(\omega) e^{-i\omega \tau} d\omega = \int_{-\infty}^{\infty} \frac{1}{\sqrt{2\pi\sigma}} e^{-\frac{\omega^2}{2\sigma^2}} e^{-i\omega \tau} d\omega = e^{-\frac{\sigma^2 \tau^2}{2}}$$

The process is summarized by the following:

1. Calculate the Fourier transform  $S(\tau)$  of  $S(\omega)$
2. Multiply  $S$  with  $G(\tau) = e^{-\frac{\sigma^2 \tau^2}{2}}$
3. Calculate the inverse Fourier transformation of  $S(\tau)G(\tau)$  which gives  $S_s(\omega)$



## **Appendix M – Content of attached data folder**

The attached file contains 3 folders.

1. Mooring:

Contains an excel sheet of calculations done on the different mooring line segments as described in section 5.2: Building the model in OrcaFlex

2. WADAM:

Contains the .FEM file created in GeniE and the WADAM workspace file.

3. OrcaFlex:

Contains the .dat files from the OrcaFlex analyses. I.e. the system modeling and corresponding input parameters. It also contains .txt-files with recorded response of the FSU during the 12 000 analysis performed with the environmental conditions as load.